Master's thesis

CHARACTERIZATION OF NOVEL GENE TARGETS INVOLVED IN BIOFILM FORMATION AND ANTIBIOTIC SUSCEPTIBILITY FROM A *STAPHYLOCOCCUS AUREUS* USA300 *BURSA AUREALIS* TRANSPOSON LIBRARY

Katri Holappa

Department of Biosciences

Faculty of Biological and Environmental Sciences

UNIVERSITY OF HELSINKI

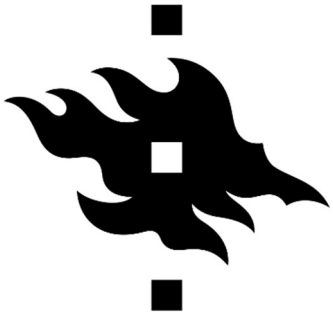

HELSINGIN YLIOPISTO
HELSINGFORS UNIVERSITET
UNIVERSITY OF HELSINKI

UNIVERSITY OF HELSINKI

Faculty	**Department**
Faculty of biological and environmental sciences	Department of biosciences

Author

Katri Holappa

Title

Characterization of novel gene targets involved in biofilm formation and antibiotic susceptibility from a *Staphylococcus aureus* USA300 *bursa aurealis* transposon library

Subject

General microbiology

Level and instructors	**Month and year**	**Number of pages**
Master's thesis Prof. Surbhi Malhotra-Kumar, Sarah De Backer, MSc.	April 2018	76 + 4 appendix pages

Abstract

Staphylococcus aureus is a commensal bacterium in humans and approximately 30% of healthy people carry it as part of their microbiome, in the nasal cavity and skin, without any harm. However, it is an opportunistic pathogen that causes severe infections in immunocompromised and hospitalized patients. Typical infections caused by *S. aureus* are wound and skin infections, pneumonia and urinary tract infections in people with a medical implanted device such as for example a catheter. *S. aureus* has gained resistance to virtually all antibiotics over the years of excessive antibiotic consumption, making treatment nearly impossible in some cases. MRSA, methicillin resistant *S. aureus*, is a worldwide problem in hospitals and the mortality rate is still rising. One of the most common MRSA lineages is USA300, a community-acquired MRSA, which is notorious not only for its antibiotic resistance but also for its ability to form prolific biofilms. Biofilm production combined with antibiotic resistance complicates treatment of *S. aureus* even further. A detailed understanding the molecular mechanisms of biofilm formation might bring us closer to a cure for infections caused by MRSA biofilms.

The study comprised two parts. First, characterize the phenotype of the mutants under static and dynamic conditions, test the minimal inhibitory concentrations (MIC's) for antibiotics and verify the gene knockout by real-time RT-PCR. Second, study gene function by transduction to the parental strain USA300-UAS391 Ery^S and a MRSA strain TCH1516 Ery^S to study the gene function in a different bacterial background. The methods used were cell culturing for static and dynamic biofilm as well as growth curve, fluorescence microscopy, antibiotic susceptibility testing and real-time RT-PCR.

In total seven strains were selected for characterization. The chosen seven knockouts were ΔHAD (HAD-superfamily hydrolase, subfamily IA, variant 1), non-coding region, *ΔausA* (non-ribosomal peptide synthetase), *ΔoppA* (Oligopeptide ABC transporter substrate-binding protein), *ΔclfB* (clumping factor B), *ΔampA* (cytosol aminopeptidase), and *ΔpgsA* (CDP-diacylglycerol--glycerol-3-phosphate 3-phosphatidyltransferase).

General characterization showed a few changes in biofilm formation for the genes *ΔoppA*, *ΔausA*, *ΔHAD* and *ΔpgsA*. Especially *ΔpgsA* is interesting because of increased ciprofloxacin resistance. The real-time RT-PCR showed some altered gene expression patterns, but no connection to poor biofilm formation. With fluorescence microscopy the growth patterns of USA300 transposon mutant strain biofilms could be described.

To verify the results of the characterization, further experimentation is needed, such as RNA sequencing and complementation. Also expanding the study to other gene hits of the screening is recommended.

Keywords

Staphylococcus aureus, transposon, *bursa aurealis*, biofilm, biofilm formation, MRSA, USA300

Where deposited

E-Thesis database of the University of Helsinki, http://ethesis.helsinki.fi/

Additional information

The experiments of this thesis were done at the University of Antwerp (Universiteit Antwerpen), at the faculty of Medicine, the Department of Medical Microbiology

HELSINGIN YLIOPISTO

Tiedekunta	**Laitos**
Bio- ja ympäristötieteellinen tiedekunta	Biotieteiden laitos

Tekijä

Katri Holappa

Työn nimi

Uusien biofilmin muodostumiseen ja antibioottiresistenssiin liittyvien geenien karakterisointi *Staphylococcus aureus* USA300 *bursa aurealis* -transposonikirjastosta

Oppiaine

Yleinen mikrobiologia

Työn laji ja ohjaaja(t)	**Aika**	**Sivumäärä**
Pro Gradu -tutkielma Prof. Surbhi Malhotra-Kumar, Sarah De Backer, MSc.	Huhtikuu 2018	76 + 4 liitesivua

Staphylococcus aureus on kommensaali bakteeri, joka on noin 30 % ihmisistä normaalimikrobiomissaan (nenänielussa ja iholla) ilman, että se aiheuttaa mitään tautia. Se on kuitenkin opportunisti patogeeni ja voi aiheuttaa pahoja iho- ja haavainfektioita, sekä keuhkokuumetta sairaalapotilailla ja virtsatieinfektioita katetroiduilla potilailla. S. aureus on vuosien saatossa muuttunut vastustuskykyiseksi lähes kaikille käytetyillä antibiooteille niiden liikakäytön vuoksi ja on siksi miltei mahdoton hoitaa joissakin tapauksissa. Metisilliinille resistentti *S. aureus* (MRSA) onkin jo maailmanlaajuinen ongelma sairaaloissa ja sen aiheuttamat kuolemat ovat yleistymässä. Yksi yleisimpiä MRSA -linjoja on USA300, ympäristöbakteeri, jolla on antibioottiresistenssin lisäksi kyky tuottaa paljon biofilmiä kasvualustaansa. Biofilmin tuotto yhdistettynä antibioottiresistenssiin vaikeuttaa entisestään infektioiden hoitoa. Siksi biofilmin muodostumisen molekulaaristen mekanismien tuntemus voi auttaa tutkijoita kehittämään uusia hoitomuotoja MRSA -infektioiden hoitoon ja torjuntaan.

Tutkimukseen käytettiin *bursa aurealis* transposonikirjastoa. Tutkimus koostui kahdesta osasta: 1. Valittujen bakteerimutanttien fenotyyppien karakterisointi sessiileissä ja dynaamisissa viljelmissä, testata mutanttien antibioottiherkkyys eri mikrobilääkkeille ja varmistaa mutatoituneen geenin hiljentyminen reaaliaika-käänteiskopiointi PCR:llä (real-time RT-PCR). 2. Tutkia geenin toimintaa toisessa isäntäbakteerissa transduktoimalla se φ11 bakteriofaagilla USA300-UAS391 Ery^S ja TCH1516 Ery^S kantoihin. Lisäksi mutanttikannat kuvattiin epifluoresenssimikroskoopilla.

Seitsemän eri mutanttia valittiin karakterisointiin: *ΔHAD* (HAD-superfamily hydrolase, alaryhmä IA, variantti 1), *ΔNCR* (koodaamaton alue), *ΔausA* (ei-ribosomaalinen peptidisyntetaasi), *ΔoppA* (oligopeptidi ABC transportterin substraattiin kiinnittyvä proteiini), *ΔalfB* (clumping factor B), *ΔampA* (sytosolinen aminopeptidaasi) ja *ΔpgsA* (CDP-diasyyliglyseroli--glyseroli-3-fosfaatti 3-fosfatidyylitransferaasi).

Karakterisoinnissa ilmeni muutoksia *ΔoppA*-, *ΔausA*-, *ΔHAD*- ja *ΔpgsA* -mutanteissa. Erityisesti *pgsA* -mutantti oli kiinnostava, sillä havaittiin myös lisääntynyt resistenssi siprofloksasiini -antibiootille. Reaaliaika RT-PCR:ssä havaittiin muutamia muutoksia geeni-ilmentymisessä, mutta niitä ei voitu varmuudella yhdistää heikentyneeseen biofilmin muodostukseen. Mikroskooppikuvista voitiin analysoida *S. aureus* USA300 kannan biofilmin rakenne- ja pinnanmuodonvaihtelua, mutta mutanttikantojen väliset erot eivät olleet suuria silmällä tarkasteltuna.

Tulosten varmistamiseksi suositeltavaa olisi toistaa dynaamiset testit ja reaaliaika RT-PCR, jotta niiden tulosten tilastollinen merkitsevyys voitaisiin vahvistaa. Lisäksi RNA-sekvensointi ja komplementaatiokokeet voisivat antaa tarkempaa tietoa geenien osuudesta biofilmin säätelyyn. Tutkimusta jatkettaneen myös muilla seulonnassa löytyneillä geeneillä.

Avainsanat

Staphylococcus aureus, transposoni, *bursa aurealis*, biofilmi, biofilmin muodostus, MRSA, USA300

Säilytyspaikka

Helsingin yliopiston E-Thesis tutkielmatietokanta, http://ethesis.helsinki.fi/

Muita tietoja

Työn kokeellinen osio on tehty Antwerpenin yliopiston (Universiteit Antwerpen) lääketieteellisen tiedekunnan kliinisen mikrobiologian osastolla.

Declaration of authorship

The work presented in this thesis is my own and performed as a part of my master's thesis project with following exceptions: the transposon mutant library was constructed by Charlotte Vanmarsenille in 2013. The original "Screening of the transposon library" project is a doctoral thesis project of Sarah De Backer. The screening of the library was done as a collective work by Sarah De Backer, Wouter Vermeulen, several technicians and me. The identification of genes (DNA isolation and sequencing) was done by Sarah De Backer, me and a technician. Characterizations presented in this thesis were done by me, under supervision of Sarah De Backer.

List of abbreviations

ACME	arginine catabolic mobile element
agr	accessory gene regulator gene
AgrBDCA	response regulator (proteins) BDCA of *agr* system
AIP	auto-inducing peptide
AmpA	cytosol aminopeptidase gene
Atl	autolysin
AusA	non-ribosomal peptide synthetase gene
Bap	biofilm-associated protein
CA-MRSA	community-acquired MRSA
cDNA	complementary DNA
ClfB	Clumping factor B gene
Coa	Coagulase
DNA	deoxyribonucleic acid
ECM	extracellular matrix
eDNA	extracellular DNA
FnBPA	fibronectin-binding protein A
FnBPB	fibronectin-binding protein B
FnBPs	fibronectin-binding proteins
HAD	HAD-superfamily hydrolase, subfamily IA, variant 1 gene
HA-MRSA	hospital-acquired MRSA
icaADBC	intercellular adhesin operon
icaR	ica regulator gene
LuxS	S-ribosylhomocysteine lyase
mecA	methicillin resistance gene
MRSA	methicillin resistant *Staphylococcus aureus*
MSCRAMM	microbial surface components recognizing adhesive matrix molecule
MSSA	methicillin sensitive *Staphylococcus aureus*
NCR	non-coding region
OppA	Oligopeptide ABC transporter substrate-binding protein coding gene
PCR	polymerase chain reaction
pgsA	CDP-diacylglycerol--glycerol-3-phosphate 3-phosphatidyltransferase gene
PIA	polysaccharide intercellular adhesin
PNAG	poly-N-acetylglucosamine
PSMs	phenol-soluble modulins
PVL	Panton-Valentine leucocidin
QS	quorum sensing
RNA	ribonucleic acid
RNAIII	regulatory ribonucleic acid III
RT-PCR	reverse transcription polymerase chain reaction
sarA	staphylococcal accessory regulator A gene
SasC	*S. aureus* surface protein C

SCCmec	staphylococcal chromosomal cassette mec
Spa	staphylococcal protein A
ST/MLST	sequence type/multilocus sequence type
σB	sigma factor B

CONTENTS

1 INTRODUCTION

A biofilm is a common life form of bacteria. They are aggregates of bacteria, which are embedded in a self-produced matrix of extracellular polymeric substances, such as exopolysaccharides, proteins and extracellular DNA. Biofilms can either emerge on surfaces or without any solid substratum. Biofilms are beneficial: they run the biogeochemical cycles of soil taking part in degradation of matter into elements (Flemming et al., 2016). While certain biofilms are beneficial, others frequently cause problems in the health care environment. An example of such a harmful biofilm is that of the bacterium *Staphylococcus aureus* (*S. aureus*). This bacterium is a common commensal in 30–50% of humans, but it can cause an infection in wounds and prostheses, especially in immunocompromised patients. The most severe infections caused by it are necrotizing pneumonia, sepsis and endocarditis, which might lead to death. The lethality of the bacterium is empowered by its selection of antibiotic resistance genes, which are becoming more and more prevalent in correlation with excessive global antibiotic usage (Chambers & Deleo, 2009; Pantosti & Venditti, 2009).

An especially problematic *S. aureus* lineage is USA300, a methicillin resistant *S. aureus* (MRSA). It is a globally spread lineage and its fitness advantages are among other a thick biofilm production in addition to antibiotic resistance and other virulence factors. USA300 is a so-called community-associated MRSA (CA-MRSA), and therefore becoming a carrier or infected by it does not require hospital treatment or even having an illness. Different MRSA lineages are, however, blending and traditional CA-MRSA can also be acquired from hospital environment as well (Pantosti & Venditti, 2009).

Biofilm formation is a highly intricate interplay between environment and quorum sensing between bacteria, after a certain cell density of the bacterial community is reached. The molecular mechanisms of how a biofilm develops and is regulated are actively being researched, but still not all genes involved have been identified yet. This study focuses on finding new key elements that participate in biofilm formation as well as antibiotic resistance. Biofilm research is needed, since it only aggravates the pandemic problem of antibiotic resistance in infectious bacteria and often leaves no other option than removal of the indwelling medical device. By understanding the process of how biofilms are developing and how signaling within the biofilm is taking place, there is a chance to find new therapeutic targets for anti-biofilm treatments that could cure MRSA infections in the future (Chambers & Deleo, 2009; McCarthy et al., 2015).

2 LITERATURE REVIEW

2.1 Biofilms

A biofilm is a community of irreversibly aggregated microbes embedded in extracellular compounds which can be water, exopolysaccharides, extracellular DNA, proteins and lipids. Non-cellular components are also present in the biofilm matrix: salts, crystals, corrosion particles, soil or blood and host organism extracellular matrix components. Bacteria in the biofilm differ from planktonic (single-cell) bacteria by their genetic phenotype as well as their metabolism. In nature, a biofilm usually is a community of several bacterial and even fungal species, which is called a multispecies biofilm (Donlan, 2002; Flemming et al., 2016; Götz, 2002). Such biofilms exist everywhere: in soil, surfaces and living organisms such as plants and animals. They have practical applications: degradation of wastewater and solid waste as well as the biogeochemical cycling processes (degradation of matter to elements) (Flemming et al., 2016). The most common biofilms in humans are, for example, beneficial lactobacilli biofilms in the mucosa of the intestine and the vagina (M. Wilson, 2001). However, some biofilms can also cause damage to humans. Biofilm can easily colonize invasive implants because of their hydrophobic surface, which is known to increase bacterial adhesion (Myint et al., 2010). In time, indwelling implants become coated with host proteins, which also facilitates the bacterial attachment (Donlan, 2002). The most prevalent harmful biofilm found in humans is the caries-causing tooth plaque (M. Wilson, 2001). A biofilm is a common phenotype of bacteria which provides advantages compared to a planktonic mode of living. For example, biofilms can store nutrients, such as carbon and phosphates, can shield bacteria from the effects of adverse environmental stress and protect them from phagocytosis by a host organism (Archer et al., 2011).

To form a biofilm, bacteria must first attach to a surface, for example skin or plastic. The initial attachment to a surface is reversible, which is followed by either detachment or irreversible attachment (Sauer, Camper, Ehrlich, Costerton, & Davies, 2002). Numerous adherence proteins, microbial surface components recognizing adhesive matrix molecules (MSCRAMMs), which are responsible of attachment, have been found. MSCRAMMs mediate protein-protein interaction when attaching to biotic surfaces and electrostatic, hydrophobic and hydrophilic interactions of surface proteins when attaching to abiotic surfaces such as glass or polystyrene (Moormeier & Bayles, 2017). Once attached, the formation of a biofilm begins. The bacteria multiply and start to produce slime, polysaccharides and other components of the

biofilm. As maturation proceeds, the biofilm usually forms three-dimensional structures, and water channels within the biofilm that bring nutrients to cells deep within the biofilm (Götz, 2002). In a mature biofilm, three layers of bacteria with different metabolic states can be identified and they are distributed in the biofilm according to the surrounding environmental factors. The outer layer (a layer not towards the substratum) consists of bacteria with aerobic metabolism because it typically faces air, and thus, oxygen can diffuse to the biofilm. The middle layer bacteria have an anaerobic metabolic state and the bacteria attached closest to the substratum are usually metabolically inactive as the bacteria, that are located closer to air source in the biofilm, consume the diffused oxygen (Flemming et al., 2016). The pH of the biofilm turns acidic in time and the acidic environment precipitates minerals into it, which typically leads to corrosion of the substratum (Donlan, 2002). When the biofilm has aged, it starts to degrade and the bacteria are released as metastatic clusters which colonize new surfaces (Götz, 2002). Figure 1 depicts the four classic stages of biofilm formation. A recently discovered additional stage to the normal paradigm of biofilm formation has been described for *S. aureus*. The stage is called 'exodus', which occurs after an early biofilm has formed, in which nuclease (*nuc)* gene expression by certain cells of the biofilm lead to degradation of extracellular DNA (eDNA) and therefore to dispersal of a portion of the biofilm, which contributes to the structure of the biofilm during maturation (Moormeier & Bayles, 2017). At the following dispersal stage, cells can convert back into planktonic cells (Sauer et al., 2002).

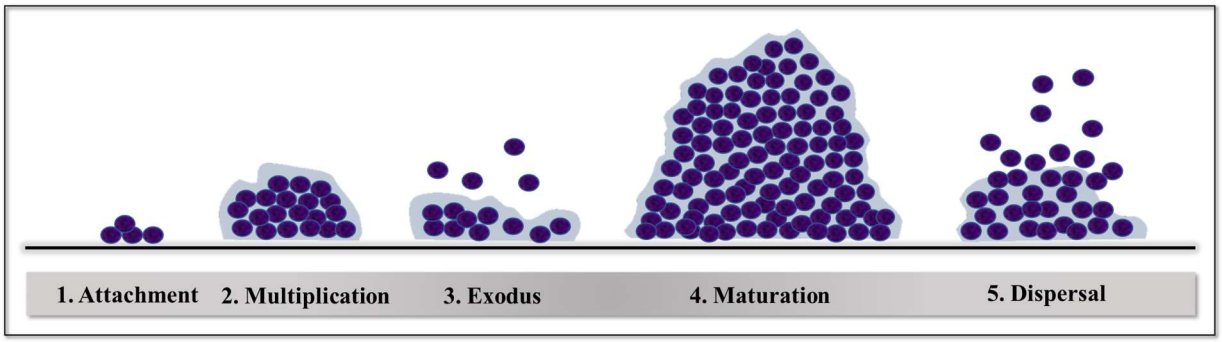

FIGURE 1. The life cycle of a biofilm. *(Blue circles depict Staphylococci and the blue-gray shade on the background of them depicts the biofilm matrix.) 1. Attachment to a surface. 2. Multiplication of the bacterial cells and production of protective matrix. 3. Mature biofilm. 4. Degradation of the biofilm; dispersal of single cells or cell clusters and colonization of new surfaces (Moormeier & Bayles, 2017).*

The biofilm matrix is mainly composed of hydrated exopolysaccharides rather than bacterial cells. The exopolysaccharides are not only produced and secreted by the bacteria, but also accumulated from the environment or the host. Water comprises up to 97% of the biofilm mass

and eDNA assists in holding the biofilm together. Biofilms also contain insoluble components depending on the surface, for example cellulose, amyloids, fimbriae, pili and flagellae (Flemming et al., 2016). *S. aureus* is known to form different types of biofilms; the phenotype depends on which part of the body it colonizes (Zapotoczna, O'Neill, & O'Gara, 2016). Biofilm types are discussed in chapter 2.2.4.5. Staphylococci are the most abundant, biofilm-associated, infection-causing bacteria mostly due to their high prevalence as commensal bacteria in humans. *S. aureus* can grow in multispecies biofilms, for example a shared biofilm with a yeast *Candida albicans* have been studied (Jey et al., 2013). In a mixed-species biofilm interspecies quorum sensing can go from competition to harmonious co-existence by inhibiting the virulence mechanisms towards one another. Such a phenomenon has been observed in a common biofilm of *Pseudomonas aeruginosa* and *S. aureus* (Otto, 2008).

Biofilm formation is a big problem especially in medical device-associated infections, because the biofilm works as a shield against antibiotics, diluting the concentration and preventing it from penetrating into the lower layers of the biofilm. Therefore, the infections last longer and are sometimes impossible to treat (Pantosti & Venditti, 2009; Vanhommerig et al., 2014), only leaving removal of the device which is not always a viable option in the case of artificial heart valves or pacemakers. The biofilm also shields the bacteria from the host immune cells. Planktonic cells are engulfed by the phagocyting leucocytes in a primary infection. In biofilm infections, the biofilm prevents phagocytosis of the bacteria by immune cells (Archer et al., 2011). Matured biofilms also disperse in the body, for example via blood circulation, which leads to new infections and might eventually cause sepsis (Sauer et al., 2002).

2.2 Staphylococcus aureus

Staphylococcus aureus is a Gram-positive, facultative anaerobic coccus, that forms clusters. When grown on a blood agar plate, it can be recognized by its yellow color and β-hemolysis (a clearing around the colony due to breaking down of red blood cells). All *S. aureus* strains form coagulase enzyme (Coa), which makes it possible for the bacterium to survive in blood and differentiates *S. aureus* from other staphylococcal strains (Zapotoczna et al., 2016). In humans, its natural habitat is in the nose, upper respiratory tract and epidermis. However, *S. aureus* is an opportunist pathogen, occurring frequently in skin, soft tissue, and wound infections, and approximately 98% of nosocomial infections are caused by the most prevalent MRSA lineage, USA300 (Thurlow et al., 2013).

2.2.1 Antibiotic resistance in *S. aureus*

Staphylococcus aureus has been remarkably successful in developing antibiotic resistance towards β-lactams. When antibiotics were first discovered in the 1940s, all strains of the bacterium *Staphylococcus aureus* studied were susceptible to penicillin. However, briefly after the introduction of penicillin, penicillinase-producing strains were found (Abraham et al., 1941; Kirby, 1944). An upgraded version of penicillin, methicillin, an antibiotic towards penicillin-resistant *S. aureus*, was soon invented, but the first reports about methicillin resistant *S. aureus* (MRSA, *S. aureus* strain resistant to β-lactams) were published at the beginning of the 1960s (Barber, 1961). By the 1970s, *S. aureus* had become resistant to all penicillins and cephalosporins, (Bran, Levison, & Kaye, 1972; Chabbert, 1967). Thus, MRSA strains are nowadays usually multi-drug resistant strains, resistant not only to β-lactams, but also varyingly to fluoroquinolones, lincosamides, macrolides, tetracyclines, aminoglycosides and vancomycin (Hope, Livermore, Brick, & Lillie, 2008; Pantosti & Venditti, 2009). Linezolid, daptomycin and an antibiotic recently approved by FDA, tedizolid, are currently the last antibiotics to treat MDR MRSA infections (Vanegas, Ocampo, Urrego, & Jiménez, 2017).

The prevalence of antibiotic resistant strains is a major challenge for health care. The antibiotic resistant strains are not only prevalent in hospitals but also in the community. Traditionally, MRSA lineages are classified as hospital-acquired MRSA (HA-MRSA) and community-acquired MRSA (CA-MRSA) (Wertheim et al., 2005) (sometimes also referred to as community-/hospital-associated/-genotype [HA, CA, HG, CG]). However, the definition is more clinical than microbiological: infection is hospital-acquired when it occurs within 48 hours or later after hospitalization (Chatterjee & Otto, 2013). The distinction between the two is overall becoming more and more loose as the lineages become more occurring in all environments. The most common lineage of community-associated MRSA is USA300 (Pantosti & Venditti, 2009).

β-lactams are antibiotics that disrupt peptidoglycan synthesis of the cell wall (Herzberg & Moult, 1987). Resistance towards penicillin is due to penicillin-binding proteins (PBPs) (Pinho, Kjos, & Veening, 2013). PBPs are enzymes that synthesize peptidoglycan on the cell wall by elongating the glycan chains and linking them together (Brown, Santa Maria, & Walker, 2013). The cell wall of Gram-positive bacteria, including staphylococci, consists of peptidoglycan, teichoic acids, teichuronic acids and other polymers that are covalently linked to the peptidoglycan. The penicillinases inactivate β-lactams by hydrolyzing the amide bond in a β-lactam ring of a penicillin molecule. The resistance towards methicillin is due to a penicillin-

binding protein 2a (PBP2a). It is encoded by the *mecA* gene which is in the chromosome carried on the staphylococcal chromosome cassette, *SCCmec* (Katayama, Ito, & Hiramatsu, 2000). The different lineages of MRSA can be differentiated by their *SCCmec*- (Liu et al., 2016), staphylococcal protein A- (SpA), and their multi-locus sequence types (MLST) (Pantosti & Venditti, 2009). The *SCCmec* element always contains the *mecA* gene, a complete or a truncated part of a *mecR1* regulatory gene and a recombination gene *ccr* (Robinson & Enright, 2004). The *mecA* gene makes *S. aureus* resistant not only to β-lactams, but also cephalosporins, carbapenems, and synthetic penicillins (Pantosti & Venditti, 2009; Pantosti et al., 2007).

2.2.2 MRSA virulence factors

The main virulence mechanisms of *S. aureus* are protein A (SpA), pore-forming cytotoxins, such as α-toxin and Panton-Valentine leucocidin (PVL), arginine catabolic mobile element (ACME), phenol-soluble modulins (PSMs), antibiotic resistance, and a biofilm that protects a sessile bacterial community (Diep & Otto, 2008). Protein A is a cell wall protein of *S. aureus* and it participates in invasion into epithelial cells, especially in airway infections (Soong et al., 2011). α-toxin is α-hemolysin, which can release iron from human erythrocytes (red blood cells), and it is a major virulence factor in pneumonia caused by *S. aureus* (Parker & Prince, 2012). PVL is a pore-forming cytotoxin, which kills human neutrophils by forming pores on the membrane causing lysis of the target cell (Lacey, Geoghegan, & McLoughlin, 2016). The ACME region participates in virulence by coding for polyamine resistance enzyme spermidine/spermine acyltransferase (SpeG). Polyamines are produced by the host organism (putrescine, spermidine, and spermine) and are essential for the wound healing process. It is also likely that the SpeG facilitates skin colonization by making the bacteria more acid tolerant (Thurlow et al., 2013). Another ACME cluster gene, *arcA,* codes for arginine deaminase pathway, and *opp3*, an oligopeptide permease system, which are known to participate in the pathogenesis of *S. aureus* by facilitating survival on the skin (Diep et al., 2008; Ellington, Yearwood, Ganner, East, & Kearns, 2008). The phenol-soluble modulins are small molecules produced by the bacteria and they have many functions, such as biofilm structuring and dispersal, proinflammatory effect, cell-killing properties (erythrocytes, phagocytic cells), antimicrobial effect towards other bacterial species, and facilitating skin colonization (Li et al., 2014; Peschel & Otto, 2013).

2.2.3 The *S. aureus* USA300 clonal lineage

USA300 CA-MRSA lineage is one of the most successful, globally spread MRSA lineages to date. The first reports about USA300 are from the beginning of 2000s in which CA-MRSA infection outbreaks were reported in prisoners (Centers for Disease Control and Prevention, 2001), sport players (Centers for Disease Control and Prevention, 2003) and wrestlers (Lindenmayer, Schoenfeld, O'Grady, & Carney, 1998). The USA300 lineage most probably originated in the east of the United States, Pennsylvania, and in few years' time, it spread across the entire country (Challagundla et al., 2018) and gradually to all continents (Vandenesch et al., 2003). It is likely that USA300 is derived from a hospital-associated USA100 lineage (Carrel, Perencevich, & David, 2015). The USA300 lineage studied in this thesis is USA300-UAS391. This multi-locus sequence type 8 (ST8) strain carries the *SCCmec* type IV that codes for *mecA* gene. (Boyle-Vavra et al., 2015; Pantosti & Venditti, 2009). UAS391 was isolated in a Belgian hospital from an abscess of a patient and it has previously been proven to be a prolific biofilm forming MRSA strain, and was therefore chosen for this study (Vanhommerig et al., 2014).

Being *S. aureus*, the USA300 lineage contains partly the same general virulence mechanisms as methicillin sensitive *S. aureus* (MSSA), but the molecular mechanisms that generate greater virulence characteristic to USA300 compared to other strains are not completely understood. Epidemiologically, the PVL gene has been linked to be the main virulence mechanism giving fitness advantage compared to the rest of the strains. However, *in vitro* studies cannot prove that yet unanimously. Other important virulence factors of USA300 are the secreted PSMs, short, α-helical peptide toxins, which also kill neutrophils. All these toxins (PVL, α-hemolysins, PSMs) are produced excessively. Therefore, it can be hypothesized that the greater virulence of USA300 is due to differences in gene expression rather than different virulence mechanisms (DeLeo, Otto, Kreiswirth, & Chambers, 2010; Diep & Otto, 2008). Low cytotoxicity, for example, has been linked to higher mortality in nosocomial pneumonia, which could be due to inability of the host to trigger immune reactions due to lack of antigens (Rose et al., 2015). Studies also show that USA300 has acquired an arginine catabolic mobile genetic element (ACME), coded by the gene *arcA*, from another skin commensal *Staphylococcus epidermidis* (Diep et al., 2006; Diep & Otto, 2008; Thurlow et al., 2013). The ACME element is located next to the *SCCmec* region in the chromosome and studies show, that the physical link between these genes gives USA300 a greater virulence, and thus, a fitness advantage. The location of these two genes in the same mobile element takes away the burden of carrying a resistance gene in a community environment where antibiotics normally are absent (Diep et al., 2008).

Additionally, the ACME element also contains a gene that encodes for SpeG, spermidine resistance factor which participates in skin colonization, but the exact mechanisms of how ACME enhances virulence are yet to be discovered (Boyle-Vavra et al., 2015).

2.2.4 Molecular basis of regulation and biofilm formation of *S. aureus*

2.2.4.1 The quorum sensing system of *S. aureus*

Quorum sensing (QS) is a system for sensing cell-to-cell communication between bacteria and it is based on autoinducing peptides (AIPs), which are short protein fragments produced by the *agr* gene. Detection and production of AIPs gives bacteria information about the cell density of the population in the biofilm and alters the gene expression of a single cell accordingly (Rutherford & Bassler, 2012). The major QS system of *S. aureus* is controlled by the accessory gene regulator (*agrBDCA*) operon, which produces RNAII and RNAIII. The system itself consists of the response regulator AgrA protein and regulatory RNAIII, which affects gene expression post-transcriptionally by binding to mRNA. The *agr* gene also contains the RNAII, which translates into two-component system (TCR) proteins AgrB, AgrC and AgrD, that are needed for the TCR signal transduction (Singh & Ray, 2014). AgrD is the precursor protein for AIPs. The AgrB post-translationally truncates AgrD into ready AIPs while it transports it out of the cell. The extracellular AIPs activate the membrane bound histidine kinase AgrC, which then phosphorylates the cellular AgrA response regulator (Bronesky et al., 2016). Phosphorylation of AgrA leads to transcription of RNAIII, as AgrA binds to the promoter P2 and P3. RNAIII both directly and indirectly activates a variety of different virulence factors while AgrA activates psmα and psmβ translation (Le & Otto, 2015). Additionally, RNAIII inhibits the repressor of toxins (*rot*), which leads to enhanced expression of virulence factors (Mootz et al., 2015). The transcriptional regulator "staphylococcal accessory regulator protein A" (SarA) is a positive regulator of the *agr* system (Figueiredo, Ferreira, Beltrame, & Côrtes, 2017). The σB stress response regulator, encoded by *sigB*, has been found to inhibit *agr* expression in USA300 strain, which leads to reduced expression of exoprotease genes, and thus, a thicker biofilm (Lauderdale, Boles, Cheung, & Horswill, 2009). High glucose concentration in the environment (growth media) downregulates the *agr* system and promotes a thicker biofilm in MRSA, whereas NaCl induces MSSA biofilm formation (O'Neill et al., 2008; Singh & Ray, 2014). The AIPs also mediate signaling in a multispecies biofilm, where it can cross-inhibit *agr* QS systems of other species (Le & Otto, 2015). Virulence factors induced by the *agr* QS sytem are α-hemolysin and bi-component leucocidins PVL and LukED, which are all

pore-forming toxins. The *agr*-controlled Spa protein can inactivate humoral immune response in host by preventing phagocytosis and triggering apoptosis in phagocytes. Other two-component QS systems have not been found to contribute to biofilm formation (Le & Otto, 2015).

2.2.4.2 Bacterial attachment to surfaces

Attachment of bacteria to surfaces is due to hydrophobic interactions of MSCRAMMs. These are bacterial surface proteins and consist of three parts, the binding domain, the cell wall-spanning domain and the domain outside the cell that mediates covalent and non-covalent binding to the extracellular matrix proteins of the host, such as fibronectin and collagen. Clumping factor A, protein A, and fibronectin-binding proteins are important MSCRAMMs of *S. aureus* (Reffuveille et al., 2017). They all contain an LPXTG-motif, which anchors the protein to the cell wall. The anchoring of the proteins is mediated by a sortase enzyme (O'Neill et al., 2008). Typically, covalent binding of bacteria is associated with indwelling medical devices, such as catheters. Generally, the adhesive molecules on the surface of bacteria tend to attach to the ECM molecules of host organism that quickly cover the medical devices after insertion. The non-covalent attachment is supported by autolysins (Atl) produced by a bacterium (Reffuveille et al., 2017). LPXTG-transmembrane motif-containing proteins, such as protein A and SasG, mediate intercellular aggregation. Serine aspartate repeat-containing proteins, a member of MSCRAMM protein family, have been found to participate in adherence (Figueiredo et al., 2017). Attachment to abiotic surfaces has been shown to be mediated by teichoic acids (plastic) and SasX and SasC surface antigen proteins. SasC has been shown to not be involved in attachment to biotic surfaces. Autolysins also seem to have a role in attachment to plastic, however their function is yet unclear (Reffuveille et al., 2017), as well as teichoic acids have been found important during attachment to abiotic surfaces by maintaining the negative net electric charge of the bacterial cell suitable for adhesion. *S. aureus* can adhere to surfaces with a slight negative charge, as van der Waals forces can overcome the repulsion of the negative charges (Gross, Cramton, Tz, & Peschel, 2001).

During attachment to surfaces, sigma factor B (σB), encoded by *sigB*, has also been found to be an important factor. Stress agents, such as nutrient deprivation, activate the *sigB* gene and thus, production of σB, which is a stress response activator protein in bacteria (Lauderdale et al., 2009; Reffuveille et al., 2017). σB upregulates the expression of the genes of adhesive proteins needed in the early stages of biofilm formation, such as fibronectin-binding protein A

(FnBPA), clumping factor (Clf) and coagulase (Coa). Additionally, σB downregulates virulence factors, that are linked to planktonic mode of living, such as toxins and proteases (Archer et al., 2011).

2.2.4.3 Exodus and maturation

After an early biofilm has formed, nuclease activity detaches microcolonies from the biofilm, which then spread to nearby areas. Exodus has a contribution to the biofilm architecture and it is different from the later dispersal phase (Moormeier & Bayles, 2017). As the maturation begins after exodus, *SarA* is upregulated, and it downregulates the thermostable nuclease gene (*nuc).* Downregulation of *nuc* allows the biofilm to mature without disturbance of nuclease or protease activity. When an early biofilm has formed, *sarA* and *agr* regulators inhibit adhesion molecule expression on the bacterial cell surface. In the meantime, virulence factors and immune-avoidance mechanisms are upregulated. For example, Hla coded α-hemolysin secretion shields the biofilm from phagocyting leucocytes (Archer et al., 2011). Autolysin production leads to cell-lysis dependent eDNA release. eDNA is an important structural component in biofilms and essential for biofilm accumulation as it binds biofilm components together during maturation. The more autolysins are produced, the more biofilm is detected (Beltrame et al., 2015). The phenol-soluble modulins (PSMs) have been found to be responsible for the formation of the fluidic channels as well as protease activity in a matured biofilm. The production of PSMs is controlled by the *agr* QS-system, leading to the formation of thick biofilms in strains which lack *agr*-QS (Periasamy et al., 2012).

2.2.4.4 Dispersal of the biofilm

As the biofilm ages, the bacteria grow slowly, and nutrient deprivation upregulates stress responses and downregulates virulence factors, especially pH homeostasis-maintaining systems. Studies have found that in the maturing biofilm, when quorum sensing auto-inducing peptides (AIPs) reach a certain threshold, *agr* is upregulated, which then downregulates expression of cell-wall associated adhesin molecules and upregulates PSM and protease production. PSMs have been found to be responsible for the protease activity, which finally leads to degradation of the biofilm and therefore its dispersal to new surfaces (Archer et al., 2011; Le & Otto, 2015; Reffuveille et al., 2017). However, the *in vivo* effect of proteases in the biofilm dispersal remains to be proven (Le & Otto, 2015). Additionally, *agr* mutant strains have shown to form more solid and smooth biofilms that attach especially well onto plastic

(polystyrene) surfaces, especially in the nosocomial environment (Le & Otto, 2015; Singh & Ray, 2014). Expression of exoproteases is indirectly related to biofilm thickness, as they degrade biofilms. Such proteases are serine proteases (Spl), cysteine proteases (Scpa-B, Sspa and V8) and metalloproteases (Lauderdale et al., 2009).

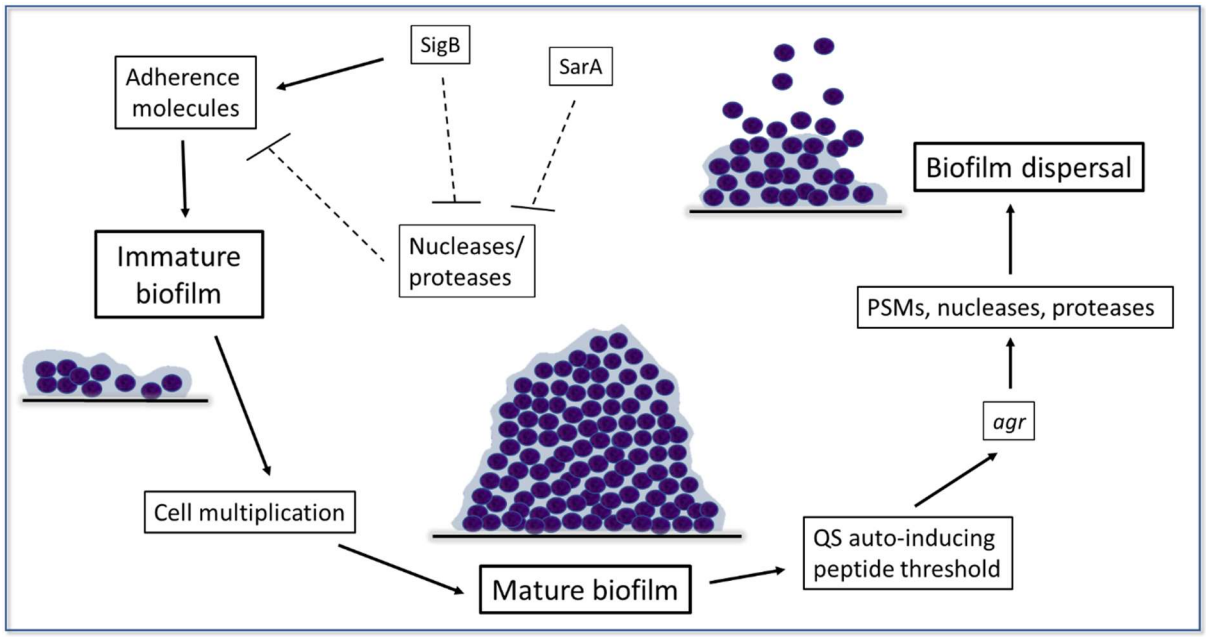

FIGURE 2. The regulation of S. aureus biofilm by agr, sarA and sigB. sarA is staphylococcal accessory regulator gene, agr is accessory gene regulator and sigB is sigmaB (σB). *When the QS auto-inducing peptide threshold is reached, auto-inducing peptides activate the agr gene expression. Protease and nuclease production degrades the biofilm and leads to dispersal. An arrow marks for upregulation and blunt-end arrow with a dashed line marks for inhibition. (According to Archer et al., 2011)*

2.2.4.5 Biofilm types of *S. aureus*

MRSA and MSSA strains form structurally different biofilms, out of which four different types are more well-known. The first type is polysaccharide biofilm formed through an intercellular adhesion operon *icaADBC* and its product polysaccharide intercellular adhesin/poly-N-acetylglucosamine (PIA/PNAG). This biofilm type mostly consists of exopolysaccharides and is common in MSSA strains as well as skin-colonizing *S. aureus* strains. The second form of a biofilm is a protein/eDNA-biofilm, in which the outer membrane proteins FnBP and BAP and extracellular DNA enhance accumulation of bacteria into a biofilm. Lysed cells also act as components of the biofilm (Zapotoczna et al., 2016). The *mecA* coded PBP2a is known to be associated with FnBP-type biofilm formation, proposedly due to upregulated protease activity (McCarthy et al., 2015). The third is a fibrin-coated biofilm which works through Coa or vWF and it is promoted in niches where the bacterium must hide from the host defense mechanisms,

such as blood. The fourth biofilm is a so-called amyloid biofilm, which is accumulated by phenol-soluble modulins (Zapotoczna et al., 2016), which are known to assist with accumulation and dispersal of the biofilm (Periasamy et al., 2012).

2.2.4.5.1 PIA-dependent biofilm formation

Currently, two pathways of biofilm formation in *S. aureus* are characterized. The first biofilm formation pathway is the *icaADBC* operon, that codes for polysaccharide intercellular adhesin (PIA), which was first discovered in *Staphylococcus epidermidis* (Arciola, Campoccia, Ravaioli, & Montanaro, 2015). The pathway is depicted in figure 3. The *icaADBC* operon consists of four genes and is regulated by the global transcriptional regulator SarA. In *S. aureus,* it affects the expression of about 120 genes either positively or negatively (O'Gara, 2007). The *icaA* gene, that codes for a transmembrane enzyme with N-glucosaminyl transferase activity, is required for synthesis of PNAG. The *icaD* gene is needed for synthesis of polymers longer than 20 residues and must be co-expressed with *icaA*. The product of *icaC* translocates PNAG to the outer surface of the bacterial cell wall and the *icaB* product deacetylates PNAG. Deacetylation is required for structural formation of the PNAG and is necessary in polysaccharide biofilms (Arciola et al., 2015). The *icaADBC* expression is downregulated by transcriptional regulators IcaR and TcaR. *icaR* is located upstream of the *icaADBC* gene. *icaR* has been found to be downregulated by Rbf transcriptional regulator. LuxS two-component system has been shown to increase PIA production notably, but its function might only be due to basic metabolism rather than regulation (Le & Otto, 2015). Rbf and TcaR regulate relatively few genes when compared to global transcriptional regulators σB and SarA (Cue, Lei, & Lee, 2013). However, PIA/PNAG mediated biofilms are typically found in MSSA strains, but not always in MRSA strains, in which the biofilm formation occurs also independent of PIA (McCarthy et al., 2015). PIA has been found responsible for the positive net charge within the biofilm matrix, but it also has zwitterionic properties due to positively charged N-acetylated and negatively charged succinate residues in its structure. The zwitterionic properties play a role in adhesion to artificial surfaces, intercellular aggregation and resistance to cationic antimicrobials. (Rohde, Frankenberger, Ahringer, & Mack, 2010)

2.2.4.5.2 PIA-independent biofilm formation

The formation of PIA-independent biofilm is less-well known than the PIA-dependent pathway, but a few proteins have found to be essential for this type of biofilm formation. In *icaADBC*

deletion studies it was found that the MSSA strain was not able to produce a biofilm (Heilmann et al., 1996), whereas an MRSA strain with *ica* mutation was (Fitzpatrick, Humphreys, & O'Gara, 2005). The PIA-independent biofilm is also known to rely on LPXTG-anchored surface proteins (MSCRAMMs) FnBPs, eDNA and teichoic acids as its building components, yielding a proteinaceous biofilm (Arciola et al., 2015). This biofilm type has also been shown to be preferred when the *mecA* gene is present in the bacteria (Pozzi et al., 2012). Also, without *ica*, the Staphylococcal Protein A (Spa) was found to be crucial for biofilm formation. In *spa* deletion containing bacteria an exogenous addition of the *spa* gene restored biofilm development, which means that, despite it being cell wall-associated, the protein need not be incorporated into the cell wall (Archer et al., 2011). Fibronectin-binding proteins (FnBPA and FnBPB) are suggested to participate in the accumulation of a biofilm through autolysin (Atl) and *sigB* regulation (McCarthy et al., 2015). Finally, Biofilm associated proteins (Bap) and related proteins were found to take part in biofilm production by cell-to-cell aggregation. Bap and *S. aureus* surface protein C (SasC) are associated with adherence to plastic. Overall, protein-mediated biofilms tend to form less thick biofilms than PIA (Archer et al., 2011; McCarthy et al., 2015). The PIA-independent biofilm formation pathway is depicted in figure 3.

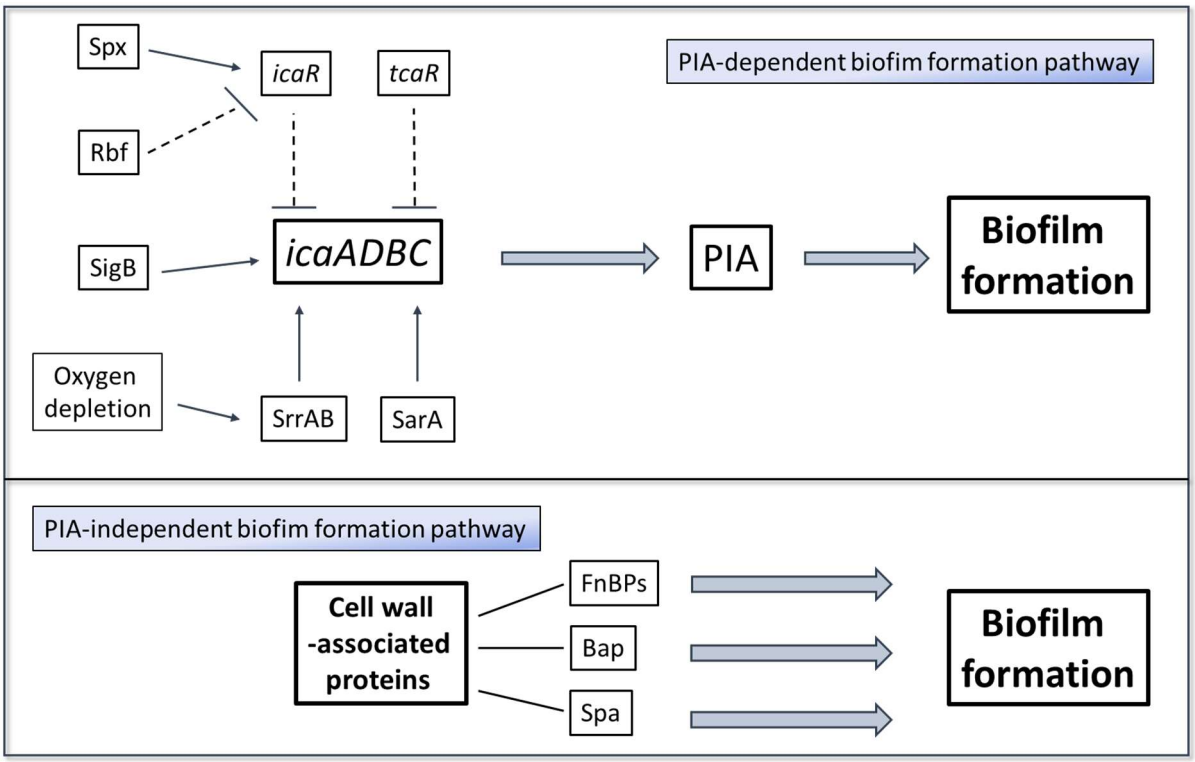

FIGURE 3. Biofilm formation pathways of S. aureus*. icaR, intracellular adhesion regulatory gene, which inhibits icaADBC expression, is regulated by Rbf and Spx proteins. An anoxic (O2=oxygen) environment upregulates SrraAB, the staphylococcal respiratory response regulator two-component system and leads to biofilm production. tcaR is a transcriptional regulator of the teicoplanin-associated locus and inhibits biofilm formation. Cell wall-associated proteins: S. aureus protein A (Spa), fibronectin-binding proteins (FnBPs) and biofilm-associated protein (Bap). SigB (σB) and SarA are global regulatory factors and promote biofilm formation in some strains. Arrow means upregulation and blunt-end arrow means downregulation of the gene expression. (According to Archer et. al., 2011 and Cue et al., 2009)*

2.2.4.6 Antibiotic resistance in the *S. aureus* biofilm

A bacterial biofilm can resist 1000-fold doses of antibiotics compared to its planktonic counterparts (Arciola et al., 2015). The antibiotic resistance in this case is not only due to antibiotic resistance genes, but also environmental factors and changes in metabolism. Biofilm formation is a method for *S. aureus* to resist antibiotics by a physical barrier which prevent the antibiotic from reaching bacteria and by diluting the antibiotic concentration close to the bacterial niche (McCann, Gilmore, & Gorman, 2008; McCarthy et al., 2015). It is also hypothesized that ions and components of the glycocalyx might bind or neutralize antibiotics (Figueiredo et al., 2017). In stress conditions, such as an antibiotic treatment, bacteria of the biofilm of *S. aureus* can slow down their growth, the metabolism, to prevent the antibiotic from working. A small part of the bacterial cells (<1%) in a biofilm can become dormant and thus practically become metabolically inactive, persister cells, which prevents the antibiotic from functioning as antibiotics mainly interfere with the metabolism of the bacteria. Persister cells

can later restart their metabolism and start a biofilm anew (McCann et al., 2008). The extreme microenvironment within the biofilm can inactivate the antimicrobials, such as macrolides, aminoglycosides and tetracyclines. The inhospitable environment is due to acidic pH, pO2, pCO2, divalent cation concentration (Mn^{2+}, Ca^{2+}), pyrimidine concentration and the level of hydration (Dunne, 2002; McCann et al., 2008).

2.3 The *bursa aurealis* transposon library

Transposon mutagenesis means inserting a transposable element into a genome of the studied organism, in which it will cause a disruption of a gene, a knockout gene. It is a particularly effective method to use for genome query of nonessential genes involved in virulence mechanisms, antibiotic resistance, growth and biofilm formation. Ideally, from a transposon library it is possible to find entire pathways involved in fitness strategies of bacteria (Bae, Glass, Schneewind, & Missiakas, 2008; Fey et al., 2013).

The *bursa aurealis* transposon library has been constructed to study biofilm formation and gene expression in the UAS391 *S. aureus* strain. The transposon *bursa aurealis* (size 2.3 kb) was chosen, as it causes a random mutation into the genome because it does not have sequence preference, unlike *Tn917* which is also used for transposon mutagenesis (Bae et al., 2004). The library was generated by inserting *HimarI*, a *mariner* family transposable element, *bursa aurealis*, thereby inactivating a random gene of USA300–UAS391 Ery^S *S. aureus* strain. UAS391 Ery^S is a plasmid-cured strain derived from the wild type USA300–UAS391 *S. aureus*. The plasmids were eliminated to prevent integration of the transposon into them, as well as to eliminate the erythromycin resistance from the strain (Bae et al., 2008). Mariner transposable elements are a group of transposons of insects; *Himar*1 is present in *Haematobia irritans* (horn fly) (Lampe, Churchill, & Robertson, 1996).

The transposon knockout strains were created by introducing plasmids pBursa (see figure 4.) and pFA545 into the UAS391 Ery^S *S. aureus* strain. The pBursa transposable element *bursa aurealis* contains *mariner* terminal inverted repeats (TIR), erythromycin resistance gene *ermC* (codes for an rRNA methylase), a promotorless *gfp* from *Aequorea victoria*, origin of replication (*oriV*) and *Bam*HI and *Aci*I restriction sites. If the transposon incorporates into the genome, erythromycin sensitive strains becomes resistant due to the *ermC* carried by the transposon and erythromycin resistance can then be used as a selective marker. The pFA545 codes for the *Himar1* transposase, which integrates the transposable element to the chromosome. In total, the library consists of 1920 mutant strains, which are knockouts in non-

essential genes. The position of the transposon can be determined via the *Bam*HI and *Aci*I restriction sites of the insert using inverse PCR and subsequent sequencing. In inverse PCR, the insert is first digested from *Bam*HI and *Aci*I sited, ligated into circular DNA fragments and then amplified with PCR by using primers that recognize the transposon sequence. After PCR, the fragments can be Sanger-sequenced and identified by bioinformatics tools (Bae et al., 2008) (such as nucleotide BLAST [www.blast.ncbi.nlm.nih.gov, access date 15.2.2017]). A similar transposon library is for example the Nebraska transposon mutant library (NTML) in *S. aureus* JE2. To date, the sequence of USA300-UAS391 is annotated (accession number CP007690.1) but also to the sequence of USA300_FPR3757 strain (accession number NC_007793.1), which is the closest clonal lineage to UAS391 that is annotated. The corresponding gene can be identified from the GenBank® (https://www.ncbi.nlm.nih. gov/genbank/, access date 15.2.2017).

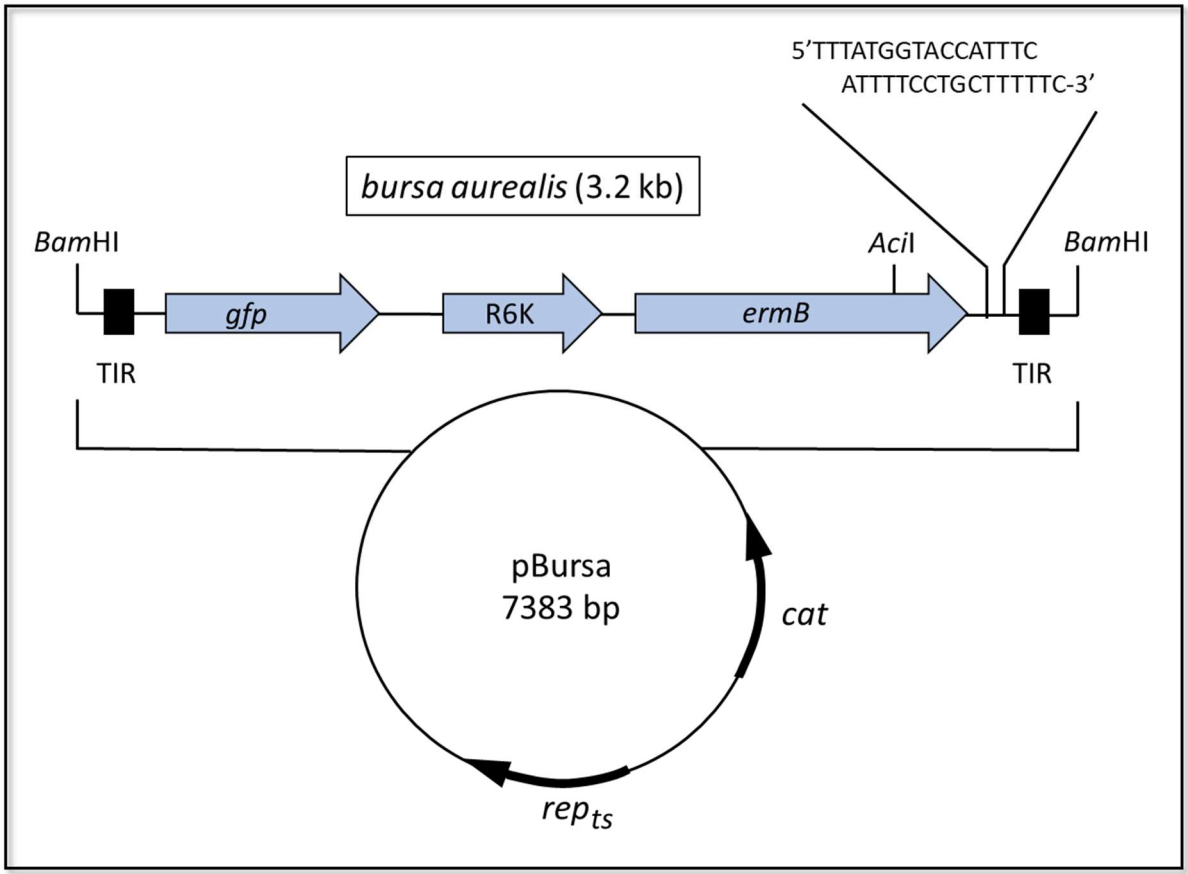

FIGURE 4. Map of plasmid pBursa. *Bursa aurealis, a mini-mariner transposable element, was cloned into pTS2, with a temperature-sensitive plasmid replicon (rep_{ts}) and chloramphenicol-resistance gene cat to generate pBursa. Bursa aurealis contains mariner terminal inverted repeats (TIR), R6K replication origin (oriV), green fluorescent protein gene (gfp), and erythromycin-resistance gene ermC (Bae et al., 2008).*

3 RESEARCH HYPOTHESIS

USA300-UAS391 in particular has been proven to be a prolific biofilm producing strain (Vanhommerig et al., 2014), and is an increasingly prevalent causative agent for skin and wound infections both in hospitalized patients and healthy people. By screening a random mutation library of USA300, it is possible to find non-essential genes that are involved in biofilm formation. The change in biofilm formation can be detected with a series of experiments that characterize the phenotype of the biofilm in relation to the non-mutated strain. By characterizing new genes involved in biofilm formation it could be possible to find new therapeutic targets for curing MRSA infections.

Prior to characterizations made for this study, a screening of the transposon mutant library was done. In total, 1920 strains were screened for their biofilm formation by a static biofilm assay, growth curve analysis and antibiotic susceptibility testing. The screening revealed around 250 mutants displaying either an increase or decrease in formed biofilm mass compared to the parental strain. The disrupted genes were identified by inverse PCR (as described on section 2.2.) and sequencing.

TABLE 1. The genes selected for characterization.

Strain	**Disrupted gene**	**Knockout gene name**
Tn0002	HAD-superfamily hydrolase, subfamily IA, variant 1	***ΔHAD***
Tn0007	non-coding region	***ΔNCR***
Tn0123	non-ribosomal peptide synthetase	***ΔausA***
Tn0428	Oligopeptide ABC transporter substrate-binding protein	***ΔoppA***
Tn1354	Clumping factor B	***ΔclfB***
Tn1433	cytosol aminopeptidase	***ΔampA***
Tn1732	CDP-diacylglycerol--glycerol-3-phosphate 3-phosphatidyltransferase	***ΔpgsA***

This thesis aimed to perform an in-depth analysis on seven mutants (table 1) of the *bursa aurealis* transposon library, focusing on the biofilm formation process. These mutants were selected based on their significantly altered biofilm formation capacity during the preliminary screening and on the mutated gene. None of the genes had earlier reports in literature about being associated with biofilm formation, except for clumping factor B. Moreover, knocking out several of these genes also resulted in a change in antibiotic susceptibility, suggesting an

interlinkage between antibiotic resistance and biofilm formation. First, results of the initial screening were reconfirmed by repeating biofilm formation assays, growth rate determinations and antibiotic susceptibility tests. Next, the seven mutants were studied using more specialized techniques, such as epifluorescence microscopy, real-time reverse transcriptase PCR (real-time RT-PCR) and transduction. Real-time RT-PCR was performed to study expression of the transposon-targeted gene in the mutants compared to the wildtype parent. Finally, transduction was performed in erythromycin-cured UAS391 and TCH1516 (USA300 lineage).

In short, the project consists out of two main objectives:

1. To characterize both biofilm formation and structure under static and dynamic conditions.
2. To confirm the disrupted gene involvement in biofilm formation by φ11 bacteriophage transduction.

4 MATERIALS AND METHODS

4.1 Culturing transposon strains

Media composition and corresponding preparation, as well as basic solutions used in this study are described in appendix II. For the transduction experiments, the phage plates and broths were provided by the VUB, which are as well described in appendix II. The broth used in culturing the transposon strains contains glucose, since it is known to induce biofilm formation (O'Neill et al., 2008). The list of all the *Staphylococcus aureus* strains used is given in table 2.

TABLE 2. S. aureus strains used for experiments in this study.

Bacterial strain	Characteristics	Experiments
ATCC 6538	*Staphylococcus aureus* subsp. *aureus* Rosenbach, positive control for biofilm formation	Static assay, growth curve
S. aureus 5374	*Staphylococcus aureus* strain known to not produce biofilm (Vanhommerig et al., 2014), negative control for biofilm formation	Static assay, growth curve
USA300–UAS391	Wild-type MRSA strain isolated from an abscess of a patient in a Belgian hospital (Vanhommerig et al., 2014), wild-type control strain	Static assay, growth curve, confocal microscopy, disk diffusion, MIC testing
USA300–UAS 391 Ery^S	Plasmid cured strain of the wild-type USA300–UAS391, the parental strain of the transposon mutated strains	Static assay, growth curve, confocal microscopy, disk diffusion, MIC testing, transduction with ϕ11 bacteriophage
ATCC 25923	CLSI recommended control strain for disk diffusion test. It is a *S. aureus* strain with no β-lactamase activity nor *mecA* gene (CLSI, 2014)	Disk diffusion
ATCC 29213	CLSI recommended *S. aureus* control strain for MIC testing (CLSI, 2014)	MIC
TCH1516	Texas Children's hospital USA300 clinical isolate associated with sepsis. The whole-genome map is identical to that of UAS391 (Sabirova et al., 2014).	Transduction with ϕ11 bacteriophage

All overnight incubations of transposon strains were done on BHI agar plates containing 5 µg/ml erythromycin to maintain the inserts within the strains. Subculturing of the UAS391 and UAS391 Ery^S parental strains was done on horse blood agar plates. All the overnight incubations were done in +37°C for 16–20 hours in aerobic conditions (Incubator: Heratherm™

Advanced protocol Microbiological Incubator, Thermo Fisher Scientific Inc.) without shaking. The planktonic cells were grown in a shaking incubator (MaxQ 6000, Thermo Fisher Scientific Inc.) at 250 rpm, at +37°C for 16–20 hours in aerobic conditions. For over-the-weekend incubations a programmable incubator was used (BK 6160, Thermo Fisher Scientific Inc.), which keeps the strains at +4°C for 48 hours and then raises the temperature to +37°C for 16 hours to obtain a fresh culture on Monday. When adjusting the McFarland (McF), a Phoenix Spec™ nephelometer (Becton-Dickinson) was used to measure the turbidity of the cell suspension. For vortexing, Vortex-Genie 2T (Scientific Industries) was used.

4.2 Biofilm formation assays

4.2.1 The static biofilm – Crystal violet assay

In the static assay, biofilm formation was quantified on a 96-well flat-bottomed polystyrene microplate (Cellstar® by Geiner Bio-One) in which the bacteria form a biofilm on the bottom of the well (O'Toole, 2011). The bacteria are grown without a flow or a supply of fresh nutrients. A 0.5 McF suspension (+/- 10%) was made into BHI broth with 0.1 % D-glucose. Of the inoculum, 20µl was added on a 96-well microplate with 180µl of fresh BHI broth. Three replicate plates were cultured. After 24 h incubation in aerobic conditions in +37 °C, the wells were gently washed thrice with 200 µl of PBS and fixed with 150µl of methanol for 20 minutes, after which these were air dried. The samples were then stained with 150µl of Hucker's crystal violet (2%) for 15 minutes and gently rinsed with running water, followed again by air drying. The dye was eluted with glacial (33%) acetic acid for 30 minutes. The amount of biofilm was measured with a Multiskan™ FC Microplate Photometer (Thermo Fisher Scientific Inc.) at a wavelength of 492 nm.

The biofilm forming capacity was compared to the parental strain UAS391 Ery^S. Static assay raw data was brought in Excel where the average and standard deviation were calculated. All plates were done as triplicates and on each plate and there were quadruples of each mutant strain. In total, 24 measurements for each strain were made. For the blank and the control strains there were 144 measurements, since they were tested on each plate. Strains that showed reduced or increased biofilm formation compared to the parental train UAS391 Ery^S were selected for inverse PCR. The formed biofilm mass in relation to the parental strain was calculated with MS Office Excel.

The static biofilm assay was also used for fluorescence microscopy. The protocol is the same as described, but instead of fixing and staining with crystal violet, the biofilm was stained with

150µl of 1µmol/ml SYTO™ 9 Green-Fluorescent nucleic acid stain (Invitrogen, Thermo Fisher Scientific Inc.).

4.2.2 The dynamic biofilm experiment

The dynamic assay was performed with the Bioflux™ shear flow system (Fluxion Biosciences Inc.), in which a biofilm is grown under fresh flow of nutrients.

For the dynamic assay, a 0.5 McF inoculum of bacteria in BHI broth with 0.1% D-glucose was made and diluted 1:10 to obtain 0.05 McF. On the Bioflux™ 200 plate, 150µl of medium was pipetted to the input well and the plate was attached to the interface and connected to the electropneumatic pump. The pressure was run from input to output well with 5 dyne/cm^2 until bottom of the output well was filled. Then, 85µl of bacterial inoculum was added to the output well and run with a backward flow of 2 dyne/cm^2 for three seconds. The bacteria were let to attach to the tube between the interconnected wells for one hour on the +37°C heating stage. After incubation, 1ml of fresh media was added to the input wells. The plate was incubated overnight at 37°C, with a continuous 0.5 dyne/cm^2 flow, for 16–17 hours. After incubation, media was changed by first emptying the output wells, followed by the input wells. Next, 400µl of media and 1µl of SYTO™ 9 Green-Fluorescent nucleic acid stain (Invitrogen, Thermo Fisher Scientific Inc.) was added to input well then. To stain the biofilm, the flow was run for 10 minutes at 0.5 dyne/cm^2. Figure 5B shows the channel between the input and output wells as well as the viewing channel where both the fluorescence and confocal laser-scanning microscopy images were taken. The viewing channel is the region of laminar flow within the plate. A picture of the Bioflux™ system is represented in Figure 6. The visualization of biofilms was done with a fluorescence microscope. The method is explained in detail in section 4.2.3. Figure 5A depicts the shear flow system of the plate.

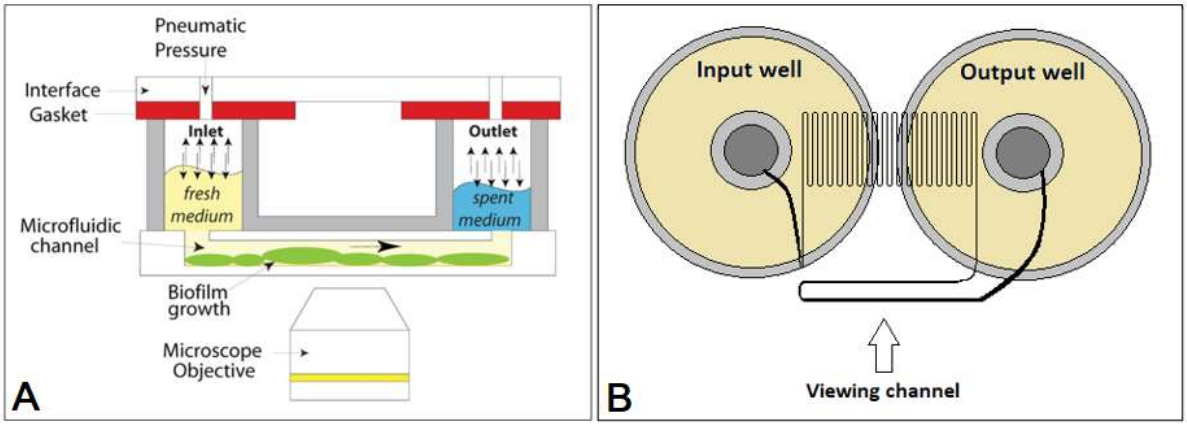

FIGURE 5. A. The shear-flow system of a Bioflux™ plate. *Fresh medium flows through the channel between the inlet and outlet wells bringing a constant flow of fresh nutrients to the biofilm. (Benoit, Conant, Ionescu-Zanetti, Schwartz, & Matin, 2010)* ***B. The structure of the Bioflux™ wells.*** *Fresh media (yellow) flows from input to output well. Biofilm grows inside the viewing channel, which can be stained and be looked under a microscope.*

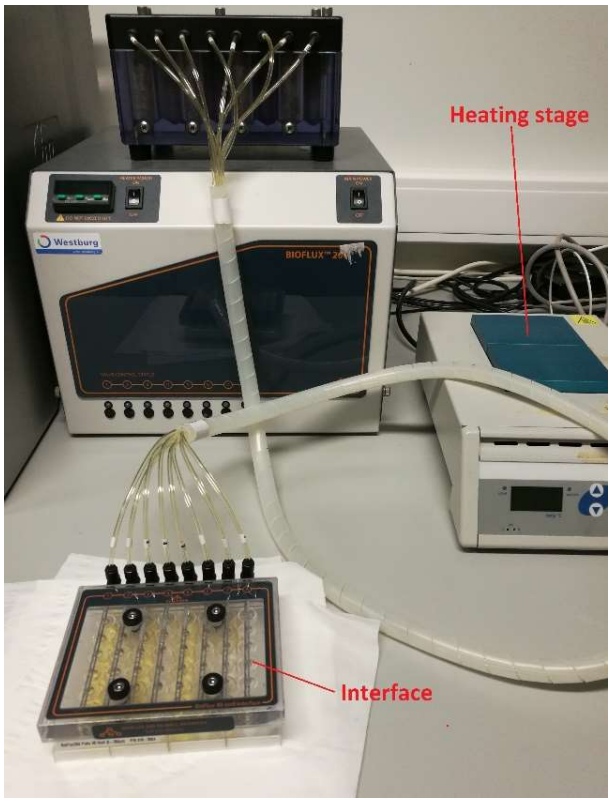

FIGURE 6. The Fluxion Bioflux™ 200 system for growing a biofilm with a constant flow of nutrients. *The interface attaches to the 48-well plate on which the biofilms grow. The electropneumatic pump pressurizes the wells and causes a shear flow system. Fresh media flows into the channel between the wells where the biofilm grows. The biofilm is stained and then observed under a microscope. (Photo: K. Holappa)*

4.2.3 Epifluorescence microscopy

Fluorescence microscopy is based on the phenomenon, in which a higher energy (smaller wavelength) light (a photon) is absorbed by an indicator, and some of the absorbed energy is then emitted as another photon of a lower energy (bigger wavelength). This emitted energy, a photon, is fluorescence. The goal is to separate the excitation light from the emitted light, which can be done with different types of filters, depending on the lasers and fluorochromes used

(Sanderson, Smith, Parker, & Bootman, 2014). With fluorescence microscopy it is possible to visualize much more details than with bright-field microscopy, whose resolution relies only on density differences within the sample. However, three-dimensional structures cannot be visualized with the basic fluorescence microscope, an epifluorescence microscope.

The selected strains were first grown as described in the dynamic biofilm assay (4.2.2) and then imaged tested with a dynamic assay, in which the biofilm is grown under a constant flow of nutrients and then stained with SYTO®9 Green-Fluorescent nucleic acid stain by Invitrogen™ (Thermo Fisher Scientific Inc.), which is a DNA probe which binds to DNA of both living and dead cells. Then, the biofilms were imaged with Observer.Z1 (Carl Zeiss™ GmbH) epifluorescence microscope with a camera (AxioCam MRm, Zeiss) attached to it. A compatible software by ZEN (Zeiss Efficient Navigation®) pro 2012 was used to maneuver the microscope and to formulate the images. An objective of 40 000-fold magnification with immersion oil was used. An image of the biofilm was built of 84 separate tiles (small pictures) of one µm², which covered the whole viewing channel. An example of such a picture is figure 7. For each picture, the intensity was set to "best fit" in the Zen program. ImageJ 1.51j8 software (Image Processing and Analysis in Java, downloaded from: https://imagej.nih.gov/ij/, access date:15.2.2017), was used to analyze integrated densities, the number of pixels, in the images to calculate the area covered by biofilm. Default "Color threshold" algorithm was used to analyze the integrated densities of the biofilms. Because the epifluorescence microscope only takes an image of a certain layer but not depth of the target, it cannot be used to estimate volumes. The microfluidic channel is 30 µm tall and 350 µm wide and it is made of polydimethylsiloxane.

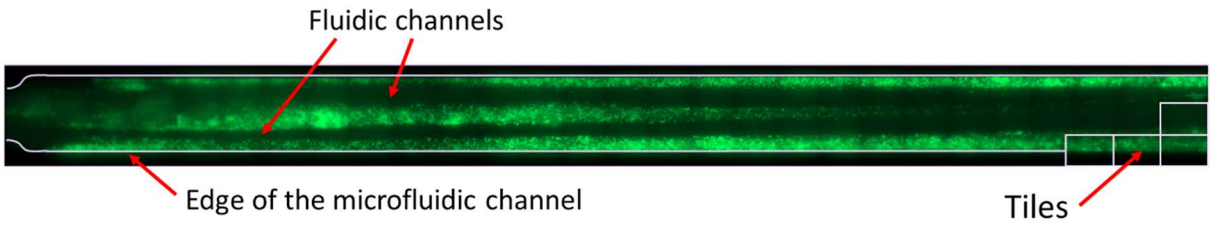

FIGURE 7. How to look at the epifluorescence microscopy pictures. *The black that is left outside (upper and lower part of the image) is outside of the microfluidic channel. The green marks for the biofilm (live and dead cells) and the brighter the fluorescence, the more cells are present. Black parts inside the microfluidic channel are either fluidic channels within the biofilm, exopolysaccharide parts of the biofilm or an area without cells. Edges of tiles might be visible in some pictures, they should not be mistaken for fluidic channels. Examples of tiles are marked with white boxes on the right.*

4.3 Characterization of growth

Growth curves were used in the screening of the transposon library to look for pleiotropic effects caused by the mutation and to test the growth speed of the mutant and transduced strains. In this assay, the transposon mutant strains are compared to the parental strain and the wild-type strain to see if the mutation has changed the growth capacity. Growth curves were measured from all the the seven selected mutant strains as well as the transduced strains on both backgrounds (THC1516 Ery^s and UAS391 Ery^s).

In the growth curve experiment, an overnight culture was made into a 0.5 McF suspension (+/- 10%) into BHI broth with 0.1% D-glucose and 20µl of the inoculum was added on a 96-well flat-bottomed polystyrene microplate (Cellstar® by Geiner Bio-One) with 180µl of fresh BHI broth (O'Toole, 2011). During 24h incubation at +37°C, optical density at a wavelength of 600 nm (OD_{600}) of the culture was measured every 15 minutes (96 measurements in total) with kinetic turbidometric measurements with the Multiskan™ GO Microplate Spectrophotometer (Thermo Fisher Scientific Inc.) device and applicable SkanIt™ software. The bacteria were grown without a flow or fresh nutrients and in background shaking to prevent biofilm formation.

Quadruple samples were made of each mutant strain. A growth curve was drawn with MS Office Excel from the OD_{600} values to illustrate the growth speed of each strain compared to the wild-type. The growth rates were calculated according to Hall et. al, with a command prompt based GrowthRates software by Hall B., downloaded from a website https://sourceforge.net/ projects/growthrates/ (access date 15.11.2017). The program calculates the increase of OD_{600} per minute at a logarithmic phase of growth, as well as the efficiency of the curve (R^2) and the maximum OD_{600} that the sample reaches (Hall, Acar, Nandipati, & Barlow, 2014). Default settings of the software were used.

4.4 Antibiotic susceptibility testing

All the seven mutant strains that showed altered biofilm forming capacity were tested for their minimum inhibitory concentration (MIC), the smallest concentration of antibiotic that inhibits the growth. MIC was tested to see whether the insertion of the transposon had caused pleiotropic effects to the mutants. MIC testing was done with commercially available e-tests according to the CLSI guidelines for MIC testing (CLSI, 2014). A list of the MIC strips used is on table 3. The MIC was determined by streaking 0.5 McF bacterial suspension on the whole surface of

Müller-Hinton agar plate and an e-test strip was added on top of the agar (see figure 8.) and then incubated at +37°C for 16–20 hours (CLSI, 2014).

TABLE 3. The e-tests used to determine the minimum inhibitory concentration.

ETEST® BioMérieux, France	Range µg/ml
Chloramphenicol (C)	0.016 - 256
Gentamicin (GM)	0.016 - 256
Ciprofloxacin (CIP)	0.002 - 32
Benzylpenicillin (P)	0.016 - 256
Erythromycin (E)	0.016 - 256
Cefoxitin (FOX)	0.016 - 256
Tetracycline (TE)	0.016 - 256
Clindamycin (CC)	0.016 - 256
Trimethoprim-sulfamethoxazole (SXT)	0.002 - 32

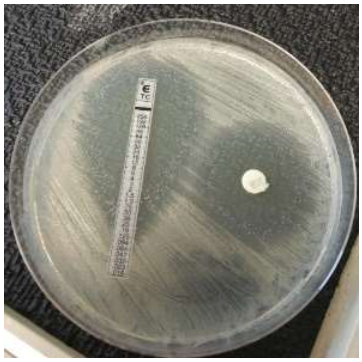

FIGURE 8. An e-test on the left and a disk diffusion test on the right. *The e-test result is read from the point where the bacterial mass meets the test strip. The disk diffusion result is the diameter of the inhibition zone around the disk. The disks were used in the screening and they are on the same plate in the image for demonstration. (Photo: K. Holappa)*

4.5 Determination of gene expression by using RT-PCR

4.5.1 Principles of reverse transcriptase polymerase chain reaction

Reverse transcriptase polymerase chain reaction (RT-PCR) is a highly developed PCR method for detecting mRNA levels in the cells, which is first converted to complement DNA (cDNA) using a reverse transcriptase enzyme. It can be used for mRNA quantification as well as comparing expression levels (relative expression level) of a treated/mutated and the original gene. Compared to traditional PCR, the amplification of the DNA fragment is measured after each cycle, which enables precise quantification of the starting material.

RT-PCR is based on the same idea as traditional PCR with denaturing, annealing and extension phases, but it is equipped with a fluorescent probe. Quantification of the initial DNA is possible because of a DNA probe, which contains a green fluorescent dye and a red quencher dye. The

quenching mechanism is based on a FRET (fluorescence resonance energy transfer) phenomenon. The green light (fluorescent dye) has a smaller wavelength than red light (the quencher) and when they are near each other, FRET occurs. The excitation of the green dye causes the green emission energy to be transferred to the red dye. However, when the probe integrates to the target DNA, the polymerase 5' activity excises the probe and the red and green dye are released into the reaction mix. The green dye and the quencher are no longer next to each other and FRET cannot occur. Therefore, the green reporter dye will no longer be quenched and the increased green fluorescent signal can be detected (Life technologies, 2014).

In this study the $2^{-\Delta\Delta Ct}$ method is used for comparing gene expression levels between samples by relying on regular expression of the housekeeping gene *gyrB*. The result, the fold-difference, tells the difference of expression in relation to the non-mutated gene. Gyrase B has been validated as a good normalizer gene for *S. aureus* for example by Sihto et. al (Sihto, Tasara, Stephan, & Johler, 2014), and in other species as well (Crawford, Singh, Metcalf, Gibson, & Weese, 2014; Wen, Chen, Xu, & Sun, 2016), and was therefore chosen.

The fold difference $2^{-\Delta\Delta Ct}$ is derived followingly:

$Ct_{GOI}^{s} - Ct_{norm}^{s} = \Delta Ct_{sample}$

$Ct_{GOI}^{c} - Ct_{norm}^{c} = \Delta Ct_{calibrator}$

$\Delta Ct_{sample} - \Delta Ct_{calibrator} = \Delta\Delta Ct$

Fold difference $= 2^{-\Delta\Delta Ct}$

A negative ΔΔCt is a decreased transcription of the gene of interest (GOI) and a positive ΔΔCt is an increased transcription of the gene of interest (Life technologies, 2014). A fold difference <1 indicates less expression of the gene of interest than the wild-type (calibrator) and a fold difference >1 indicates elevated expression compared to the wild-type (Livak & Schmittgen, 2001). Standard curves were measured for each gene as a control for the efficiency of the reaction but were not used in calculations.

When running the PCR, a real-time amplification plot is drawn. An example of an amplification plot is in figure 9. Threshold is a value set to distinguish statistically significant amplification of the fluorescence from the background fluorescence, which is called the baseline. Therefore, the amplification cycle, when the DNA amount (fluorescent signal) rises above the threshold value, it is considered relevant amplification and is therefore called the threshold cycle, $\mathbf{C_t}$. The

software of the PCR instrument usually sets the threshold at 10 times the standard deviation, but it can be set manually as well. C_t values can be used to calculate the amount of starting material, because it is inversely related to the starting amount of the target gene (Life technologies, 2014).

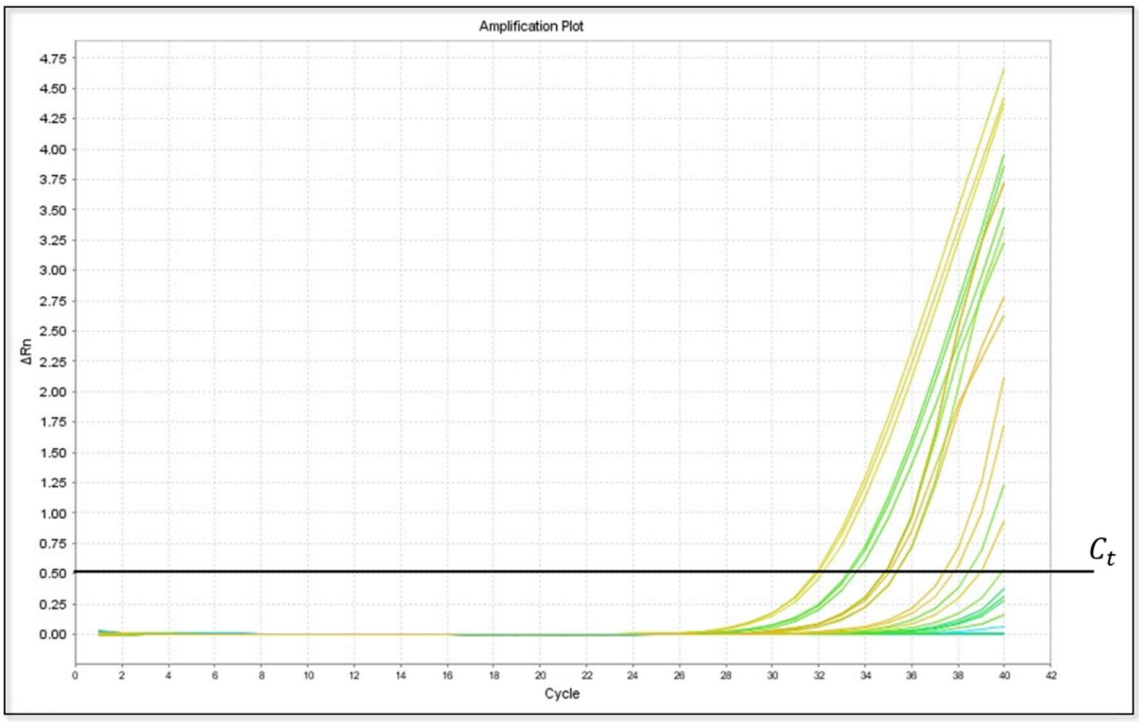

FIGURE 9. Example of a linear amplification plot. *The fluorescent signal above C_t threshold is considered significant.*

At the end of the run, a melt curve analysis was done to exclude a chance of non-specific as well as primer dimer amplification during the PCR run (Life technologies, 2014).

4.5.2 The protocol for real-time RT-PCR

4.5.2.1 Collecting planktonic cells

Each studied strain was inoculated to 15 ml of BHI broth with 0.1 % D-glucose and incubated with shaking 250 rpm at +37 °C for 3 hours. OD600 was measured and the McF was adjusted to 0.5. The cultures were incubated for 24 h shaking 250 rpm at +37 °C. The cells were pelleted with full speed in a centrifuge and the supernatant was discarded. On the pellet, 2ml of RNA protect was added, and the sample was homogenized by vortexing. One milliliter of the suspension was transferred into a 1.5ml microcentrifuge tube and incubated at room temperature for 5 minutes. The samples were vortexed and then pelleted at 5000 x *g* for 10

minutes at +4 °C (Eppendorf™ Centrifuge 5430 R). All the supernatant was removed, and the samples was stored at -80 °C for the RNA preparation.

4.5.2.2 Collecting biofilm cells

On a 20cm diameter polystyrene petri dish 5ml of 1 McF inoculum solution of each strain, and 95 ml of BHI medium with 0.1% D-glucose was added and incubated for 24h at +37°C. The media was carefully removed and 2ml of RNA protect was added on the dish. The biofilm was scraped off with a glass triangle. Into two 1.5 ml microcentrifuge tubes, 1ml of the suspension was pipetted. Samples were incubated at room temperature for 5 minutes. The samples were homogenized by vortexing and centrifuged at 5000 x G for 10 minutes at +4°C (Eppendorf™ Centrifuge 5430 R). All the supernatant was removed, and the sample was stored at -80°C for the RNA preparation.

4.5.2.3 Bacterial lysis and RNA preparation

Total RNA was extracted from both biofilm and planktonic cells. RNA extraction was done with Qiagen® RNeasy™ Minikit. The required solutions are listed on table 4.

TABLE 4. The reagents needed for bacterial lysis and RNA extraction in addition to the buffers provided by the kit.

Solutions	Contents
Biofilm cells	TE buffer with 5 mg/ml lysostaphin + 20 mg/ml lysozyme (Enzymes: Sigma Aldrich)
Planktonic cells	TE buffer with 1 mg/ml lysostaphin + 20 mg/ml lysozyme
TE buffer	1.211g Tris (10 mM), 0.372g EDTA (1mM), 1L milliQ water, set to pH 8.0 and then autoclaved
RTL with β-mercaptoethanol	10µl β-MEtOH per 1ml of buffer RTL (RNeasy® Minikit, Qiagen)

The samples were thawed at room temperature before 200µl of TE buffer with lysozyme and lysostaphin (concentrations mentioned in table 4.) and 20µl of Proteinase K (Invitrogen) was added to the samples. Samples were resuspended and vortexed for 10 seconds and incubated at RT for 10 minutes with shaking. Of the lysate, 5µl was taken and added to 1500µl RLT buffer containing 1:100 β-MEtOH and vortexed for 10 seconds. One milliliter of the suspension was

transferred to a Safe-lock tube containing glass beads (Lysing Matrix B, MP Biomedicals). Bacteria were homogenized with FastPrep instrument (MP Biomedicals) twice for 40 seconds with an intensity of 5.5 and with a 5-minute incubation on ice in between the runs. The samples were centrifuged at 13 500 x G for 10 minutes at 4 °C. Supernatant was transfer into a new microcentrifuge tube. 1300µl of 80% EtOH was added to the supernatant and mixed by pipetting. Then, 700µl of the lysate was transferred to RNeasy Mini spin column and the column was centrifuged for 15s at 12 000 x G. Flow-though was discarded and another 700µl of lysate was added to the column. 350µl of Buffer RW1 was added to the RNeasy Mini spin column and centrifuged for 15s at 12 000 × G, after which flow-through was discarded and the collection tube was replaced with a new one. 80µl of DNase I solution was added (1:10 dilution of DNase I to DNase buffer for each sample) to the RNeasy Mini spin column, directly to the membrane. The column was incubated at room temperature (15–25°C) for 20 minutes. The column was put into a new collection tube and 500µl RPE buffer (with ethanol) was added to it and centrifuged for 15s at 12 000 × G. Flow-through was discarded. 500 µl of RPE buffer was added to the tube and centrifuged for 15s at 12 000 × G. Flow-through was discarded and the tube centrifuged for 2 minutes at maximum speed. The column was placed into a new 1,5 ml microcentrifuge tube and incubated at RT for 2 minutes with the lid open. 30µ of RNA storage solution was added directly to the spin column membrane and the column incubated at RT for 2 minutes. The tubes were centrifuge for 1 min at 12 000 ×G to elute the RNA. The eluate was pipetted back to the RNeasy Mini spin column and incubated at RT for 2 minutes and centrifuge for 1 min at 12 000 × G.

RNA quality and concentration were measured by Agilent RNA 6000 Nano Kit and Agilent Bioanalyzer 2100 instrument according to manufacturer's instructions. The RNA was denatured at +72°C for 2 minutes before analyzing. The RNA was again frozen at -80°C before cDNA conversion and qRT-PCR. Samples with RNA integrity value (RIN) 7.5 or higher (max. value 10) and concentration more than 90 ng/µl were accepted to cDNA conversion.

4.5.2.4 Reverse transcription

For RNA conversion into cDNA, the Reverse Transcription System (Promega) kit was used. Random primers were chosen to reverse transcript the whole length of RNA. 2µg of total RNA was incubated at +70°C for 10 minutes in a microcentrifuge tube and then placed on ice. A reaction mix done according to manufacturer's instructions and adjusted to each RNA amount

separately. The reaction mix components are listed on table 5. Kanamycin was used as a positive control for the reverse transcription reaction and was provided by the kit.

TABLE 5. The reagents for the cDNA conversion. *A reaction mix is done before pipetting them to the reaction with mRNA.*

Components reverse transcription reaction	**Amount**	**µL**	**10**
MgCl2	4µl	4	**40**
Reverse transcription 10x buffer	2µl	2	**20**
dNTP mixture, 10mM	2µl	2	**20**
recombinant Rnasin ribonuclease inhibitor	0.5µl	0,5	**5**
AMV reverse transcriptase	15U	0,68	**6,8**
oligo(dT) primer OR **random primers**	0.5µg	1	**10**
1,2kb kanamycin positive control RNA (2µL) OR poly(A)+ mRNA OR total RNA	1 µg	2	**20**
nuclease free water to a total volume of 20µL		7,82	**78,2**
		20	**200**

Reactions were first incubated at room temperature for 10 minutes and then at 42°C for 15 minutes. The Reverse Transcriptase enzyme was inactivated by heating the samples to 95°C for 5 minutes and then the cDNA was diluted to 100µl of nuclease free water. The samples were stored to -80°C prior to real-time RT-PCR.

4.5.2.5 Reverse transcription PCR

The components for one reaction are listed on table 6. A master mix was prepared of nuclease-free water and Power® SYBR Green PCR master mix (ABI). Each sample was run with its own primer (see appendix I). *GyrB* (DNA gyrase subunit B) a "housekeeping gene", a constantly expressed gene, was used as a reference for expression. The parental strain UAS391 Ery^S was used as a calibrator gene to which the mutant expression is compared to. The test also included an NTC control for the reaction mix (no sample), an RNA control RTC (RNA sample of the same transposon strain) and a Kanamycin resistance gene (the control of the cDNA kit) was used as a positive control for reverse transcription. The RT-PCR instrument and the program used were the StepOnePlus™ Real-Time PCR system (Thermo Fisher Scientific Inc.). The RT-PCR program is described on table 7. The results were calculated with the comparative quantification algorithm, the $2^{-\Delta\Delta Ct}$, in which the normalizer gene and the gene of interest are used for calculations. A standard curve efficiency was calculated to control the quality of the PCR reaction.

TABLE 6. Reagents for one RT-PCR reaction.

Component	Volume (µl)
Nuclease-free H_2O	7.2
Power® SYBR Green PCR master mix (ABI)	10
Fw primer	0.4
Rw primer	0.4
cDNA	2

TABLE 7. The PCR program for RT-qPCR

Temperature	Time	Cycles
95 °C	10 min	1 cycle
95 °C 62 °C	15 s 1 min	35 cycles
95 °C 62 °C +0.3 °C 95 °C	15 s 1 min 15 s	Melt curve

4.6 Generalized transduction

4.6.1 Principles of generalized transduction with φ11 bacteriophage

The φ11 is a *Staphylococcus aureus* specific bacteriophage, a virus that infects bacteria. It was chosen due to its high transducing efficiency and it is well-studied. It has a linear double-stranded DNA, 46.604 kbps genome. It belongs to the Siphoviridae family and to the Phietavirus genus (GenBank accession number AF424781, retrieved 5.10.2017). It is capable of transducing, which is an ability to transfer genomic and plasmid DNA from one strain to another (Iandolo et al., 2002). Generalized transduction occurs relatively often; viruses use the translation system of the host organism to construct new virions, and sometimes, while packing the viral DNA into the virion, mispacking of bacterial DNA into the bacteriophage capsid happens. However, the mispacked virion does transfer the genetic material into the new host bacterium normally. In generalized transduction the gene transfer is random, whereas in specialized transduction the gene targeted to a certain gene. In horizontal gene transfer the propagation of the genetic material is not due to cell duplication, but the genetic source lies outside the cell (Olson, 2014). Other horizontal gene transfer methods exist, such as conjugation, in which bacteria transfer genetic material to each other via pilus (Thomas &

Nielsen, 2005). Transduction can be used as a method of studying gene function in another cell background to see if the gene function is universal or only strain specific (Olson, 2014).

Bacteriophages are used in molecular biology to alter bacterial strains. If the transferred gene contains a marker, such as an antibiotic resistance gene, the correctly transduced strains can easily be isolated with selective media (Olson, 2014).

4.6.2 The protocol for transduction

The φ11 bacteriophages and lab facilities for working were kindly provided by the Faculty of Sciences and Bio-engineering Sciences at Vrije Universiteit Brussel. The media and solutions used are described in appendix II.

4.6.2.1 Preparation of the transducing phage

Two recipient bacterial strains were used: USA300 UAS391 Ery^S and TCH1516 Ery^S. Erythromycin resistance was used as a selective marker. The cultures of *S. aureus* containing the screened mutation were grown overnight in 10 ml BHI broth with 0.01 % D-glucose in a shaker incubator in +37 °C. Then, 20 µl of the culture was further growth in 2 ml of LB for 4 hours in a shaker incubator at +37°C. A 100 µl of the transducing phage and 150 µl of transposon mutated *S. aureus* were mixed together with 5 ml of molten top agar and poured over a phage base agar. Viral dilutions of 10^{-3}, 10^{-4} and 10^{-5} (the original phage stock was estimated 2–4*10^6 pfu/ml) were used. The plates were incubated overnight at +37 °C. On the same day, recipient bacterial strains were also inoculated on Luria broth and grown overnight in a shaker incubator at +37°C.

4.6.2.2 Transduction

The 10^{-4} phage dilution was enough to completely lyse the bacterial cells on top agar and was therefore used for harvesting the transducing phage. The top layer from the phage plate was removed and the plate rinsed with 2 ml LB medium, which was added to the removed top agar. The removed top agar was centrifuged at 15 000 rpm for 10 min. The supernatant was then sterile filtered through a 0.45µm filter (Millipore®, Merck).

Overnight cultures of the recipient *S. aureus* strains (UAS391 Ery^S and TCH1516) were harvested by centrifuging at 10 000 rpm for 10 min, the supernatants were discarded, and the pellet resuspended in 1 ml of LB with 10 mM $CaCl_2$. 500 µl of bacterial cells was added to 1

ml of LB broth with 10 mM $CaCl_2$ and 500 µl of phage stock. A negative control was included: (strains without the phage) 500 µl of resuspended bacteria and 1.5 ml of LB with 10 mM $CaCl_2$. Samples were incubated in a 37°C water bath for 25 min, followed by incubation at 37°C for 15 min with shaking at 200 rpm. The samples were then quickly put on ice and 1 ml of ice-cold 0.02 M sodium citrate was added to bind Ca^{2+} ions needed for phage adsorption. The cells were harvested by centrifuging at 10 000 rpm for 10 min and the supernatant was removed. The cells were resuspended in 1 ml of ice-cold 0.02 M sodium citrate and incubated on ice for 2h. A 100 µl of phage stock was plated on LB medium for sterility test. 100 µl aliquots were spread on LB agar plates containing 0.05% sodium citrate and the selective antibiotic erythromycin 5 mg/ml and incubated up to 48 hours at 37°C. Single colonies were purified from phages by plating them twice on LB (0.05% sodium citrate) containing erythromycin 5 mg/ml and incubating overnight +37°C. Figure 10. is a picture of the transduced colonies. The smaller colonies were hypothesized to be false positive, because of their small size and their carotenoid expression; the resistance was due to a random mutation, not the transduction. The big, light-colored colonies were chosen for characterization.

FIGURE 10. Transduced strains on 0.05% sodium citrate LB agar plate with erythromycin 5 mg/ml. *The big colonies were real transduced strains whereas the small colonies have most likely gained erythromycin resistance through a spontaneous mutation in the chromosome. (Photo: K. Holappa)*

4.6.2.3 Confirmation of transduction on genomic level

The verification of the transduction of the donor genome into the recipient strain was done by PCR. The forward primer used was the transposon insert primer and the reverse was the end part of each mutated gene. The PCR was run with Veriti 96-well Fast thermal cycler (Applied Biosystems). The forward primer is Buster (sequence on part 4.4.1 on Table 7 Inverse PCR primers). The reverse primers are listed on Table 8. The mastermix used for the PCR is given in table 9 and the PCR program is in Table 10.

TABLE 8. The reverse primers for the verification of transduction PCR

Reverse primers for mutated genes
Tn0002-R 5' – TGTCGGCGTTAAACCAAACG –3'
Tn0002-R 5' – TGGCTTCTCATAGGCATCCG –3'
Tn0007-R 5' – GGTGTAATTCCCAACCGGCA –3'
Tn0123-R 5' – ACCTCGTGGCGAAATGTGAT –3'
Tn0428-R 5' – GCCATTTGCGTTTCCTTTTGC –3'
Tn1354-R 5' – ACCGAGCAAAGGCACCTAAA –3'
Tn1433-R 5'– GCAGCAGCTTTATCATCGCC –3'
Tn1732-R 5' – TCAATGTTGCCAATGGATCACC –3'

TABLE 9. The mastermix for the verification of transduction PCR

Compound	**Specified compound**	**Manufacturer**	**Concentration**	**µl for 1 reaction**
H_2O		Ambion		15
Nucleotides	dNTPs	Invitrogen	1 mmol/ml	1.5
Buffer	Platinum Taq	Invitrogen	10 X	2.5
Primer Fw	Buster-F	Sigma Aldrich	10 pmol/ml	1
Primer Rev	Tn-R	Sigma Aldrich	10 pmol/ml	1
$MgCl_2$		Invitrogen	50mmol/ml	1
Enzyme	Platinum Taq Invitrogen	Invitrogen	5 U/ml	0.5
			Total	**22.5**
DNA	Transduced transposon DNA		+/- 100 ng/µl	2.5

TABLE 10. The PCR program for the verification of transduction

Temperature	**Time**	**Cycles**
95°C	10 min	1 cycle
95°C	1 min	40 cycles
65°C	30 secs	
72°C	3 min	
72°C	10 min	1 cycle
4°C	∞	

The PCR product was analyzed on 2.0% agarose gel (Ultrapure™ Agarose, Lifetechnologies) with Gelred™ (Biotium). Here, 2.4g agarose was dissolved in 144 ml of distilled water and 16 ml of 5x TBE buffer by heating and 16 µl of GelRed™ was added prior to casting the gel. 5 µl of DNA was loaded on gel with 5 µl of gelloading buffer. The ladder used was (5 µl) MassRuler DNA Ladder Mix (Thermo Fisher Scientific Inc.). The gel was run for 50 minutes with 150 volts / 200 mA. The gel was visualized with a UV light camera.

4.6.3 Phenotypic analysis of the transduced mutant stains

To characterize the phenotype of the transduced mutant strains the static biofilm assay and the growth curve were repeated. Dynamic biofilms were also observed under fluorescence microscope.

4.7 Data analysis methods

Raw data of the experiments was processed with MS Office Excel. The growth curves were analyzed with MS Excel and the GrowthRates program (Hall et al., 2014). For epifluorescence microscopy, ImageJ program was used as well as MS Excel. For statistical testing (Student's independent samples t-test) IBM SPSS Statistics 25 was used.

5 RESULTS

5.1 Characterization of the transposon mutant strains

5.1.1 Static assay

The static biofilm assay is used for screening the library, but it can also give information about the biofilm formation in relation to the parental strain and the wild-type strain (100%). Significant difference was found in strains Tn0002 ΔHAD (OD=0.420, 121%, p=0.023) Tn0428 *ΔoppA* (OD=0.463, 133%, p=0.003) and Tn1354 *ΔclfB* (OD=0.245, 70%, p=0.001), when variances were assumed equal and significance level was set to $p<0.05$. However, Tn1354 *ΔclfB* is not significantly different from the wild-type strain UAS391 (OD=0.348, p=0.257). The results of the static assay shown in figure 11 and the p-values on table 11.

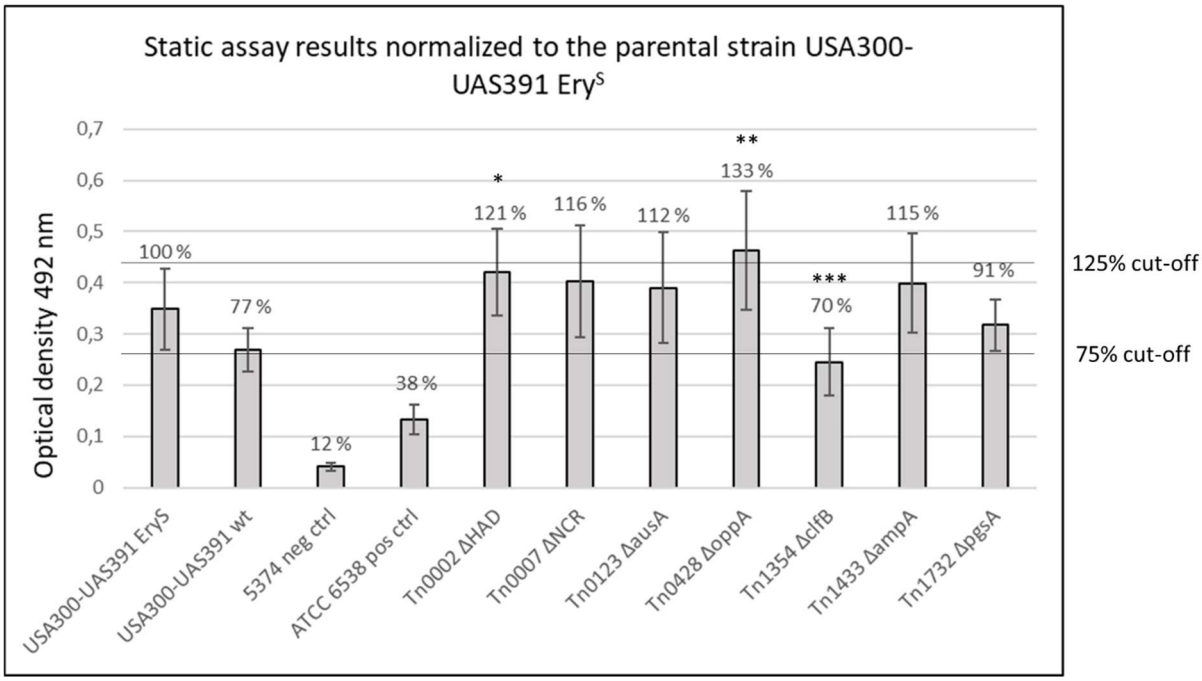

FIGURE 11. Optical densities of the static assays of the transposon mutants*. The OD_{600} values were normalized to the parental strain UAS391 Ery^S. Statistically significant values are marked with asterisks. *p < 0.05, **p ≤ 0.01, ***p ≤ 0.001*

TABLE 11. The p-values of the static assay results. *The strains were compared with independent variables t-test to the parental strain UAS391 Ery^S. Significance limit is p<0.05. Asterisks mark the significance level: *p < 0.05, **p ≤ 0.01, ***p ≤ 0.001 and n.s. = non-significant.*

Two-tailed t-test			
Strain	**p-value**	**Significance**	**n**
USA300-UAS391 wt	0.002	**	16
5374 neg ctrl	0.000	***	8
ATCC 6538 pos ctrl	0.000	***	8
Tn0002 *ΔHAD*	0.023	*	16
Tn0007 *ΔNCR*	0.131	n.s.	16
Tn0123 *ΔausA*	0.231	n.s.	16
Tn0428 *ΔoppA*	0.003	**	16
Tn1354 *ΔclfB*	0.001	***	16
Tn1433 *ΔampA*	0.126	n.s.	16
Tn1732 *ΔpgsA*	0.207	n.s.	16

5.1.2 Testing the minimum inhibitory concentration of antibiotics

MIC values were determined of each strain to see if the transposon mutated gene is linked with antibiotic resistance genes. The strain Tn1732 *ΔpgsA* was intermediate resistant towards ciprofloxacin in the screening and showed a rise in resistance towards it in MIC test too, with a result between sensitive and intermediate susceptibility. The rest of the strains did not show remarkable changes in susceptibilities. Clindamycin and chloramphenicol resistance were provided by the transposon insertion. The results are on table 12.

TABLE 12. Minimum inhibitory concentration values of the transposon strains. *Antibiotic susceptibilities are color-coded in the table: green marks for sensitive, white is between sensitive and intermediate, yellow is intermediate and red is resistant. Ciprofloxacin (CIP), gentamicin (GM), trimethoprim/sulfamethoxazole (SXT), cefoxitin (CFX), chloramphenicol (C), erythromycin (E), penicillin (P), tetracyclin (TC) and clindamycin (CC) MICs were tested.*

	S	Between I and S	I	R					
	Antibiotic								
Strain	**CIP**	**GM**	**SXT**	**CFX**	**C**	**E**	**P**	**TC**	**CC**
UAS391	0,25	0,38	0,047	32	6	32	24	0,19	0,125
UAS391 Ery^S	0,38	0,38	0,047	32	8	0,38	6	0,25	0,125
Tn0002 *ΔHAD*	0,25	0,38	0,032	24	12	>256	4	0,25	>256
Tn0007 *ΔNCR*	0,25	0,38	0,047	24	12	>256	4	0,38	>256
Tn0123 *ΔausA*	0,25	0,38	0,047	24	12	>256	6	0,38	>256
Tn0428 *ΔoppA*	0,25	0,38	0,032	24	12	>256	4	0,19	>256
Tn1354 *ΔclfB*	0,25	0,38	0,032	24	12	>256	4	0,25	>256
Tn1433 *ΔampA*	0,25	0,38	0,047	24	16	>256	6	0,19	>256
Tn1732 *ΔpgsA*	1,5	0,38	0,032	32	24	>256	6	0,38	>256

5.1.3 Growth curves of the transposon mutants

Growth rates and growth curves of the cells were measured to see whether the transposon mutation had impacted the growth capacity of the cells. According to the graph (figure 12., page 48), the UAS391 cell lines, mutated and non-mutated, have a similar exponential growth phase and all reach the plateau phase in approximately the same time. The results are the same when looking at growth rate and lag time (table 13). The only exception is the positive control strain ATCC 6538, which grows less efficiently (growth rate 0.019 increase of OD_{600}/min) and seems to enter the death phase, which begins where the curve starts to decline. All the other strains do not enter death phase during 24-hour growth. The wild-type strain UAS391 seems to grow the fastest, but the UAS391 Ery^S strain has a slightly higher growth rate and eventually the maximum OD is comparable (0.611 vs 0.591).

TABLE 13. The growth rates of the mutant strains and the control strains.

Strain	Growth Rate	R	Max OD	Lag time (minutes)
UAS391 wt	0.02229	0.99968	0.611	39.5
UAs391 Ery^S	0.02287	0.99963	0.591	24.4
ATCC 6538	0.01877	0.99829	0.419	49.1
5374	0.02375	0.99935	0.591	35.8
Tn0002 *ΔHAD*	0.02336	0.99874	0.567	26.8
Tn0007 *ΔNCR*	0.02199	0.99947	0.552	42.1
Tn0123 *ΔAusA*	0.02371	0.99932	0.556	33.3
Tn0428 *ΔOppA*	0.0228	0.99916	0.554	32.1
Tn1354 *ΔClfB*	0.02282	0.99936	0.534	41.5
Tn1433 *ΔAmpA*	0.02504	0.99969	0.535	44.3
Tn1732 *ΔpgsA*	0.02244	0.99936	0.574	19.5

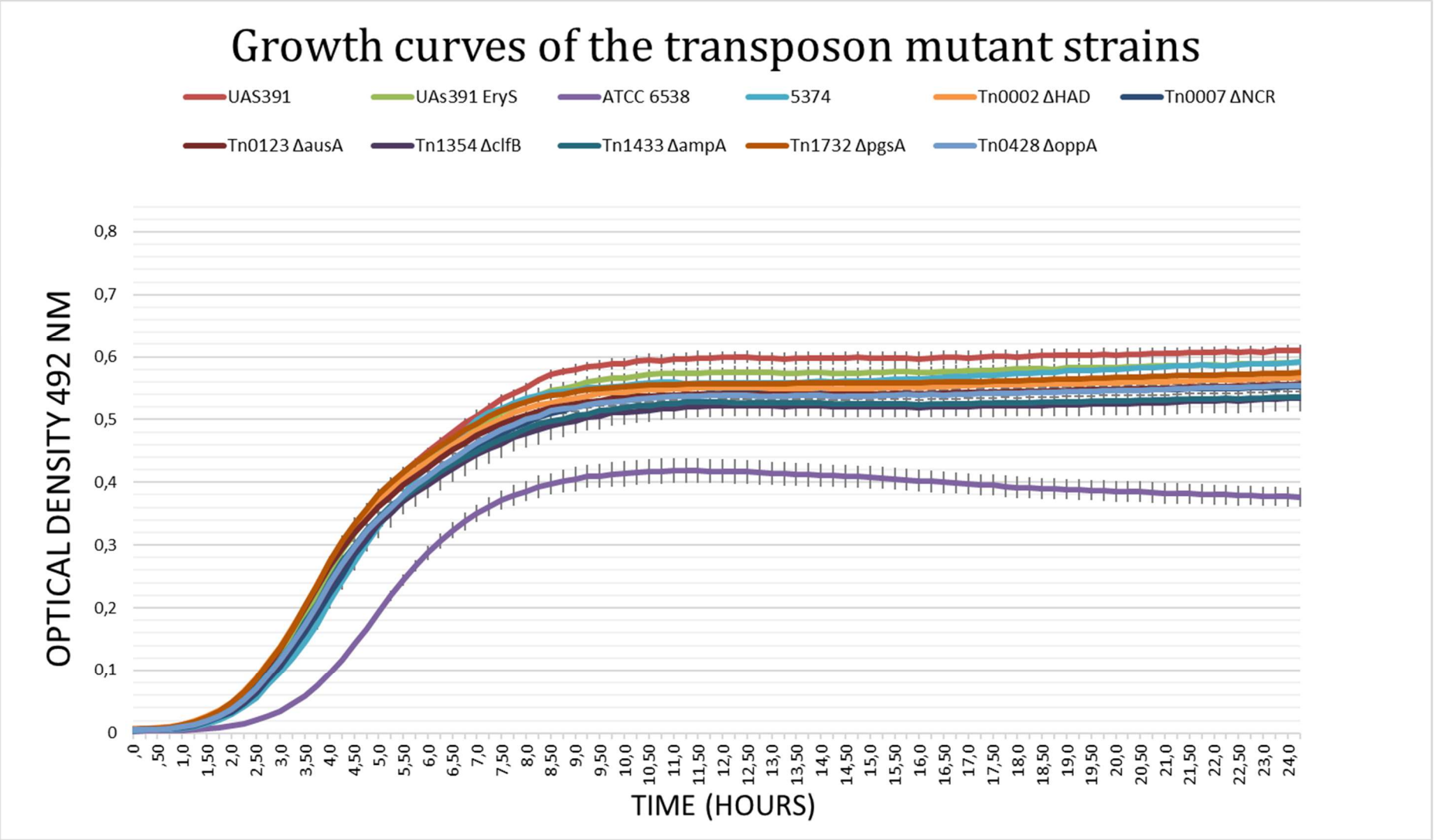

FIGURE 12. The growth curves of the transposon mutant strains.

5.1.4 Transposon mutants under epifluorescence microscope

The pictures of the biofilms grown in shear flow system (the dynamic biofilms) were analyzed both visually and with the ImageJ program. However, the standard deviation of the pixel analysis was quite large and more images would have been needed per biofilm than was feasible during this study; for this reason, the statistics were excluded from the results. The biofilm images can be used for qualitative analysis. How the pictures were taken is described in the section 4.2.3. All images were taken with 40x oil objective.

Looking at the wild-type and the parental strain images. certain features can be distinguished: an intricate formation of cells, matrix and fluidic channels. The biofilm grows throughout the whole viewing channel and it seems to have concentrated colonies of cells, which show as saturated fluorescent spots on the images. The fluorescence microscopy pictures can be seen in figures 13–21.

Basically, the mutant strains showed similar structures compared to the wild-type and parental strain. There were small differences, such as more clumped colonies, indistinct fluidic channels and lack of solid biofilm. Such patterns could be seen for example in *ΔHAD*, *ΔoppA* and *ΔpgsA* strains.

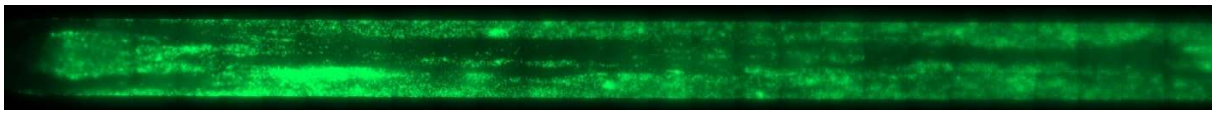

FIGURE 13. Epifluorescence microscopy picture of the USA300-UAS391 strain. *The wild-type UAS391 produced a rich and intricate biofilm inside the viewing channel under a flow of nutrients.*

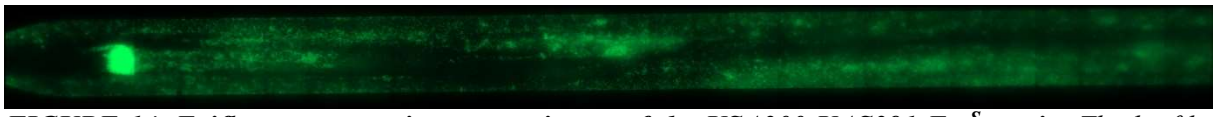

FIGURE 14. Epifluorescence microscopy picture of the USA300-UAS391 Ery^S strain. *The biofilm structure looks the same as in figure 13. (UAS391).*

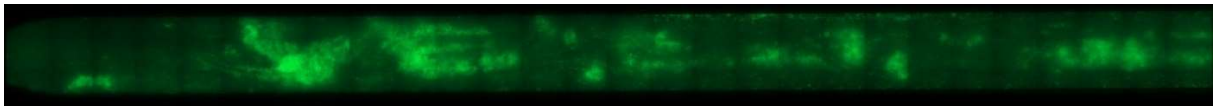

FIGURE 15. Epifluorescence microscopy picture of ΔHAD UAS391 (Tn0002) strain. *The biofilm structure looks clumpy compared to the parental strains.*

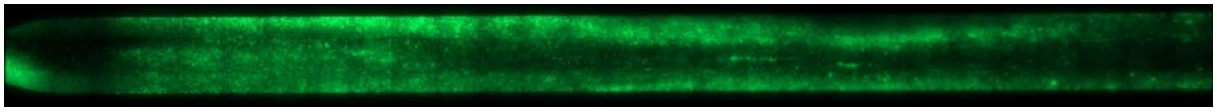

FIGURE 16. Epifluorescence microscopy picture of ΔNCR UAS391 (Tn0007) strain. *The biofilm is abundant and fills the whole length of the viewing channel.*

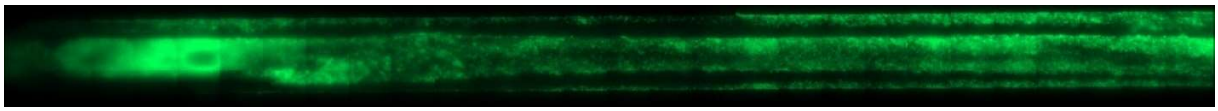

FIGURE 17. Epifluorescence microscopy picture of ΔausA UAS391 (Tn0123) strain. *The biofilm looks very thick and intricate with its fluidic channels, and it fills the whole viewing channel.*

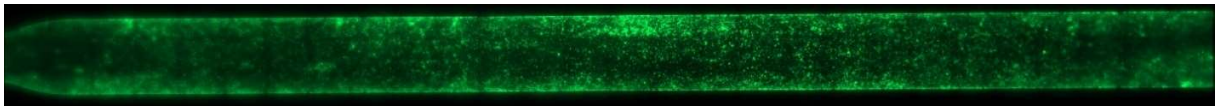

FIGURE 18. Epifluorescence microscopy picture of ΔoppA UAS391 (Tn0428) strain*. This strain seems to have produced only little biofilm and basically only loose cells float in the viewing channel.*

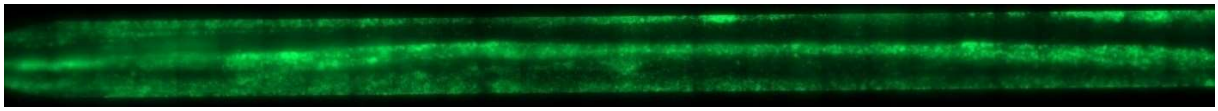

FIGURE 19. Epifluorescence microscopy picture of ΔclfB UAS391 (Tn1354) strain. *The strain has produces an intricate biofilm and the fluidic channels are visible as well.*

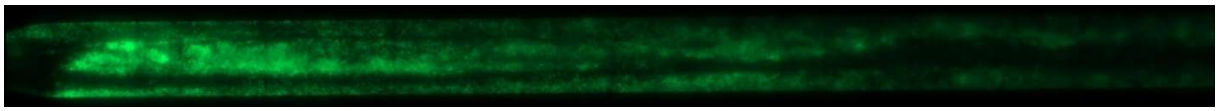

FIGURE 20. Epifluorescence microscopy picture of ΔampA UAS391 (Tn1433) strain. *The strain seems to have produced a thick biofilm which would explain the poor penetration of the fluorescent dye in it, especially at the right end of the viewing channel.*

FIGURE 21. Epifluorescence microscopy picture of ΔpgsA UAS391 (Tn1732) strain*. Only detectable biofilm is the fluorescent portion on the left side of the viewing channel. It could imply a weakened ability to produce a biofilm in flow conditions.*

The static biofilms were also imaged with fluorescence microscope. They were grown and stained as described in section 4.2.1. All strains were grown both on glass and polystyrene wells. No remarkable differences in the biofilm morphology were detected between the biofilms. Depending on the imaged spot, some images showed denser areas with cells and protruding structures. In the figure 22 there are pictures of the parental strain UAS391 Ery^S and *ΔpgsA* imaged with fluorescence microscope both on polystyrene and glass wells. From the images it can be said that the surface of the biofilm has some structures and protrusions, and the cells are not evenly distributed, but they are in clusters.

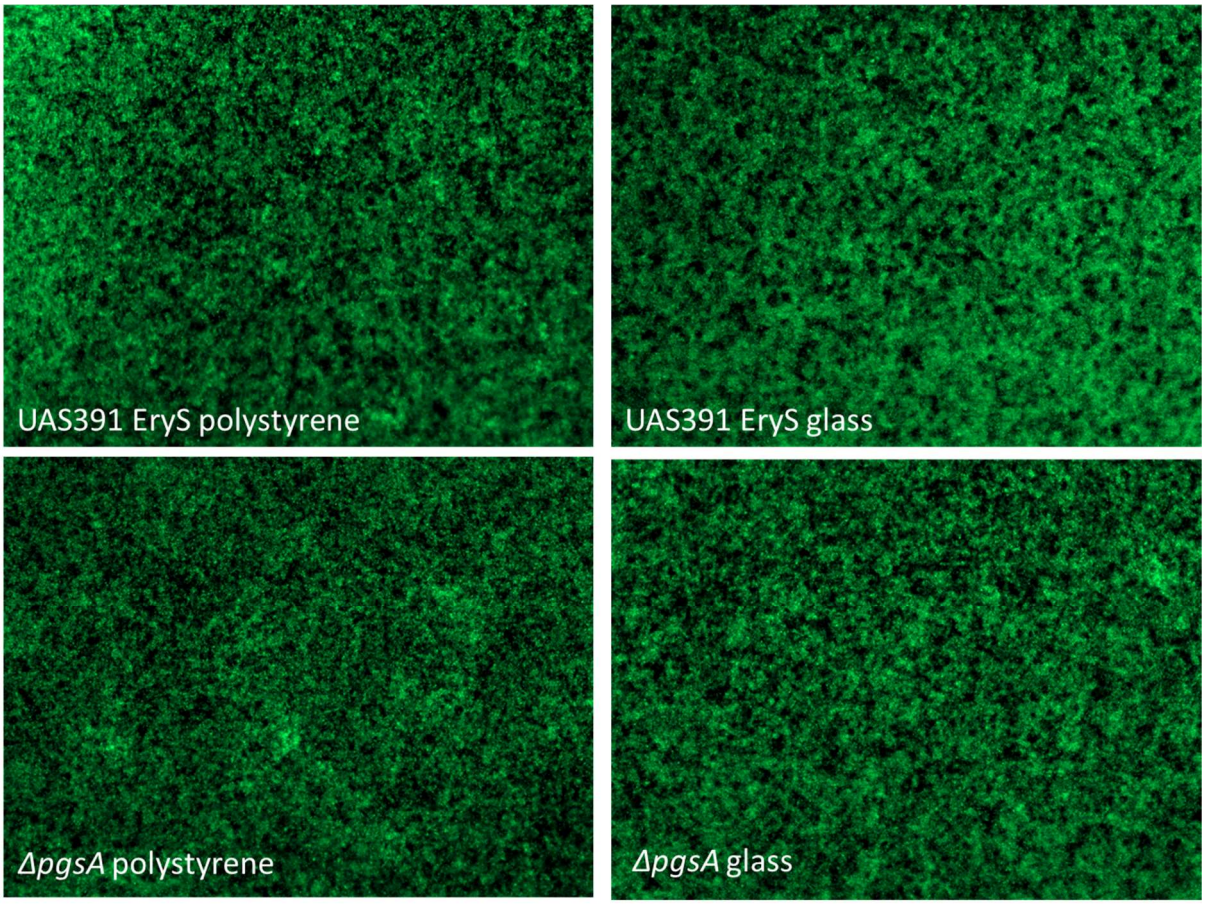

FIGURE 22. Comparison of the static biofilms grown on polystyrene and glass wells. *Syto9 stains the live and dead cells. No remarkable differences were observed between the images, nor in other strains (not shown). 40x oil objective was used.*

5.1.5 Detection of gene expression by using real-time RT-PCR

A real-time RT-PCR was run for the strains to see if the mutation influenced the gene expression and could therefore explain the differences in biofilm formation. The results of the RT-PCR are seen in figure 23. The PCR was run with RNA, that was extracted both from cells grown of a biofilm and cells grown in a planktonic culture (described in sections 4.5.2.2 and 4.5.2.1, respectively) and converted into cDNA before the RT-PCR. The results are presented as fold differences calculated with $2^{-\Delta\Delta Ct}$ method, as was described in section 4.5.1.

The *ΔpgsA* seems to have slightly less expression than the parental strain (fold-change 0.611 planktonic [pl] and 0.811 biofilm [bf]). In the cases of *ΔNCR* (pl. 0.131, bf. 0.490) and *ΔausA* (pl. 0.002, bf. 0.001) the gene expression is much less in comparison with the parental strain. *ΔHAD* (pl. 1.232, bf. 3.500), *ΔclfB* (pl. 2.107, bf. 2.787) and *ΔampA* (pl. 1.926, bf. 1.685) have a fold change >1, which indicates that there is more expression of the gene in relation to parental strain but the standard deviations are too high to confirm this; a maximum for a reliable result is 0.2. SD bars also overlap the line of fold-change 1. *ΔoppA* seems to have a slight decreased

fold-change (0.655) in expression in a planktonic culture but slightly elevated expression (1.109) in the biofilm culture. However, the SD of the biofilm fold-change is 1.137 and that also is left unconfirmed. Correlation coefficients R^2 of the measurements vary, which on its part explains the high standard deviations. An R^2 value less than 0.95 is typically considered as a cut-off value for a successful reaction. The fold-changes, standard deviations and R^2 values are listed on table 14. According to R^2 values, for example, *ΔausA*, *ΔoppA* and *ΔclfB* should be repeated.

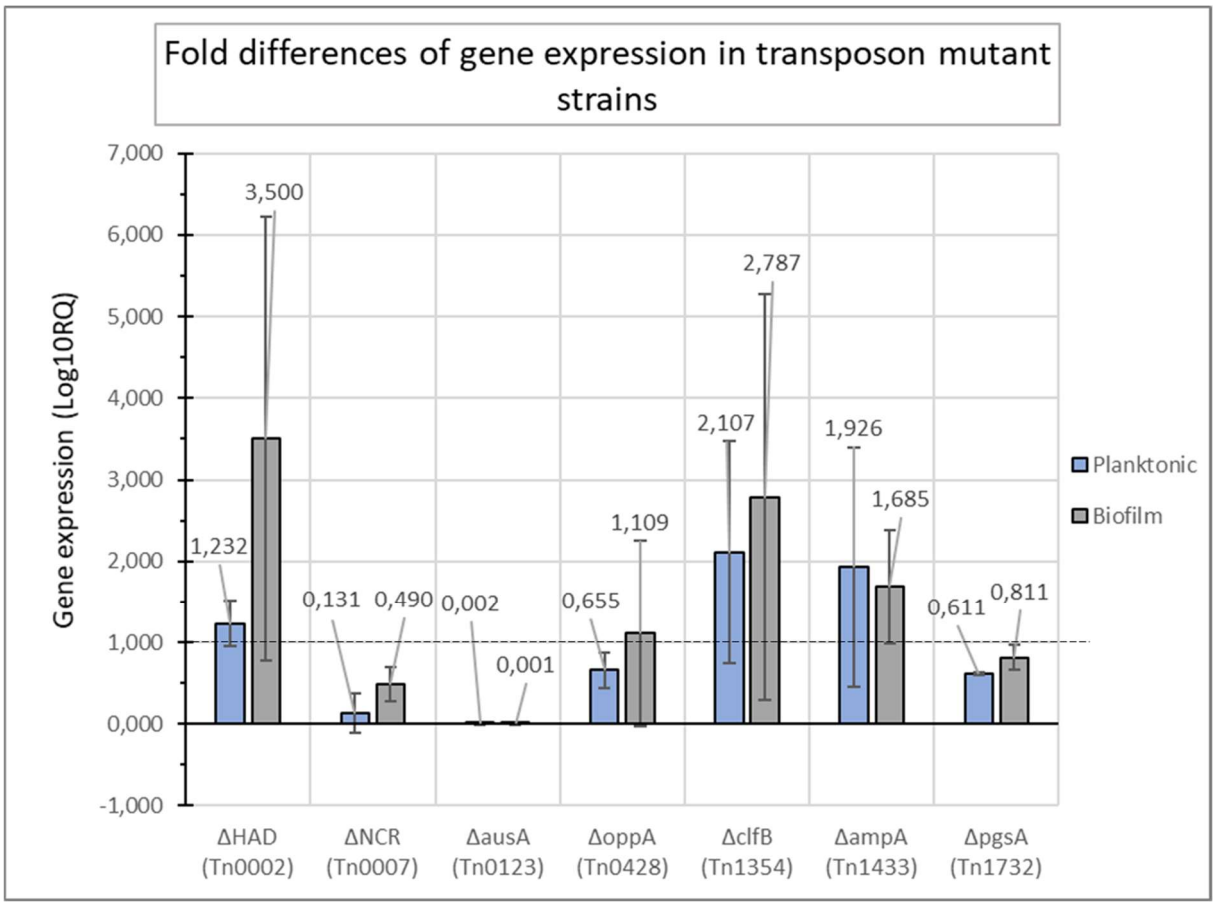

FIGURE 23. The-fold changes of gene expression of the planktonic and biofilm grown bacteria. *The dashed line at 1.000 marks the expression level of the parental strain. Bars reaching above 1.000 indicate more than 1-fold increase of gene expression and bars left below 1.000 mark for decreased gene expression in relation to the parental strain UAS391 Ery^S. The calculations are done with $2^{(-\Delta\Delta Ct)}$ method, which is used for analyzing relative changes in gene expression without quantifying the starting amount of RNA. Because of the logarithmic scale, the bars are not symmetric.*

TABLE 14. The calculated fold-changes, standard deviations of the RT-PCR of the transposon mutants. *Correlation coefficients (R^2) of the standard curves were also calculated to evaluate the efficiency of the PCR reaction.*

	Planktonic			Biofilm		
Strain	**Mean $2^{-\Delta\Delta Ct}$**	**SD**	**R^2 of standard curve**	**Mean $2^{-\Delta\Delta Ct}$**	**SD**	**R^2 of standard curve**
ΔHAD (Tn0002)	1.232	0.282	0.90	3.500	2.727	0.62
ΔNCR (Tn0007)	0.131	0.240	0.91	0.490	0.207	0.90
ΔausA (Tn0123)	0.002	0.000	0.41	0.001	0.000	0.53
ΔoppA (Tn0428)	0.655	0.223	0.55	1.109	1.137	0.95
ΔclfB (Tn1354)	2.107	1.370	0.76	2.787	2.489	0.68
ΔampA (Tn1433)	1.926	1.470	0.95	1.685	0.696	0.77
ΔpgsA (Tn1732)	0.611	0.020	0.95	0.811	0.151	0.95

5.2 Characterization of the transduced transposon mutant strains

Transduction was performed with to the transposon strains to study the gene universality in a different bacterial background. The transposon containing gene of transposon strains was transduced into UAS931 Ery^S and MRSA TCH1516 strains, after which static assay, growth curve and imaging of the biofilm were done to detect the possible changes in phenotype of the biofilm.

5.2.1 Static assays of the transduced transposon mutants

The static assay was done for each transduced strain to see if the mutation effects would also occur also in the recipient strain. After transduction to the UAS391 Ery^S strain, only *ΔpgsA* Tn1732 showed a significant difference compared to the parental strain ($p = 0.033$). Notable is however, that the wild-type strain gave an even lower result than *ΔpgsA*. Therefore, it could not be stated as significantly different result. The results of the transduction into UAS391 Ery^S are represented in figure 24. The p-values are listed in table 15 (n = 24, except for *ΔclfB* UAS391 and *ΔampA* UAS391 n = 36).

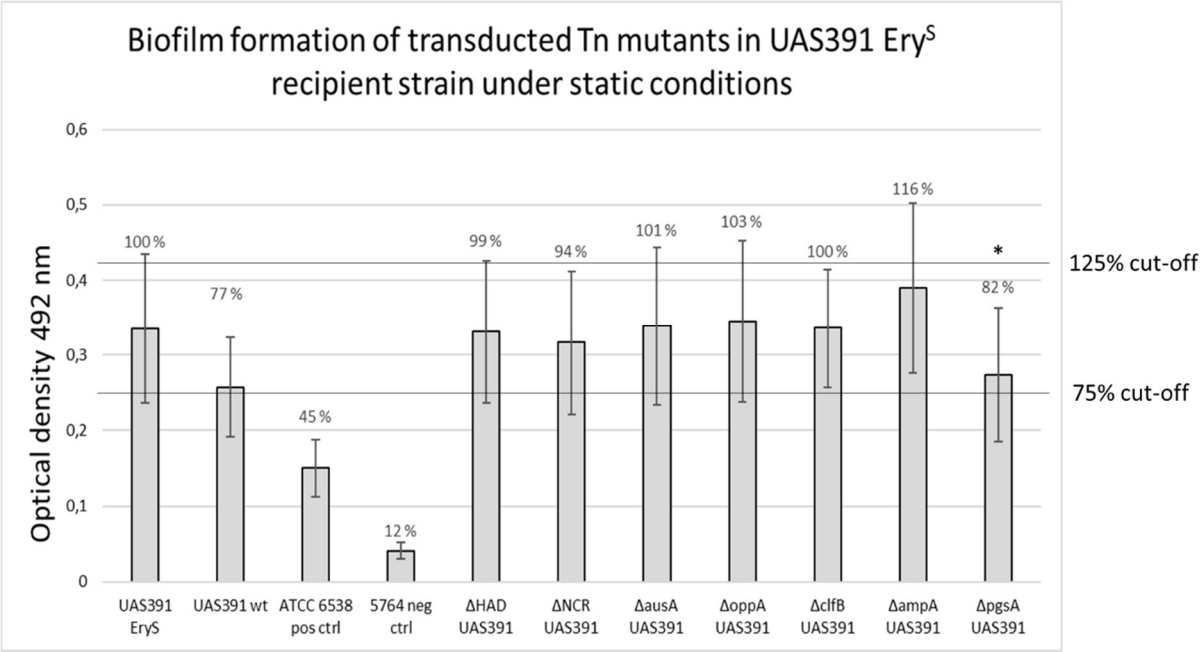

FIGURE 24. The transduced transposon strains in UAS391 Ery^S recipient strain. *The transduced strains are normalized to the UAS391 Ery^S strain. The controls and parental strains were not transduced and are shown in the figure for reference. Statistically significant values are marked with asterisks. *=p < 0.05, **=p ≤ 0.01, ***=p ≤ 0.001.*

TABLE 15. The p-values of two-tailed t-tests of the transduced UAS391 transposon stains. *The strains were compared with independent variables t-test to the recipient strain used in transduction, UAS391 Ery^S here. Significance limit is p<0.05. Asterisks mark the significance level: *p < 0.05. **p ≤ 0.01. ***p ≤ 0.001 and n.s. = non-significant. [1)]Control strains were not transduced and are only shown for reference.*

	Transduced into UAS391EryS		
Strain	**Max OD492**	**p-value**	**Significance**
UAS391 wt [1)]	0.335	0.003	**
UAS391 Ery^S [1)]	0.257		
ATCC 6538 pos ctrl [1)]	0.150	0.000	***
5764 neg ctrl [1)]	0.041	0.000	***
Tn0002 *ΔHAD*	0.331	0.874	ns
Tn0007 *ΔNCR*	0.316	0.512	ns
Tn0123 *ΔausA*	0.339	0.899	ns
Tn0428 *ΔoppA*	0.345	0.743	ns
Tn1354 *ΔclfB*	0.336	0.668	ns
Tn1433 *ΔampA*	0.390	0.066	ns
Tn1732 *ΔpgsA*	0.274	0.033	*

After transduction to the TCH1516 strain, only *ΔausA* (Tn0123) showed a significant difference compared to the parental strain (OD=0.356, p < 0.001). The *ΔausA* seemed to form 1.51 times more biofilm than the TCH1516 strain. UAS391 Ery^S strain alone grew a 1.42-fold thicker biofilm than TCH1516. Other mutants did not show a change in biofilm formation. The results

of TCH1516 transduction are in figure 25 and the p-values of the tests are in table 16 (n = 24, except for *ΔclfB* TCH1516 and *ΔampA* TCH1516 n= 20).

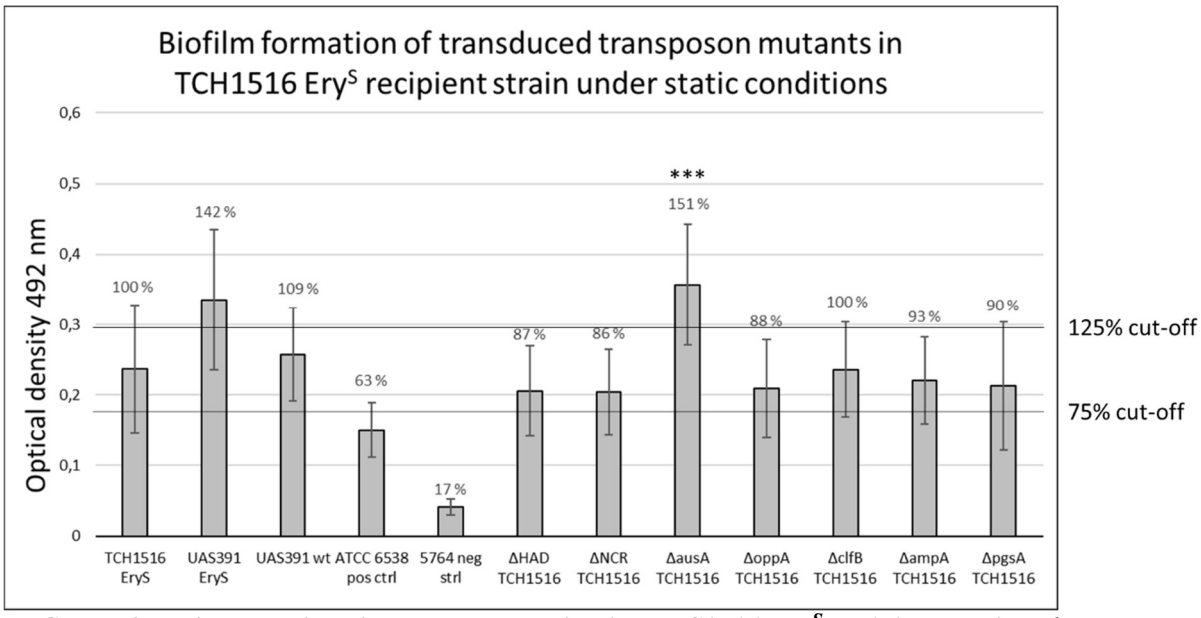

FIGURE 25. The transduced transposon strains in THC1516 Ery^S recipient strain. *The strains are compared to TCH1516 Ery^S. The controls and parental strains were not transduced and are shown in the figure for reference. Statistically significant values are marked with asterisks. *p < 0.05, **p ≤ 0.01, ***p ≤ 0.001.*

TABLE 16. The p-values of two-tailed t-tests of the transduced transposon stains. *The strains were compared with independent variables t-test to the recipient strain used in transduction, TCH1516 Ery^S in this case. Significance limit is p<0.05. Asterisks mark the significance level: *p < 0.05. **p ≤ 0.01. ***p ≤ 0.001 and n.s. = non-significant. [1)]Control strains were not transduced and are only shown for reference.*

	Transduced into TCH1516		
Strain	**Max OD492**	**p-value**	**Significance**
UAS391 wt[1)]	0.335	0.380	ns
UAS391 Ery^S [1)]	0.257	0.001	**
ATCC 6538 pos ctrl [1)]	0.150	0.000	***
5764 neg ctrl [1)]	0.041	0.000	***
Tn0002 *ΔHAD*	0.206	0.193	ns
Tn0007 *ΔNCR*	0.204	0.165	ns
Tn0123 *ΔausA*	0.356	0.000	***
Tn0428 *ΔoppA*	0.209	0.249	ns
Tn1354 *ΔclfB*	0.236	0.987	ns
Tn1433 *ΔampA*	0.220	0.500	ns
Tn1732 *ΔpgsA*	0.213	0.379	ns

5.2.2 Growth curves of the transduced transposon mutants

Similarly as for the mutants strains, growth curves were measured for each transduced strains. According to the growth rates algorithm, all the transduced strains grew with the same rate. Correlation coefficients (R^2) tell that the curves grew linearly. All R^2 values are above 0.95, meaning that the test is reliable. The growth rates are presented in table 17 and the growth curves are in figures 26 and 27.

TABLE 17. The growth rates of the transduced strains. *The growth rate tells the increase of OD_{600} per minute during the logarithmic growth phase. R^2 should be >0.95 for the test to be reliable.*

Transduced strains	**Growth rate (increase of OD_{600}/min)**	**R^2**	**Max OD_{600}**
UAS391 wt	0.022	0.998	0.636
UAS391 Ery^S	0.022	0.999	0.603
ATCC 6538 pos ctrl	0.022	0.999	0.428
5374 neg ctrl	0.024	0.997	0.583
TCH1516 Ery^S	0.023	0.999	0.499
ΔHAD Tn0002 UAS391	0.025	0.999	0.574
ΔNCR Tn0007 UAS391	0.027	0.999	0.510
ΔausA Tn0123 UAS391	0.022	0.998	0.568
ΔoppA Tn0428 UAS391	0.023	0.999	0.567
ΔclfB Tn1354 UAS391	0.024	0.999	0.570
ΔampA Tn1433 UAS391	0.025	0.999	0.601
ΔpgsA Tn1732 UAS391	0.026	0.996	0.580
ΔHAD Tn 0002 TCH1516	0.025	0.999	0.529
ΔNCR Tn0007 TCH1516	0.024	0.999	0.522
ΔausA Tn0123 TCH1516	0.021	0.999	0.572
ΔoppA Tn0428 TCH1516	0.026	0.999	0.508
ΔclfB Tn1354 TCH1516	0.024	0.999	0.508
ΔampA Tn1433 TCH1516	0.026	0.998	0.509
ΔpgsA Tn1732 TCH1516	0.025	0.999	0.508

Figure 27 (page 57) represents the growth curves of the TCH1516 transduced mutants. *ΔausA* (Tn0123 in TCH1516) looks to grow more like the wild-type and the UAS391 Ery^S strains while the rest of the transduced strains grow more similarly to the recipient strain TCH1516. In a two-tailed t-test (variances assumed the same), the difference between TCH1516 and *ΔausA* is significantly different ($p = 0.038$) but not between parental strain UAS391 Ery^S and *ΔausA* ($p = 0.257$). *ΔausA* is drawn in orange in figure 27.

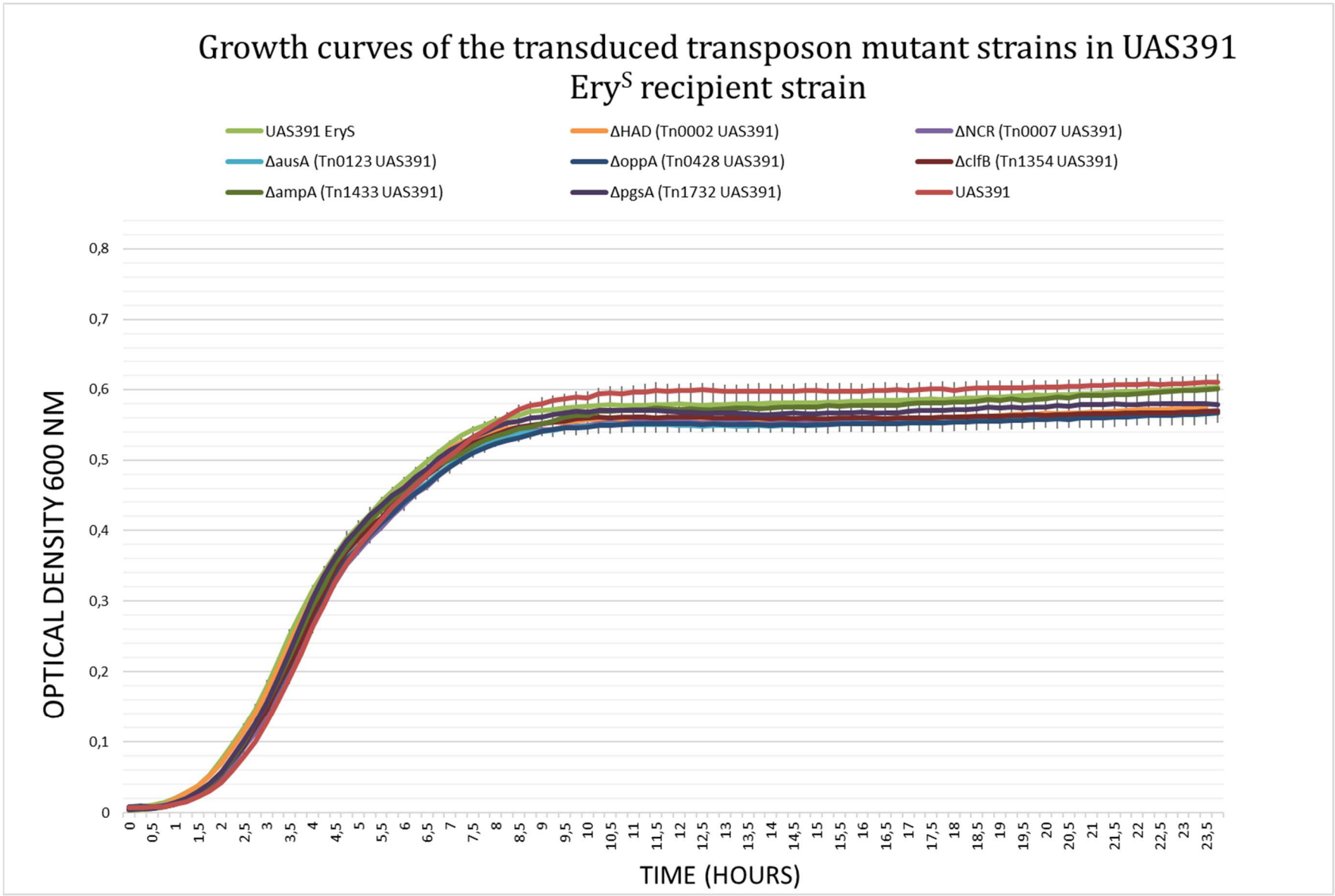

FIGURE 26. The growth curves of the transduced mutants in the UAS391 Ery^S background.

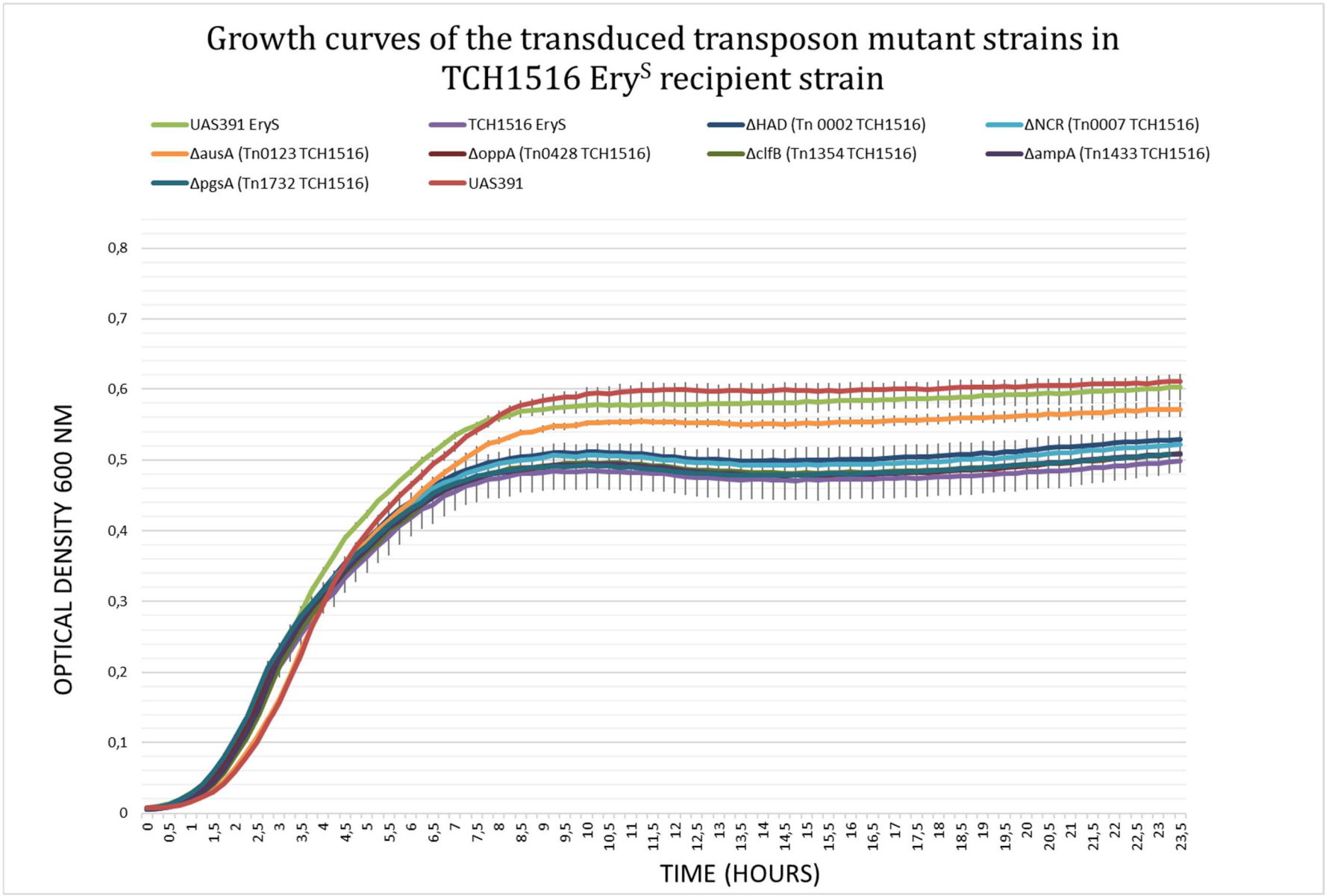

FIGURE 27. The transduced mutant strains in TCH1516 Ery^S background.

5.2.3 Epifluorescence microscopy imaging of the biofilms

The transduced strains were imaged similarly as the original mutants with epifluorescence microscope to see whether the disrupted gene function would cause changes in the biofilm phenotype of the transduced strains. As can be seen in figures 28–43, all strains produced a biofilm. However, not all strains as strongly as others. The TCH1516 transduced strains performed a thinner biofilm, and all the biofilms of TCH1516 looked about the same, except *ΔausA*, which did not produce a lot of biofilm. The biofilm is fluffy and cells are rather evenly distributed among the biofilm, while in UAS391 strains the biofilm morphology seems vary much more. All images were taken with 40x oil objective. Each biofilm is described in figure legends.

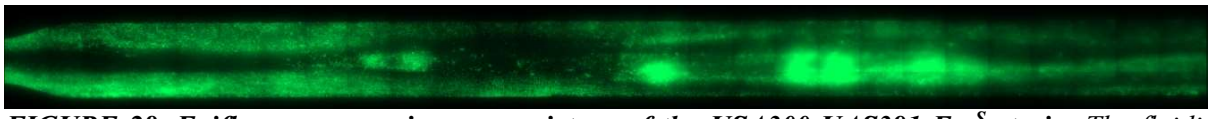

FIGURE 28. Epifluorescence microscopy picture of the USA300-UAS391 Ery^S strain. *The fluidic channels are visible (black) and the biofilm fills almost the whole viewing area.*

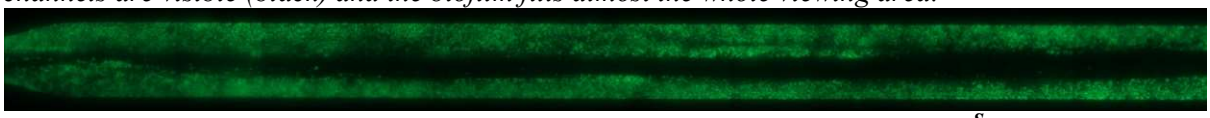

FIGURE 29. Epifluorescence microscopy picture of the USA300 TCH1516 Ery^S strain. *The biofilm fills the whole viewing area and has a fluidic channel in the middle.*

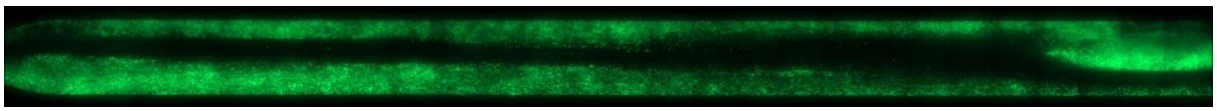

FIGURE 30. Epifluorescence microscopy picture of ΔHAD (Tn0002) UAS391. *The biofilm fills the viewing area and it has a distinct fluidic channel in the middle.*

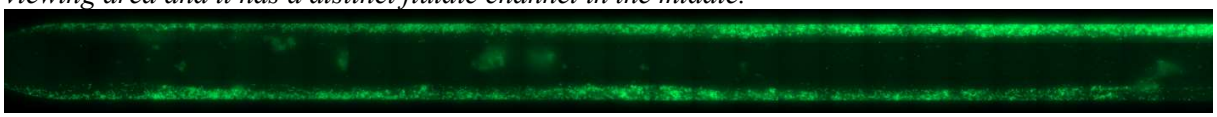

FIGURE 31. Epifluorescence microscopy picture of ΔHAD (Tn0002) TCH1516. *The biofilm mass is less than in the UAS391 background and mainly on the walls of the viewing channel.*

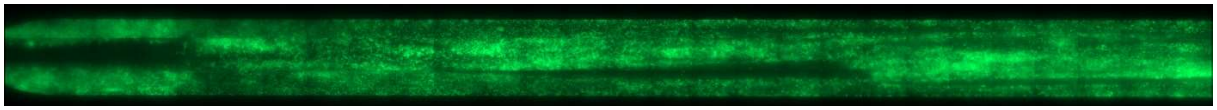

FIGURE 32. Epifluorescence microscopy picture of ΔNCR (Tn0007) UAS391. *Biofilm fills the viewing channel and the fluidic channels are narrow and hardly visible at this plane of focus.*

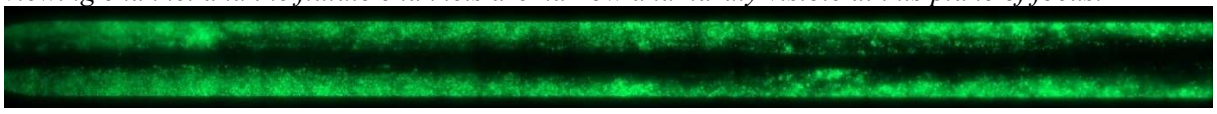

FIGURE 33. Epifluorescence microscopy picture of ΔNCR (Tn0007) TCH1516. *The biofilm grows mainly on the sides of the tube and no other fluidic channels are visible but the channel in the middle.*

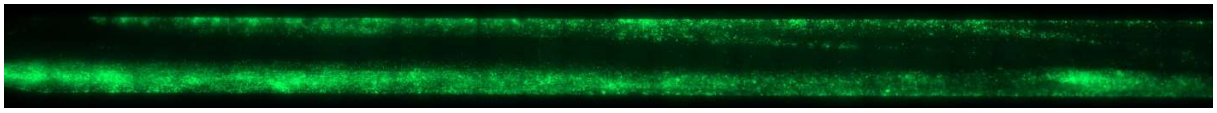

FIGURE 34. Epifluorescence microscopy picture of ΔausA (Tn0123) UAS391. *The biofilm has formed thickly on the walls of the tube and some fluid channels are also visible on in addition to the big channel in the middle.*

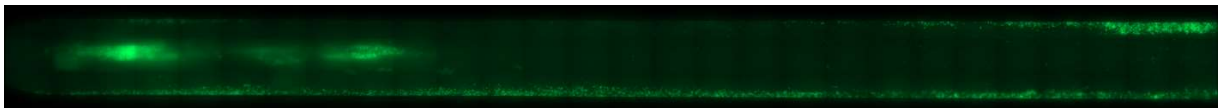

FIGURE 35. Epifluorescence microscopy picture of ΔausA (Tn0123) TCH1516. *Some biofilm accumulated in the tube, and there is a larger biofilm islet on the left side of the viewing channel.*

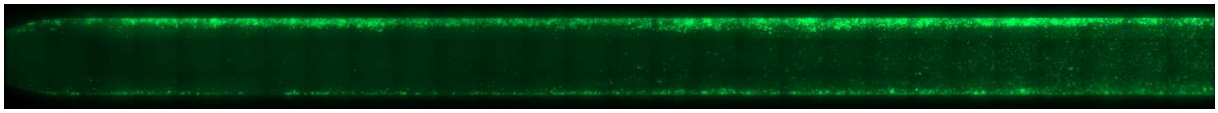

FIGURE 36. Epifluorescence microscopy picture of ΔoppA (Tn0428) UAS391. *This strain seems to have formed only a little biofilm on the viewing channel.*

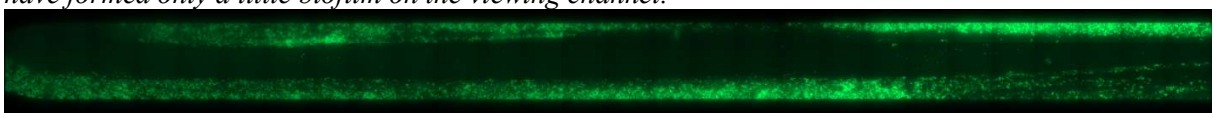

FIGURE 37. Epifluorescence microscopy picture of ΔoppA (Tn0428) TCH1516. *This strain seems to have formed a smooth, waving biofilm on the edges of the viewing channel.*

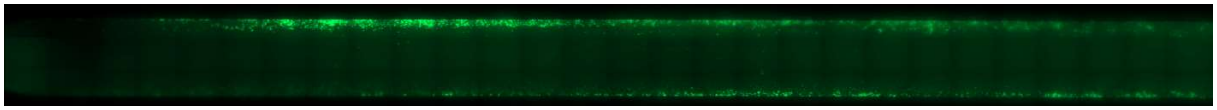

FIGURE 38. Epifluorescence microscopy picture of ΔclfB (Tn1354) UAS391. *The strain formed only little biofilm in the viewing channel.*

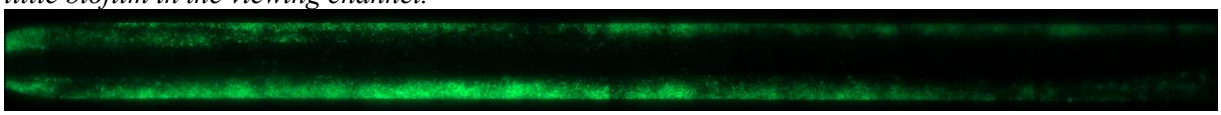

FIGURE 39. Epifluorescence microscopy picture of ΔclfB (Tn1354) TCH1516. The strain formed some biofilm on the walls but relatively little compared to the parental strain.

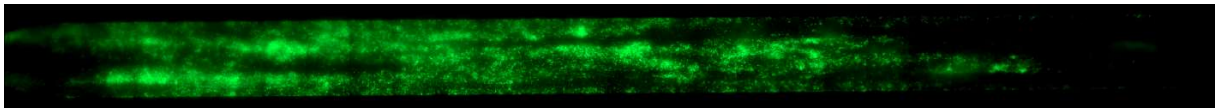

FIGURE 40. Epifluorescence microscopy picture of ΔampA (Tn1433) UAS391. *This biofilm was abundant and filled the viewing channel and partly prevented the dye from reaching all cells of it.*

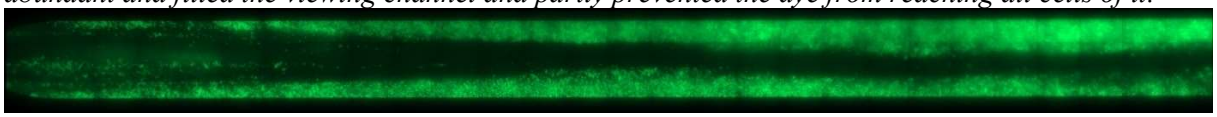

FIGURE 41. Epifluorescence microscopy picture of ΔampA (Tn1433) TCH1516. *The biofilm looks like the other TCH1516 transduced strains, there is biofilm of the walls of the viewing channel and one fluidic channel formed by the shear-flow.*

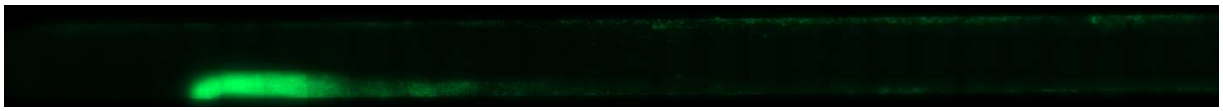

FIGURE 42. Epifluorescence microscopy picture of ΔpgsA (Tn1732) UAS391. *Again this mutant failed to perform a biofilm like the parental strain. Similar effect was seen in figure 20.*

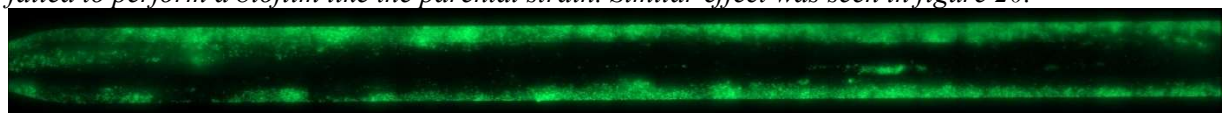

FIGURE 43. Epifluorescence microscopy picture of ΔpgsA (Tn1732) TCH1516. *In TCH1516 background ΔpgsA performed a lot more biofilm than the original mutant and in the UAS391 background. For comparison, see figures 21 and 42.*

6 DISCUSSION

6.1 Evaluation of the gene involvement in biofilm formation

The aim of the study was to find out whether the transposon mutated genes found in the screening are involved in biofilm formation of *S. aureus* USA300 UAS391 as well as to study the behavior of the gene in a φ11 transduced UAS391 Ery^S and TCH1516 Ery^S strains. The results look promising, however they differed from the screening, in which all strains showed decreased biofilm formation capacity as well as some showed changes in antibiotic susceptibility (mainly risen resistance). Each gene is analyzed individually in this discussion.

Transposon mutation in *psgA* resulted in decreased biofilm formation under flow conditions. However, the same trend could not be shown under static conditions. Growth curve analysis confirmed the absence of pleiotropic effects caused by the mutation, while the mutant did display an increase in resistance towards ciprofloxacin from 0.38 (wild-type) into 1.5µg/ml. The RT-PCR revealed that due to the mutation the expression levels dropped to 0.6 -fold in planktonic cells and to 0.8 -fold in biofilm cells, meaning that there was still some expression of *pgsA*, however less than in the parental strain. The biofilm phenotype did not change significantly when the mutation was transduced into a different background. The *psgA* gene codes for CDP-diacylglycerol-glycerol-3-phosphate 3-phosphatidyl-transferase (glycerol-phosphate phosphatidyltransferase) in USA300_FPR3757 (http://aureowiki.med.unigreifs-wald.de/ SAUSA300_1176, access date 1.3.2018). Earlier the same gene has been associated with daptomycin resistance (Peleg et al., 2012). Daptomycin is a cyclic lipopeptide antibiotic produced by *Streptomyces roseosporus* (Steenbergen, Alder, Thorne, & Tally, 2005). It has been studied as a knockout in *Escherichia coli* (*E. coli*) where it caused growth arrest (Suzuki, Hara, & Matsumoto, 2002). Involvement of *pgsA* in biofilm formation has not earlier been studied in *S. aureus*. PgsA is a component of the membrane and it participates in the biosynthesis of fatty acids and phospholipids (http://www.ebi.ac.uk/interpro/entry/IPR004570, access date 6.3.2018). Fatty acids are known to affect biofilm formation, as fatty acid kinase A (*fakA*) has been shown to inhibit biofilm formation in *S. aureus* USA300 strain (Sabirova et al., 2011). Therefore, *pgsA* involvement in biofilm formation is not far-fetched, even though it could not be proven with these data. Overall, *pgsA* is an interesting target for future research due to its possible effect on antibiotic susceptibility.

Tn1354 has a mutation in the clumping factor B gene, *clfB*. In the results, the disruption of *clfB* could be noticed as 70% biofilm formation compared to the parental strain UAS391 Ery^S (p=0.001). The RT-PCR results suggest that both planktonic and biofilm cells have 2.1 and 2.7 -fold increase in expression of *clfB*, however, this cannot be stated with confidence due to the large standard deviation, as well as the efficiencies of standard curves were not ideal. The transduction did not reveal significant differences in biofilm formation according to the static assay and the growth curve, however in the epifluorescence microscopy image, to a naked eye, they seemed to form less biofilm than the parental, the wild-type strain and the original transposon mutant. The transduced mutant in the TCH1516 background formed less biofilm than the UAS391 Ery^S parental strain, however the results were the same as for the TCH1516 Ery^S parental strain, and therefore remain indefinite. According to previous studies of *clfB*, it is a cell-wall anchored protein and it functions in cell adhesion by binding fibrinogen, but not in the presence of cofactors, such as Ca^{2+} and Mn^{2+} (Eldhin et al., 1998). It has also been shown that ClfB is important for biofilm formation in calcium-chelating conditions in *S. aureus* USA300 JE2 strain. In the same study, the strains were also aureolysin (an extracellular metalloprotease) depleted, and in the presence of aureolysins the ClfB-mediated biofilms could not grow. Therefore, it was hypothesized that aureolysins might degrade ClfB (Abraham & Jefferson, 2012). Lantibiotics have also been shown to decrease staphylococcal infections and adhesion to polystyrene surfaces by preventing FnBP and ClfB functions in adhesion (Pimentel-Filho, Martins, Nogueira, Mantovani, & Vanetti, 2014). As the ClfB has been reported to participate in biofilm formation, a decrease in biofilm formation detected in this study as well as in the preliminary screening supports earlier research. However, it would be advisable to redo the RT-PCT and image more dynamic biofilms to get more statistical assurance.

Tn0123 is a strain with a mutation in the non-ribosomal peptide synthetase *ausA*. The tests with transposon mutants and transduced UAS391 Ery^S mutants did not reveal a significant difference between the mutant and the parental strain. No changes were detected in growth rate nor in the MIC tests of antibiotics. The transposon insertion is in the operon, within the last third of the gene. According to the RT-PCR data, the expression of *ausA* was very low, fold-change close to zero in both planktonic and biofilm cells, compared to the parental strain, which likely explains the results. A slight uncertainty to the results comes from low R^2 values of the standard curves, and the results would need more repetitions to confirm the expression level. In the TCH1516 transduced mutant differences were seen: the static biofilm was 151% thicker compared to the TCH1516 parental strain ($p < 0.001$). The parental strain UAS391 Ery^S was

142% compared to TCH1516. The disruption of the *ausA* gene seems, therefore, to have increased the biofilm growth after transduction into TCH1516. The same result was seen in the growth curve (page 56) in which the *ΔausA* grew similarly to the original parental strain UAS391 Ery^S (p=0.257) than the transduction recipient strain TCH1516 (p=0.038). On the other hand, the dynamic biofilm of *ΔausA* in TCH1516 (figure 35, page 58) showed less biofilm formation, while the original transposon mutant (figure 17, page 49) produced similar biofilm as the parental strain. According to earlier studies, *ausA* belongs to a protein family of AMP-binding enzymes (http://aureowiki.med.uni-greifswald.de/SAUSA300 _0181, access date 7.1.2017). The *aus* gene cluster codes for a highly conserved non-ribosomal peptide synthetase (D. Wilson, Shi, Teitelbaum, Gulick, & Aldrich, 2013) It has been reported that the *aus* gene cluster produces cyclic dipeptides aureusimines A and B (tyrvalin and phevalin, respectively, also referred to as pyrazinones), which upon discovery where mistakenly deemed to be involved in virulence (Sun et al., 2010; Wyatt et al., 2010). Secor *et al*. have found out that AusB protein amount is higher in *S. aureus* biofilms than in planktonic cells (Secor et al., 2012). While the biological function of the AusA stays undiscovered, in the light of the results of this study, it might have different roles in different *S. aureus* strains regarding biofilm formation, despite the conserved structure of the protein.

In the case of transposon mutant Tn0002, the mutation had occurred in the HAD superfamily hydrolase gene. In the results obtained in this study, the static assay revealed an increased biofilm formation capacity, which was 21 percentage units higher than the parental strain UAS391 Ery^S (p=0.023) and 44 percentage units higher than the wild-type UAS391 (p<0.001). The same pattern did not show in the static assay of the transduced strains where significant differences were not detected. The dynamic assay revealed a clumpy-looking biofilm in the transposon mutant (figure 15, page 48), but the transduced strains looked the same as the parental strains (figures 30 and 31, page 58). In the growth curves no changes in growth patterns were detected nor any changes in the MIC test of antibiotics. Notable is, that the transposon mutation did not necessarily cause a knockout gene, but might have yielded a production of truncated proteins that still can somewhat function as purposed because the transposon insertion was located within the last third of the gene. The RT-PCR results imply that there is a 3.5-fold increase of expression in the biofilm cells compared to the parental strain and a 1.2-fold increase in planktonic cells. However, the standard deviation being very high in biofilm PCR results, more repetitions should be done to verify the result. The exact function of this hydrolase enzyme has not been described in literature, but haloacid dehalogenase-like hydrolases are known to

comprise a variety of enzymes with a wide array of functions from ATPases to phosphatases and haloacid dehalogenases with actions such as cation (Mg^{2+}) transport and phosphorylating ATP (Ridder & Dijkstra, 1999). By finding out the exact enzyme target, it could be possible to also find out its involvement in biofilm formation, which herein, despite the interesting static assay results and the dynamic biofilm result, stays unconfirmed.

Tn0428 has a mutation in the oligopeptide ABC transporter substrate-binding protein coding gene *oppA*. It is a lipid-anchored cell-wall protein and transports metallophores (cation and nickel transport) The operon also contains the *oppF*. *oppB* and *oppC* genes, which function together when translated (http://aureowiki.med.uni-greifswald.de/SAUSA300_0891, access date 1.3.2018). In the static assay, the mutant strain gave a significantly higher biofilm result, 133% compared to the parental strain UAS391 Ery^S ($p=0.003$). Growth rates did not differ significantly, nor did the MIC results. The transposon insertion is in the operon, within the last third of the gene length and in the middle of a coding sequence. RT-PCR data suggested a slight negative fold-change (0.655) in planktonic cells and a mild positive fold-change in biofilm cells (1.1). However, the standard deviation was large, and more repetitions would be needed to confirm the results. In the transduced strains, no significant difference was noticed between the mutants and the parental strains. The dynamic biofilms of both the original mutant as well as the transduced mutant in the UAS391 Ery^S background grew poorly, when visually compared to the parental strain. This was not noticed in the THC1516 transduced mutant. According to PubMed (access date 1.3.2018), *oppA* has no earlier reports about being associated with the *S. aureus* biofilm, but in *Vibrio fluvialis*, a knockout in *oppA* caused it to produce more biofilm than the wild-type (Lee et al., 2004). In the case of the transposon mutant, the static assay and RT-PCR results coincided with those results, where possible decreased expression of the gene led to increased biofilm formation. The location of the transposon might imply that despite the detected expression, the translated proteins might be truncated or dysfunctional, and therefore yield the thicker biofilm. The opposite results were detected in the dynamic assay of this study. The differences might be due to different substratum materials. The static assay result is, however, more reliable than the dynamic because of more repetitions. With these data, *oppA* could be linked to biofilm formation in USA300, but more experiments are needed to confirm the result.

Tn 1433 has a mutation in the cytosol aminopeptidase gene *ampA*. In USA300_FPR3757, it participates in amino acid metabolism by degrading peptides (http://aureowiki.med.uni-greifswald.de/SAUSA300_0845, access date 5.3.2018), most likely by hydrolysing leucine

http://www.genome.jp/dbget-bin/www_bget?saa:SAUSA300_0845, access date 22.3.2018). The results showed no significant difference between the mutant and the parental strain in any of the tests, including transduction. The RT-PCR result indicates that the expression levels of RNA are 1.9- and 1.7- fold higher after mutation than in the parental strain, but high standard deviations leave some uncertainty to the results, yet less than two-fold increase in expression are not considered major. Previously *ampA* has been studied in *E. coli,* in which it was found to remove N-terminal leucine from peptides and its cofactor is Mn^{2+} (http://www.uniprot.org/uniprot/ P68767, access date 5.3.2018) and in lactobacilli it has shown specificity to certain amino acid composition containing peptides (Christensen, Dudley, Pederson, & Steele, 1999). Overall, different kinds of aminopeptidases exist and their function is to recycle amino acids to subsequent use within the cell (Christensen et al., 1999; Dong et al., 2005). AmpA has no earlier reports about being associated with biofilm formation in *S. aureus*, nor in other bacteria in PubMed (access date 5.3.2018). In the light of the results of this study, at least direct contribution to biofilm formation of *ampA* seems unlikely.

Tn0007 transposon insertion was mapped to an intergenomic DNA sequence, a non-coding region. With these data it is not possible to say where in the genome the transposon insertion is and whether the region is, for example, a regulatory region. No changes in biofilm formation were detected in any of the experiments, nor the growth was harmed due to the transposon insertion. According to RT-PCR, hardly any expression was detected, which is logical as the region should not code for RNA. In the initial screening the mutation seemed to have caused a remarkable decrease of biofilm formation (35%), but according to the results of this large-scale characterization, the mutation most likely did not influence the biofilm formation despite the promising screening result.

6.2 About the methodology

The static assay is a classically used for screening, as the small volume of the media will cause nutrient depletion and accumulation of signaling molecules. However, the static assay is a very popular method and widely used for its straightforwardness and low cost (Benoit et al., 2010; Coenye & Nelis, 2010). The flow-system (Bioflux™ in this study) is more accurate when it comes to describing the biofilm formation, although in this study the analysis of the dynamic biofilms could not be performed due to lack of repetitions. When interpreting the results, it should be noted that the static assay was done on a polystyrene microplate and the dynamic (flow) biofilms grow on a polydimethylsiloxane (PDMS, silicone elastomer) tube. *S. aureus*

might use different adhesion molecules in adherence to the materials, not to mention glass wells that were tested with confocal microcopy. Also, should the mutation cause a decrease in biofilm formation, it cannot be indefinitely stated at this point that it would be caused by an incapability, as it can also be due to less efficient initial adherence to the surface. As well the biofilm formation might be slower, but not decreased by the effect of the mutation, which cannot now be distinguished. The results of the static assay and the dynamic biofilm do not however coincide, as they measure different things and the changes cannot necessarily detected in both cases. The problem with static assay is the persistently large standard deviation within the stain. The negative and positive controls (ATCC 6538 and 5437) were used to as controls between the plates and they seemed to perform in the assays in a much more consistent manner than the mutant strains. However, large variation within a bacterial strain, especially in the screening, were detected despite that the accuracy of the protocol has been studied (Stepanović, Vuković, Dakić, Savić, & Švabić-Vlahović, 2000). Therefore, technical faults can be considered as minor sources of error in the static assay. The biological variation is quite high when quantifying the biofilm with any of the biofilm methods used in this study, despite the constant conditions in the techniques. A good sign was, that growth of the strains was not harmed practically at all due to the transposon insert, as all the growth curves resembled each other and they all grew exponentially until they reached the stationary phase. None of the mutants entered the death phase, which would have shown as a declining curve after the stationary phase. Thus, the differences in biofilm formation capacity cannot be due to a change in growth of single cells.

The RT-PCR results were somewhat controversial, as in some of the samples the standard deviations were too large to make accurate conclusions. RT-PCR is prone to errors starting from the RNA quality to DNA contaminations and fluctuations in pipetting. To bring more accuracy to RT-PCR result interpretations standard curves were included in the measurements, even though the absolute quantification of the gene expression was not done. As the efficiencies of the standard curves (R^2, table 14 on page 52) stayed under 0.95 in many cases, in those instances the results can only be considered as guiding. The results were calculated from three replicates from one run. It would be advisable to re-run all the samples to obtain more statistical assurance. In the future, it would be advisable to also run the RT-PCR to transduced strains, which would again confirm the gene involvement in the strains in which biofilm formation was altered.

By imaging the biofilms, it is possible to obtain valuable information about the biofilm behavior in different conditions. The images taken for this study confirmed that the biofilms do not act

consistently despite the constant circumstances, as was seen from the dynamic biofilms (as well as the static assay, where the standard deviation of the replicates were high). However, when grown under a shear flow and with fresh nutrients, the biofilms grew into much more intricate structures than when grown in static conditions without fresh nutrients. Improvements to imaging the biofilm would be exopolysaccharide staining with for example FilmTracer™ SYPRO® Ruby biofilm matrix stain (Thermo Fisher Scientific Inc.) to distinguish the fluidic channels from the biofilm matrix components. Another improvement would be to be able to image all biofilms with confocal laser scanning microscope, which would make it possible to quantify the biofilm amount. It would give very valuable information about the biofilm, as the *in vivo* biofilms rarely grow in such a static environment that was created for the static biofilms in this study. Ideally, the biofilms would be observed with a time-lapse camera during the whole growth process, therefore the possible effects of each mutated gene could be evaluated from each phase of biofilm formation.

6.3 Conclusions

Seven selected knockout mutants from the *bursa aurealis* library were investigated to define the relationship between the inactivated genes and biofilm formation in *S. aureus*. According to the results obtained in this study, a further characterization of the genes *pgsA, ausA*, *HAD* and *oppA* might also reveal interesting results regarding biofilm formation. PgsA showed interesting results and even suggested a linkage between ciprofloxacin resistance and biofilm formation. In the future, this mutant phenotype should be reconfirmed with the experiments used in this thesis, and further knowledge should be broadened with complementation studies as well as RNA sequencing. Knockout mutation of *clfB* resulted in decreased biofilm formation, as has been extensively reported in literature. This confirms that the *bursa aurealis* library has potential value as a screening tool for genetic targets associated with biofilm formation. Furthermore, strains carrying a knockout mutation in genes which have already been associated with biofilm formation in scientific literature, could serve as a control for the tests in addition to the wild-type (UAS391), parental (UAS391 Ery^S) and non-biofilm-forming strain (*S. aureus* 5734) in future. This characterization is a contribution to the exhaustive search for genes involved in biofilm formation, which will hopefully lead to the discovery of critical genes for biofilm formation and subsequently to new therapeutic targets.

ACKNOWLEDGEMENTS

The journey of finishing this master's thesis has been long and winding. I deeply thank my supervisors PhD candidate Sarah De Backer and Professor Surbhi Malhotra-Kumar for inviting me in the laboratory and teaching me a great deal of microbiology.

I am grateful to Professor Herman Goossens and Christine Lammens for accepting me as a visitor to the Medical Faculty of the University of Antwerp. Secondly, I would like to thank Liesbeth Bryssinck for introducing me to the laboratory and teaching the techniques and guidelines of working, otherwise my encounters in the lab would have been even messier.

Many thanks to Professor Jean-Pierre Hernalsteens from Vrije Universiteit Brussel who introduced me to bacteriophage laboratory work and taught me many useful facts about them. Also thank you for letting us use your laboratory to our experiments.

Thank you, Tomi, Mattia, Michael and Matilda for adopting me to your lunch crew and making the lunch hour even more enjoyable. Also, I would like to thank the rest of staff and students of the laboratory: you have made my time in Antwerp unforgettable.

I would also like to express my gratitude to our Professor Sarah Butcher and Professor Benita Westerlund-Wikström and PhD Ritva Virkola from the University of Helsinki for supporting me with my adventurous exchange in my academic pursuits. Your guidance and insight made this project possible.

Lastly, special thanks to my family, for your emotional and financial support, my studies abroad would not have been possible without you. Thank you also for my dear friends who visited me in Antwerp and made me feel slightly less home sick during my time abroad.

In Helsinki, 9.4.2018

Katri Holappa

REFERENCES

Abraham, E. P., Phil Oxfd Chain, D. E., M Fletcher, C. C., Camb, M., D Gardner, M. A., Oxfd, D., … Adelaide, M. (1941). Further observations on penicillin. *The Lancet*, *2*, 177–188.

Abraham, N. M., & Jefferson, K. K. (2012). *Staphylococcus aureus* clumping factor B mediates biofilm formation in the absence of calcium. *Microbiology (United Kingdom)*, *158*(6), 1504–1512.

Archer, N. K., Mazaitis, M. J., William, J., Leid, J. G., Powers, M. E., & Shirtliff, M. E. (2011). *Staphylococcus aureus* biofilms: Properties, regulation and roles in human disease. *Virulence*, *2*(5), 445–459.

Arciola, C. R., Campoccia, D., Ravaioli, S., & Montanaro, L. (2015). Polysaccharide intercellular adhesin in biofilm: structural and regulatory aspects. *Frontiers in Cellular and Infection Microbiology*, *5*, Article 7.

Bae, T., Banger, A. K., Wallace, A., Glass, E. M., Åslund, F., Schneewind, O., & Missiakas, D. M. (2004). *Staphylococcus aureus* virulence genes identified by bursa aurealis mutagenesis and nematode killing. *PNAS*, *101*(33), 12312–12317.

Bae, T., Glass, E. M., Schneewind, O., & Missiakas, D. (2008). Generating a Collection of Insertion Mutations in the *Staphylococcus aureus* Genome Using bursa aurealis. In A. L. Osterman & S. Y. Gerdes (Eds.), *From: Methods in Molecular Biology: Microbial Gene Essentiality* (Vol. 416, pp. 103–116). Totowa, NJ: Humana Press Inc.

Barber, M. (1961). Methicillin-resistant staphylococci. *Journal of Clinical Pathology*, *14*, 385–393.

Beltrame, C. O., Cortes, M. F., Bonelli, R. R., De Almeida Correa, A. B., Nunes Botelho, A. M., Americo, M. A., … Sa Figueiredo, A. M. (2015). Inactivation of the autolysis-related genes lrgB and yycI in staphylococcus aureus increases cell Lysis-Dependent eDNA Release and enhances biofilm development in vitro and in vivo. *PLoS ONE*, *10*(9), 1–20.

Benoit, M. R., Conant, C. G., Ionescu-Zanetti, C., Schwartz, M., & Matin, A. (2010). New device for high-throughput viability screening of flow biofilms. *Applied and Environmental Microbiology*, *76*(13), 4136–4142.

Boyle-Vavra, S., Li, X., Alam, T., Read, T. D., Sieth, J., Cywes-Bentley, C., … Daum, R. S. (2015). USA300 and USA500 Clonal Lineages of *Staphylococcus aureus* Do Not Produce a Capsular Polysaccharide Due to Conserved Mutations in the cap5 Locus. *mBio*, *6*(2), e02585-14.

Bran, J. L., Levison, M. E., & Kaye, D. (1972). Survey for Methicillin-Resistant Staphylococci. *Antimicrobial Agents and Chemotherapy*, *1*(3), 235–236.

Bronesky, D., Wu, Z., Marzi, S., Walter, P., Geissmann, T., Moreau, K., … Romby, P. (2016). Staphylococcus aureus RNAIII and Its Regulon Link Quorum Sensing, Stress Responses, Metabolic Adaptation, and Regulation of Virulence Gene Expression. *Annual Review of Microbiology*, *70*, 299–316.

Brown, S., Santa Maria, J. P., & Walker, S. (2013). Wall Teichoic Acids of Gram-Positive Bacteria. *Annual Review of Microbiology*, *67*, 313–336.

Carrel, M., Perencevich, E. N., & David, M. Z. (2015). USA300 methicillin-resistant S*taphylococcus aureus*, United States, 2000-2013. *Emerging Infectious Diseases*, *21*(11), 1973–1980.

Centers for Disease Control and Prevention. (2001). Methicillin-Resistant *Staphylococcus aureus* Skin or Soft Tissue Infections in a State Prison --- Mississippi, 2000. *MMWR Morbidity and Mortality Weekly Report*, *50*, 919–922. Retrieved from https://www.cdc.gov/mmwr/preview/mmwrhtml/mm5042a2.htm

Centers for Disease Control and Prevention. (2003). Methicillin-Resistant *Staphylococcus aureus* Infections Among Competitive Sports Participants --- Colorado, Indiana, Pennsylvania, and Los Angeles County, 2000--2003. *MMWR Morb Mortal Wkly Rep*, *52*(5), 88. Retrieved from https://www.cdc.gov/mmwr/preview/mmwrhtml/mm5205a4.htm

Chabbert, Y. A. (1967). Behaviour of methicillin hetero-resistant staphylococci to cephaloridine. *Postgraduate Medical Journal*, *43*, Suppl 43:40-2.

Challagundla, L., Luo, X., Tickler, I. A., Didelot, X., Coleman, D. C., Shore, A. C., … Robinson, D. A. (2018). Range Expansion and the Origin of USA300 North American Epidemic Methicillin-Resistant *Staphylococcus aureus*. *mBio*, *9*(1), e02016-17.

Chambers, H. F., & Deleo, F. R. (2009). Waves of Resistance: *Staphylococcus aureus* in the Antibiotic Era. *Nature Reviews Microbiology*, *7*(9), 629–641.

Chatterjee, S. S., & Otto, M. (2013). Improved understanding of factors driving methicillin-resistant *Staphylococcus aureus* epidemic waves. *Clinical Epidemiology*, *5*(July), 205–217.

Christensen, J. E., Dudley, E. G., Pederson, J. A., & Steele, J. L. (1999). Peptidases and amino acid catabolism in lactic acid bacteria. *Antonie van Leeuwenhoek*, *76*, 217–246.

CLSI. (2014). *M100-S24 Performance Standards for Antimicrobial susceptibility testing*.

Coenye, T., & Nelis, H. J. (2010). In vitro and in vivo model systems to study microbial biofilm formation. *Journal of Microbiological Methods*, *83*(September), 89–105.

Crawford, E. C., Singh, A., Metcalf, D., Gibson, T. W., & Weese, S. J. (2014). Identification of appropriate reference genes for qPCR studies in *Staphylococcus pseudintermedius* and preliminary assessment of icaA gene expression in biofilm-embedded bacteria, *7*, 1–6.

Cue, D., Lei, M. G., & Lee, C. Y. (2013). Activation of sarX by Rbf is required for biofilm formation and icaADBC expression in *Staphylococcus aureus*. *Journal of Bacteriology*, *195*(7), 1515–1524.

Cue, D., Lei, M. G., Luong, T. T., Kuechenmeister, L., Dunman, P. M., O'Donnell, S., … Lee, C. Y. (2009). Rbf promotes biofilm formation by *Staphylococcus aureus* via repression of icaR, a negative regulator of icaADBC. *Journal of Bacteriology*, *191*(20), 6363–6373.

DeLeo, F. R., Otto, M., Kreiswirth, B. N. B., & Chambers, H. F. H. (2010). Community-associated meticillin-resistant *Staphylococcus aureus*. *The Lancet*, *375*(9725), 1557–1568.

Diep, B. A., Gill, S. R., Chang, R. F., Phan, T. H., Chen, J. H., Davidson, M. G., … Perdreau-Remington, F. (2006). Complete genome sequence of USA300, an epidemic clone of community-acquired meticillin-resistant *Staphylococcus aureus*. *Lancet*, *367*(9512), 731–739.

Diep, B. A., & Otto, M. (2008). The role of virulence determinants in community-associated MRSA pathogenesis. *Trends in Microbiology*, *16*(8), 361–369.

Diep, B. A., Stone, G. G., Basuino, L., Graber, C. J., Miller, A., des Etages, S.-A., … Chambers, H. F. (2008). The arginine catabolic mobile element and staphylococcal chromosomal cassette mec linkage: convergence of virulence and resistance in the USA300 clone of methicillin-resistant *Staphylococcus aureus*. *The Journal of Infectious Diseases*, *197*(11), 1523–30.

Dong, L., Cheng, N., Wang, M.-W., Zhang, J., Shu, C., Zhu, D.-X., … Zhu, X. (2005). The leucyl aminopeptidase from Helicobacter pylori is an allosteric enzyme. *Microbiology*, *151*, 2017–2023.

Donlan, R. M. (2002). Biofilms: Microbial life on surfaces. *Emerging Infectious Diseases*, *8*(9), 881–890.

Dunne, W. M. J. (2002). Bacterial Adhesion: Seen Any Good Biofilms Lately? *Clinical Microbiology Reviews*, *15*(2), 155–155.

Eldhin, D. N., Perkins, S., Francois, P., Vaudaux, P., Höök, M., & Foster, T. J. (1998). Clumping factor B (ClfB), a new surface-located fibrinogen-binding adhesin of *Staphylococcus aureus*. *Molecular Microbiology*, *30*(2), 245–257.

Ellington, M. J., Yearwood, L., Ganner, M., East, C., & Kearns, A. M. (2008). Distribution of the ACME-arcA gene among methicillin-resistant *Staphylococcus aureus* from England and Wales. *Journal of Antimicrobial Chemotherapy*, *61*, 73–77.

Fey, P. D., Endres, J. L., Yajjala, V. K., Widhelm, T. J., Boissy, R. J., Bose, J. L., & Bayles, K. W. (2013). A genetic resource for rapid and comprehensive phenotype screening of nonessential *Staphylococcus aureus* genes. *mBio*, *4*(1), 1–8.

Figueiredo, A. M. S., Ferreira, F. A., Beltrame, C. O., & Côrtes, M. F. (2017). The role of biofilms in persistent infections and factors involved in ica -independent biofilm development and gene regulation in *Staphylococcus aureus*. *Critical Reviews in Microbiology*, *Online pub*, 1–19.

Fitzpatrick, F., Humphreys, H., & O'Gara, J. P. (2005). Evidence for icaADBC-independent biofilm development mechanism in methicillin-resistant *Staphylococcus aureus* clinical isolates. *Journal of Clinical Microbiology*, *43*(4), 1973–1976.

Flemming, H.-C., Wingender, J., Szewzyk, U., Steinberg, P., Rice, S. A., & Kjelleberg, S. (2016). Biofilms: an emergent form of bacterial life. *Nature Reviews Microbiology*, *14*(9), 563–575.

Gross, M., Cramton, S. E., Tz, F. G., & Peschel, A. (2001). Key Role of Teichoic Acid Net Charge in *Staphylococcus aureus* Colonization of Artificial Surfaces. *Infection and Immunity*, *69*(5), 3423–3426.

Götz, F. (2002). *Staphylococcus* and biofilms. *Molecular Microbiology*, *46*(6), 1367–1378.

Hall, B. G., Acar, H., Nandipati, A., & Barlow, M. (2014). Growth rates made easy. *Molecular Biology and Evolution*, *31*(1), 232–238.

Heilmann, C., Schweitzer, O., Gerke, C., Vanittanakom, N., Mack, D., & Götz, F. (1996). Molecular basis of intercellular adhesion in the biofilm-forming *Staphylococcus epidermidis*. *Molecular Microbiology*, *20*(5), 1083–1091.

Herzberg, O., & Moult, J. (1987). Bacterial Resistance to beta-Lactam Antibiotics: Crystal Structure of beta-Lactamase from *Staphylococcus aureus* PCi at 2.5 Å Resolution. *Science*, *236*(4802), 694–701.

Hope, R., Livermore, D. M., Brick, G., & Lillie, M. (2008). Non-susceptibility trends among staphylococci from bacteraemias in the UK and Ireland, 2001– 06. *Journal of Antimicrobial Chemotherapy*, *62*(Supplement 2), ii65-ii74.

Iandolo, J. J., Worrell, V., Groicher, K. H., Qian, Y., Tian, R., Kenton, S., … Roe, B. A. (2002). Comparative analysis of the genomes of the temperate bacteriophages φ11, φ12 and φ13 of *Staphylococcus aureus* 8325. *Gene*, *289*(1–2), 109–118.

Jey, Y., Alsad, L., Vogel, F., Koppar, S., Auguste, F., Seymour, J., … Nevarez, L. (2013). Interactions between Candida albicans and *Staphylococcus aureus* within mixed species biofilms. *Bios*, *84*(1), 30–39.

Katayama, Y., Ito, T., & Hiramatsu, K. (2000). A new class of genetic element, staphylococcus cassette chromosome mec, encodes methicillin resistance in *Staphylococcus aureus*. *Antimicrobial Agents and Chemotherapy*, *44*(6), 1549–55.

Kirby, W. M. M. (1944). Extraction of a highly potent penicillin inactivator form penicillin resistant Staphylococci. *Science*, *99*(2579).

Lacey, K. A., Geoghegan, J. A., & McLoughlin, R. M. (2016). The Role of *Staphylococcus aureus* Virulence Factors in Skin Infection and Their Potential as Vaccine Antigens. *Pathogens*, *5*, 22–39.

Lampe, D. J., Churchill, M. E., & Robertson, H. M. (1996). A purified mariner transposase is sufficient to mediate transposition in vitro. *The EMBO Journal*, *15*(19), 5470–9.

Lauderdale, K. J., Boles, B. R., Cheung, A. L., & Horswill, A. R. (2009). Interconnections between sigma b, agr, and proteolytic activity in *Staphylococcus aureus* biofilm maturation. *Infection and Immunity*, *77*(4), 1623–1635.

Le, K. Y., & Otto, M. (2015). Quorum-sensing regulation in staphylococci — an overview. *Frontiers in Microbiology*, *6*(Article 1174).

Lee, E. M., Ahn, S. H., Park, J. H., Lee, J. H., Ahn, S. C., & Kong, I. S. (2004). Identification of oligopeptide permease (opp) gene cluster in *Vibrio fluvialis* and characterization of biofilm production by oppA knockout mutation. *FEMS Microbiology Letters*, *240*(1), 21–30.

Li, S., Huang, H., Rao, X., Chen, W., Wang, Z., & Hu, X. (2014). Phenol-soluble modulins: novel virulence-associated peptides of staphylococci. *Future Microbiology*, *9*(2), 203–16.

Life technologies. (2014). Real-time PCR handbook.

Lindenmayer, J., Schoenfeld, S., O'Grady, R., & Carney, J. (1998). Methicillin-Resistant *Staphylococcus aureus* in a High School Wrestling Team and the Surrounding Community. *Archives of Internal Medicine*, *158*, 895–899.

Liu, J., Chen, D., Peters, B. M., Li, L., Li, B., Xu, Z., & Shirliff, M. E. (2016). Staphylococcal chromosomal cassettes mec (SCCmec): A mobile genetic element in methicillin-resistant *Staphylococcus aureus*. *Microbial Pathogenesis*, *101*, 56–67.

Livak, K. J., & Schmittgen, T. D. (2001). Analysis of relative gene expression data using real-time quantitative PCR and. *Methods*, *25*, 402–408.

McCann, M. T., Gilmore, B. F., & Gorman, S. P. (2008). *Staphylococcus epidermidis* device-related infections: pathogenesis and clinical management. *Journal of Pharmacy and Pharmacology*, *60*(12), 1551–1571.

McCarthy, H., Rudkin, J. K., Black, N. S., Gallagher, L., O'Neill, E., & O'Gara, J. P. (2015). Methicillin resistance and the biofilm phenotype in *Staphylococcus aureus*. *Frontiers in Cellular and Infection Microbiology*, *5*(1).

Moormeier, D. E., & Bayles, K. W. (2017). *Staphylococcus aureus* biofilm: a complex developmental organism. *Molecular Microbiology*, *104*(3), 365–376.

Mootz, J. M., Benson, M. A., Heim, C. E., Crosby, H. A., Kavanaugh, J. S., Dunman, P. M., … Horswill, A. R. (2015). Rot is a key regulator of *Staphylococcus aureus* biofilm formation. *Molecular Microbiology*, *96*(2), 388–404.

Myint, A. A., Lee, W., Mun, S., Ahn, C. H., Lee, S., & Yoon, J. (2010). Influence of membrane surface properties on the behavior of initial bacterial adhesion and biofilm development onto nanofiltration membranes. *Biofouling*, *26*(3), 313–321.

O'Gara, J. P. (2007). ica and beyond: Biofilm mechanisms and regulation in *Staphylococcus epidermidis* and *Staphylococcus aureus*. *FEMS Microbiology Letters*, *270*(2), 179–188.

O'Neill, E., Pozzi, C., Houston, P., Humphreys, H., Robinson, D. A., Loughman, A., … O'Gara, J. P. (2008). A novel *Staphylococcus aureus* biofilm phenotype mediated by the fibronectin-binding proteins, FnBPA and FnBPB. *Journal of Bacteriology*, *190*(11), 3835–3850.

O'Toole, G. A. (2011). Microtiter Dish Biofilm Formation Assay. *Journal of Visualized Experiments*, *47*.

Olson, M. (2014). Bacteriophage Transduction in *Staphylococcus aureus*. In *Methods in Molecular Biology* (pp. 257–284). Springer Science+Business Media New York.

Otto, M. (2008). Staphylococcal biofilms. *Current Topics in Microbiology and Immunology*, *322*, 207–228.

Pantosti, A., Sanchini, A., & Monaco, M. (2007). Mechanisms of antibiotic resistance in *Staphylococcus aureus*. *Future Microbiology*, *2*(3), 323–334.

Pantosti, A., & Venditti, M. (2009). What is MRSA? *European Respiratory Journal*, *34*(5), 1190–1196.

Parker, D., & Prince, A. (2012). Immunopathogenesis of *Staphylococcus aureus* Pulmonary Infection. *Seminars in Immunopathology*, *34*(2), 281–297.

Peleg, A. Y., Miyakis, S., Ward, D. V., Earl, A. M., Rubio, A., Cameron, D. R., … Eliopoulos, G. M. (2012). Whole genome characterization of the mechanisms of daptomycin resistance in clinical and laboratory derived isolates of *Staphylococcus aureus*. *PLoS ONE*, *7*(1), e28316.

Periasamy, S., Joo, H.-S., Duong, A. C., Bach, T.-H. L., Tan, V. Y., Chatterjee, S. S., … Otto, M. (2012). How *Staphylococcus aureus* biofilms develop their characteristic structure. *PNAS Proceedings of the National Academy of Sciences of the United States of America*, *109*(4), 1281–1286.

Peschel, A., & Otto, M. (2013). Phenol-soluble modulins and staphylococcal infection. *Nature Reviews Microbiology*, *11*(10), 664–673.

Pimentel-Filho, N. de J., Martins, M. C. de F., Nogueira, G. B., Mantovani, H. C., & Vanetti, M. C. D. (2014). Bovicin HC5 and nisin reduce *Staphylococcus aureus* adhesion to polystyrene and change the hydrophobicity profile and Gibbs free energy of adhesion. *International Journal of Food Microbiology*, *190*, 1–8.

Pinho, M. G., Kjos, M., & Veening, J.-W. (2013). How to get (a)round: mechanisms controlling growth and division of coccoid bacteria. *Nature Reviews Microbiology*, *11*(9), 601–614.

Pozzi, C., Waters, E. M., Rudkin, J. K., Schaeffer, C. R., Lohan, A. J., Tong, P., … O'Gara, J. P. (2012). Methicillin resistance alters the biofilm phenotype and attenuates virulence in *Staphylococcus aureus* device-associated infections. *PLoS Pathogens*, *8*(4).

Reffuveille, F., Josse, J., Vallé, Q., Josse, J., Mongaret, C., & Gangloff, S. C. (2017). *Staphylococcus aureus* Biofilms and their Impact on the on the Medical Field. *The Rise of Virulence and Antibiotic Resistance in Staphylococcus Aureus*.

Ridder, I. S., & Dijkstra, B. W. (1999). Identification of the Mg2+-binding site in the P-type ATPase and phosphatase members of the HAD (haloacid dehalogenase) superfamily by structural similarity to the response regulator protein CheY. *The Biochemical Journal*, *339*, 223–226.

Robinson, D. A., & Enright, M. C. (2004). Multilocus sequence typing and the evolution of methicillin-resistant *Staphylococcus aureus*. *Clinical Microbiology and Infection*, *10*(2), 92–97.

Rohde, H., Frankenberger, S., Ahringer, U., & Mack, D. (2010). Structure, function and contribution of polysaccharide intercellular adhesin (PIA) to *Staphylococcus epidermidis* biofilm formation and pathogenesis of biomaterial-associated infections. *European Journal of Cell Biology*, *89*, 103–111.

Rose, H. R., Holzman, R. S., Altman, D. R., Smyth, D. S., Wasserman, G. A., Kafer, J. M., … Shopsin, B. (2015). Cytotoxic virulence predicts mortality in nosocomial pneumonia due to methicillin-resistant *Staphylococcus aureus*. *Journal of Infectious Diseases*, *211*, 1862–1874.

Rutherford, S. T., & Bassler, B. L. (2012). Bacterial quorum sensing: its role in virulence and possibilities for its control. *Cold Spring Harbor Perspectives in Medicine*, *2*(a012427).

Sabirova, J. S., Hernalsteens, J.-P., De Backer, S., Xavier, B. B., Moons, P., Turlej-Rogacka, A., … Malhotra-Kumar, S. (2011). Fatty acid kinase A is an important determinant of biofilm formation in *Staphylococcus aureus* USA300. *BMC Genomics*, *16*.

Sabirova, J. S., Xavier, B. B., Hernalsteens, J.-P., De Greve, H., Ieven, M., Goossens, H., & Malhotra-Kumar, S. (2014). Complete Genome Sequences of Two Prolific Biofilm-Forming *Staphylococcus aureus* Isolates Belonging to USA300 and EMRSA-15 Clonal Lineages. *Genome Announcements*, *2*(3), e00610-14.

Sanderson, M., Smith, I., Parker, I., & Bootman, M. (2014). Fluorescence Microscopy. In *Cold Spring Harb Protocols Fluorescence Microscopy: From Principles to Biological Applications* (pp. 97–142). Cold Spring Harbor Laboratory Press.

Sauer, K., Camper, A. K., Ehrlich, G. D., Costerton, J. W., & Davies, D. G. (2002). *Pseudomonas aeruginosa* displays multiple phenotypes during development as a biofilm. *Journal of Bacteriology*, *184*(4), 1140–1154.

Secor, P. R., Jennings, L. K., James, G. A., Kirker, K. R., Pulcini, E. de L., McInnerney, K., … Stewart, P. S. (2012). Phevalin (aureusimine B) production by *Staphylococcus aureus* biofilm and impacts on human keratinocyte gene expression. *PLoS ONE*, *7*(7).

Sihto, H.-M., Tasara, T., Stephan, R., & Johler, S. (2014). Validation of reference genes for normalization of qPCR mRNA expression levels in *Staphylococcus aureus* exposed to osmotic and lactic acid stress conditions encountered during food production and preservation. *FEMS Microbiology Letters*, *365*, 134–140.

Singh, R., & Ray, P. (2014). Quorum sensing-mediated regulation of staphylococcal virulence and antibiotic resistance. *Future Microbiology*, *9*(5), 669–81.

Soong, G., Martin, F. J., Chun, J., Cohen, T. S., Ahn, D. S., & Prince, A. (2011). *Staphylococcus aureus* protein A mediates invasion across airway epithelial cells through activation of RhoA GTPase signaling and proteolytic activity. *The Journal of Biological Chemistry*, *286*(41), 35891–35898.

Steenbergen, J. N., Alder, J., Thorne, G. M., & Tally, F. P. (2005). Daptomycin: a lipopeptide antibiotic for the treatment of serious Gram-positive infections. *Journal of Antimicrobial Chemotherapy*, *55*(3), 283–288.

Stepanović, S., Vuković, D., Dakić, I., Savić, B., & Švabić-Vlahović, M. (2000). A modified microtiter-plate test for quantification of staphylococcal biofilm formation. *Journal of Microbiological Methods*, *40*(2), 175–179.

Sun, F., Cho, H., Jeong, D. W., Li, C., He, C., & Bae, T. (2010). Aureusimines in *Staphylococcus aureus* Are Not Involved in Virulence. *PLoS ONE*, *5*(12).

Suzuki, M., Hara, H., & Matsumoto, K. (2002). Envelope Disorder of *Escherichia coli* Cells Lacking Phosphatidylglycerol. *Journal of Bacteriology*, *184*(19), 5418–5425.

Thomas, C. M., & Nielsen, K. M. (2005). Mechanisms of, and barriers to, horizontal gene transfer between bacteria. *Nature Reviews Microbiology*, *3*(9), 711–721.

Thurlow, L. R., Joshi, G. S., Clark, J. R., Spontak, J. S., Neely, C. J., Maile, R., & Richardson, A. R. (2013). Functional Modularity of the Arginine Catabolic Mobile Element Contributes to the Success of USA300 Methicillin-Resistant *Staphylococcus aureus*. *Cell Host & Microbe*, *13*(1), 100–107.

Vandenesch, F., Naimi, T., Enright, M. C., Lina, G., Nimmo, G. R., Heffernan, H., … Etienne, J. (2003). Community-Acquired Methicillin Resistant *Staphylococcus aureus* Carrying Panton-Valentine Leukocidin Genes: Worldwide Emergence. *Emerging Infectious Diseases*, *9*(8), 978–984.

Vanegas Múnera, J. M., Ocampo Ríos, A. M., Urrego, D. M., & Jiménez Quiceno, J. N. (2017). In vitro susceptibility of methicillin-resistant *Staphylococcus aureus* isolates from skin and soft tissue infections to vancomycin, daptomycin, linezolid, and tedizolid. *The Brazilian Journal of Infectious Diseases*.

Vanhommerig, E., Moons, P., Pirici, D., Lammens, C., Hernalsteens, J. P., De Greve, H., … Malhotra-Kumar, S. (2014). Comparison of biofilm formation between major clonal lineages of methicillin resistant *Staphylococcus aureus*. *PLoS ONE*, *9*(8), 1–8.

Wen, S., Chen, X., Xu, F., & Sun, H. (2016). Validation of Reference Genes for Real-Time Quantitative PCR (qPCR) Analysis of Avibacterium paragallinarum. *PLoS ONE*, *11*(12), e0167736.

Wertheim, H. F. L., Melles, D. C., Vos, M. C., Leeuwen, W. Van, Belkum, A. Van, Verbrugh, H. a, & Nouwen, J. L. (2005). Review The role of nasal carriage in *Staphylococcus aureus* infections. *The Lancet Infectious Diseases*, *5*, 751–762.

Wilson, D., Shi, C., Teitelbaum, A. M., Gulick, A. M., & Aldrich, C. C. (2013). Characterization of AusA: A Dimodular Nonribosomal Peptide Synthetase Responsible for Production of Aureusimine Pyrazinones. *Biochemistry*, *52*(5), 926–937.

Wilson, M. (2001). Bacterial biofilms and human disease. *Science Progress*, *84*(3), 235–254.

Wyatt, M. A., Wang, W., Roux, C. M., Beasley, F. C., Heinrichs, D. E., Dunman, P. M., & Magarvey, N. A. (2010). *Staphylococcus aureus* nonribosomal peptide secondary metabolites regulate virulence. *Science*, *329*(5989), 294–296.

Zapotoczna, M., O'Neill, E., & O'Gara, J. P. (2016). Untangling the Diverse and Redundant Mechanisms of *Staphylococcus aureus* Biofilm Formation. *PLoS Pathogens*, *12*(7), 1–6.

Internet references

AureoWiki http://aureowiki.med.uni-greifswald.de/Main_Page (access date 15.2.2018)

Basic local alignment search tool by NCBI (Blastn) www.blast.ncbi.nlm.nih.gov (access date 15.2.2017)

GenomeNet http://www.genome.jp/ (access date 22.3.2018)

PubMed https://www.ncbi.nlm.nih.gov/pubmed/ (access date 1.3.2018)

UniProt http://www.uniprot.org/ (access date 15.2.2017)

APPENDICES

APPENDIX I. – Real-time RT-PCR primers (designed inhouse)

Primers	Primer sequence
qPCR GyrB-F	5’ – GTAACACGTCGTAAATCAGCG - 3’
qPCR GyrB-R	5’ – CGTAATGGTAAAATCGCCTGC - 3’
RTTn0002CDR-F	5’ - ATGGTGGTGCATAAGCCACT-3’
RTTn0002CDR-R	5’ – TGTCGGCGTTAAACCAAACG -3’
RTTn0002HAD-F	5’ – ACGGGACAAGATACAACCGAC -3’
RTTn0002HAD-R	5’ – TGGCTTCTCATAGGCATCCG -3’
RTTn0007-F	5’ – TACGATACCGGCAACTGGTC -3’
RTTn0007-R	5’ – GGTGTAATTCCCAACCGGCA -3’
RTTn0123-F	5’ – TTGGCTGTATCATTGGGCAC -3’
RTTn0123-R	5’ – ACCTCGTGGCGAAATGTGAT -3’
RTTn0428-F	5’ – AGGGGAATCTGGTTGCGGTA -3’
RTTn0428-R	5’ – GCCATTTGCGTTTCCTTTTGC -3’
RTTn1354-F	5’ – TCACCATCAGCACTTCCACC -3’
RTTn1354-R	5’ – ACCGAGCAAAGGCACCTAAA -3’
RTTn1732-F	5’ – TCGTAAGTGCAGCTGGTCAA -3’
RTTn1732-R	5’ – TCAATGTTGCCAATGGATCACC -3’
RTTn0460-F	5’ - TGATGAGCGATTTGATTTGAAAGAG-3’
RTTn0460-R	5’ - TGCACTTTTCCCTTTCTGGTTTC-3’
Tn1433-F	5’-TATTGTCGGAGTGCTTGCGT-3’
Tn1433-R	5’-GCAGCAGCTTTATCATCGCC-3’
Tn0123-F	5’-TCGTTTGTTACCCGATGGCA-3’
Tn0123-R	5’-TGGCATAGCAAGTGTTCGGT-3’
Tn0428-F	5’-AGACTTACAAGCCGGTGCAT-3’
Tn0428-R	5’-CCATTAGGCCTTTCGCAAT-3’

APPENDIX II. – Media. buffers and solutions used in this study

Media used for culturing transposon strains and control strains.

Medium	Manufacturer	Ingredients	Preparation
BBL™ Müller-Hinton II Broth (cation adjusted)	Becton-Dickinson	Beef Extract 3.0 g/l. Acid Hydrolysate of Casein 17.5 g/l. Starch 1.5 g/l	22 g/l in distilled water. autoclave
BBL™ Brain-Heart Infusion Broth (BHI)	Becton-Dickinson	Brain Heart. Infusion from (solids) 6.0g/l Peptic Digest of Animal Tissue 6.0g/l Pancreatic Digest of Gelatin 14.5g/l Dextrose 3.0 g/l Sodium Chloride 5.0 g/l Disodium Phosphate 2.5 g/l	37 g/l powder in distilled water. autoclave
Luria Broth	Sigma Aldrich	Tryptone 10 g/l. Yeast Extract 5 g/l. NaCl 5 g/l	20 g/l in distilled water. then autoclaved
Horse blood agar	Sigma Aldrich	Agar 15 g/l. Meat extract 10 g/l. Peptone 10 g/l. Sodium chloride 5 g/l Defibrinated horse blood	40g/l blood agar base. autoclave. before plating add 60ml/l horse blood
Müller-Hinton agar		See BBL™ Müller-Hinton II Broth (cation adjusted)	22 g/l MH Broth powder. 15g/l Bacto agar in distilled water. autoclave. pour when cooled to 50°C
BHI agar with erythromycin	Sigma Aldrich	See BBL™ Brain-Heart Infusion broth	20 g/l in distilled water. then autoclaved. before plating add 5 µg/ml erythromycin
Bacto™ Agar	Becton-Dickinson		15 g/l with wanted medium base. autoclave. pour when cooled to 50°C

Media used for the transduction of the transposon strains

Medium/solution	**Preparation**
1 M Calcium chlorate stock solution ($CaCl_2$)	Weigh 110.98g and dissolve into 800 ml distilled water. volume adjusted to 1L of distilled water. autoclaved
0.02M Sodium citrate solution	0.59g in 100 ml distilled water. autoclaved
Citric acid stock solution	21g in 1l distilled water
Sodium citrate stock	14.7g sodium citrate in 500 ml distilled water
10% Sodium citrate solution	82 ml of citric acid solution mixed with 18 ml of sodium citrate solution and distilled water added up to 500 ml. pH adjusted to 6.0 with 1M NaOH (40g in 1L distilled water). final volume adjusted to 1L with distilled water. autoclaved
Phage broth	Oxoid™ Nutrient broth No. 2 (Thermo Fisher Scientific Inc.) 20 g/l in distilled water. autoclaved - *Contents: 'Lab-Lemco' powder 8.0 g. Peptone 8.0 g. Sodium chloride 4.0 g*
Phage base agar with 10 mM $CaCl_2$	Phage broth and 10 g/L of agar (15g phage broth and 7.5g agar in 750 ml)- autoclaved. 5 ml of 1M $CaCI_2$ added in 495 ml of top agar after melting
Phage top agar with 10 mM $CaCl_2$	Phage broth and 3.5 g/l of agar (15g phage broth and 2.63g agar in 750 ml). autoclaved. 7.5 ml $CaCl_2$ added in 742.5 ml of base agar after melting
LB broth with 10 mM $CaCl_2$	As described in section 4.3 Table 2. 1 ml of 1M $CaCl_2$ stock to 99 ml of LB broth
BHI agar with 5 and 10 µg/l erythromycin	As described in section 4.3 Table 2.
LB agar with 0.05% sodium citrate	As described in section 4.1 Table 2. but 3.75 ml of 10% sodium citrate was added to 746.25 ml LB agar after it has cooled down to 55°C

Buffer solutions used in this study

Solution	Manufacturer	Ingredients	Preparation
Distilled water "MilliQ"	Merck Millipore		Autoclaved if needed
Phosphate buffered saline (PBS)	Invitrogen by Thermo Fisher Scientific Inc.	10 X PBS	Diluted 1:10. autoclaved
TBE (Tris/Borate/EDTA) buffer		54 g of Tris base. 27.5 g of boric acid.20 ml of 0.5 M EDTA (pH 8.0) Adjust pH to 8.3 with HCl	Dissolve in 1l od distilled water and adjust pH.
Hucker's Crystal Violet (CV) (2%)	Sigma Aldrich	Crystal violet powder. 95% ethanol. ammonium oxalate. distilled water	20 g crystal violet is dissolved in 200mL of 95% ethanol and mixed with a solution of 8g ammonium oxalate in 800ml of distilled water
Methanol	Merck millipore	≥99.9% pure reagent	
Glacial Acetic Acid (33%)	Sigma Aldrich	Acetic acid and distilled water	1/3 dilution of pure acetic acid in water
2-β-Mercaptoethanol	Sigma Aldrich	>98% pure reagent	
TE buffer	Epicentre®. Illumina® company	10 mM Tris-HCl [pH 7.5]. 1 mM EDTA	Ready-to-use solution
RNA Protect® Bacteria Reagent	Qiagen	Contents not provided	Ready-to-use solution